DISSERTATION

ADSORPTIVE SEPARATIONS OF PHYTOCANNABINOIDS AND PESTICIDES IN THE LIQUID PHASE

Submitted by

Jamie H. Cuchiaro

Department of Chemistry

In partial fulfillment of the requirements

For the Degree of Doctor of Philosophy

Colorado State University

Fort Collins, Colorado

Fall 2022

Doctoral Committee:

Advisor: Melissa Reynolds

Delphine Farmer
Jean Chung
Ken Reardon

ABSTRACT

ADSORPTIVE SEPARATIONS OF PHYTOCANNABINOIDS AND PESTICIDES IN THE LIQUID PHASE

Cannabis sativa L. is among the oldest crops, and globally distributed by humans for fibrous, medicinal, and recreational uses. Cannabis is perhaps best known for biosynthesis of physiologically active molecules called cannabinoids. There are over 120 known cannabinoids produced by *Cannabis sativa L.* but quantitative analysis of most is limited by their low abundance in the plant. Research on those lesser-studied cannabinoids has the potential to open a broad field of applications for the cannabis plant and the burgeoning cannabis industry. A primary agricultural, commercial, and user health concern with cannabis is pesticide contamination. Contamination by unapproved pesticides necessitates remediation prior to sale, which can be difficult to perform, as well as temporally and materially expensive. At the benchtop-scale, cannabinoids and pesticides are commonly resolved and quantitated using high-performance liquid chromatography (HPLC) coupled with either diode-array (DAD) or tandem mass spectrometry (QQQ) as the detection method. The cannabis plant is notoriously complex, necessitating creative approaches to separation strategies.

Chapter 2 reports on the development of an HPLC-QQQ method for simultaneously detecting 25 cannabinoids and 9 pesticides and advances the field of cannabis chemistry in five ways. First, to my knowledge, quantifying 25 cannabinoids in a single HPLC-QQQ method is more than has previously been reported, allowing for deeper investigations of cannabis. Second, this method simultaneously measures pesticides and cannabinoids in numerous sample types,

addressing a primary concern for the industrial cannabis chemistry. Third, this method improves the LOD and LOQ of HPLC-DAD methods (neat solvent) by approximately 50x. Fourth, this method chromatographically resolves Δ8-tetrahydrocannabinol (Δ8-THC) and Δ9-tetrahydrocannabinol (Δ9-THC), two cannabinoids with high structural similarity but different regulatory statuses. Fifth, this work reports preliminary investigations into the use of extracted hops flower as a calibration matrix.

Chapter 3 evaluates the suitability of MIL-53(Al), a commercially available metal-organic framework (MOF) as a stationary phase for cannabinoid separations. The suitability of a MOF for a given separation is limited by the ability of a given molecule to enter the pore of the MOF. To evaluate the extent of possible adsorptive interactions between cannabinoids and the interior surface area of MIL-53(Al), the Radii of Gyration (R_g) and Solvent Accessible Surface Areas (SASAs) were calculated for three cannabinoids: cannabidiol (CBD), cannabinol (CBN), and Δ9-THC, as well as the MOF. These values were used to calculate the theoretical adsorption capacity of the MOF, using four competing adsorption models. The R_g of cannabinoids (4.1 Å) is larger than one MOF pore aperture dimension (4.0 x 5.0 Å). The adsorption capacity was measured by relating a decrease in cannabinoid concentration in acetonitrile when exposed to 100 mg MOF. Cannabinoid uptake by the MOF was estimated using the relative standard deviation (RSD) of the soaking solution assay, as the Decomposition-Corrected RSD as Uptake (DCRU). The DCRU was calculated as $0.007 \pm 0.004\ \mu g_{cannabinoids}/mg_{MOF}$. These findings indicate that most of the MOF surface area was inaccessible for adsorption by cannabinoids due to size-exclusion effects. The implication of this work is that the suitability of a MOF for adsorptive separations, such as liquid chromatography, must have an upper limit for size of the

analyte. Additionally, MOFs may generally be more suitable for separations in the gas phase, where adsorbates are not hindered by the presence of a solvation shell.

Chapter 4 reports on a benchtop-scale high performance liquid chromatographic method that was developed as a proof-of-concept for preparative-scale liquid chromatographic separation. Six industrial hemp process matrices were spiked (flower, ethanol crude extract, CO_2 crude extract, distillate, distillation mother liquors, and distillation bottoms) with commonly used pesticides carbaryl, boscalid, and Spinosad, then evaluated differences of spike recovery and pesticide retention based on sample matrix through a 2.7 µm octyldecylsilane column. Then, the retention times of carbaryl, boscalid, Spinosad, and 8 additional unapproved pesticides were compared to those of 26 cannabinoids and the cannabinoid precursor olivetol for possible simple fractionation. Clothianidin, imidacloprid, carbaryl, olivetol, diuron, Spinosad, and myclobutanil eluted in the first 3.6 minutes, and all cannabinoids (except for 7-OH-CBD) eluted in the final 12.6 minutes of the 19-minute gradient for all matrices evaluated. Thus, the present method is suitable for 6/11 pesticides and 25/26 cannabinoids evaluated, and 7-OH-CBD (RT: 3.4 min), pyrethrins I and II (RT_A: 6.8 min, RT_B: 10.5 min), permethrin (RT_A: 11.9 min, RT_B: 12.2 min), and piperonyl butoxide (RT_A: 8.3 min, RT_B: 11.7 min), will require additional purification steps than presently reported. Preliminary separations using larger particle-size C18 are ongoing but require further optimization prior to method transfer. The resolution of pesticides from cannabinoids in this method indicates that eluent fractionation is a highly attractive solution for pesticide remediation of contaminated cannabis materials and targeted isolation of cannabinoids.

The work presented in this dissertation advances the field of cannabis chemistry and cannabinoid separations by increasing the number of cannabinoids and pesticides simultaneously analyzed by HPLC-QQQ, quantitative resolution of Δ8- and Δ9-THC, the first report of using a

MOF for adsorptive separation of cannabinoids, observation of matrix-specific pesticide extraction efficiencies, and development of a benchtop-scale method toward the goal of preparative-scale method for strategic fractionation, remediation, and isolation of 26 cannabinoids and 11 pesticides.

ACKNOWLEDGEMENTS

This research was performed in the Panacea Life Sciences Cannabinoid Research Center at Colorado State University. Dynamic Light Scattering experiments were performed in the Analytical Research Core at Colorado State University.

I am deeply grateful to have received fellowships in support of this work. Thank you to the Gary E. Maciel Fellowship; the C. Michael Elliott Scholarship; Daughters of the American Revolution William Robert Findley Graduate Chemistry Scholarship; the Alexander Foundation Graduate Scholarship.

Thank you to my advisor, Dr. Melissa Reynolds, for mentoring me as a chemist and professional. I am grateful for your leadership during the COVID pandemic, supporting my academic endeavors throughout, and ensuring our group always had a well-communicated safety plan. Thank you for being my advocate within the university, and supporting my pursuit of life, liberty, and the pursuit of happiness. Thanks for the tip about wearing comfortable shoes. I am lucky to have been a part of your group.

Thank you to the Reynolds Group for collaboration, friendship, and baked goods. It was my privilege to work with Dr. Chris Allison, Dr. Alyssa Galvin, Dr. Robert Reeves Tuttle, Dr. Jon Thai, Andrea Selkow, Maga Mohnike, Maddie Roach, Tracey Wick, Dr. Jessi Vlcek, Dr. Yanyi Zang, Sarah Stanley, Yaman Peksenar.

Thank you to my family, friends, teachers, professors, mentors, grad committee

CU-Boulder, CU-Denver, CSU-Fort Collins

Thank you to Darren Stewardson and John Thurman at Phenomenex (Torrance, CA) for providing the Phenomenex Luna C18 (PREP) 10 µm column used in Chapter 4.

Thank you

DEDICATION

Not so much a dedication as a direction.

The Way You've Not Yet Been

By Greg Hobbs

Lift your eyes to the hills,
Plant your feet among the trees,
The way that is before you
Is the way you've not yet been.

Gather in your family,
Bring along your friends,
Raise yourself for each other
Then the mountains will be seen.

TABLE OF CONTENTS

CHAPTER 1 – INTRODUCTION

1.1 Overview

Cannabis sativa L. is one of the oldest crops, and globally distributed by humans for fibrous, medicinal, and recreational uses.[1] It may have been used as long as 10,000 years ago, and cultivation in China has been documented for at least 6000 years.[2–4] Cannabis is the most common illegal drug crop in the world, but has recently seen a trend towards legalization as attitudes towards prohibition change.[5–7] In Colorado alone, cannabis sales were over $2.2 billion in 2020 and 2021, and $906 million for January-June 2022.[8]

Cannabis is perhaps best known for biosynthesis of physiologically active molecules called cannabinoids. There are over 120 known cannabinoids produced by Cannabis sativa L. but quantitative analysis of most of these cannabinoids is limited by their low abundance in the plant.[9–12] It is known that cannabinoids elicit physiological effects within the body via interactions with CB1 and CB2 receptors in the endocannabinoid system, but much of what is known about these effects is limited to a small number.[12–14] Research on those lesser-studied cannabinoids has the potential to open a broad field of applications for the cannabis plant and the burgeoning cannabis industry.[10,15]

Pesticide contamination is a primary agricultural, commercial, and user health concern for cannabis.[16–18] State regulatory agencies set acceptability criteria for approved and non-approved pesticides. In Colorado, acceptable pesticides and concentration in consumer cannabis products are set by the Marijuana Enforcement Division (MED).[19,20] As of August 2022, there are 417 MED-approved pesticides.[21] Contamination by unapproved pesticides necessitates remediation prior to sale, which can be difficult to perform, as well as temporally and materially

expensive.

At the benchtop-scale, cannabinoids and pesticides are commonly resolved and quantitated using high-performance liquid chromatography (HPLC) coupled with either diode-array (DAD) or tandem mass spectrometry (QQQ) as the detection method.[22,23] The benefit of this approach is that cannabinoids can be resolved in reverse-phase HPLC methods.[24–26] The literature tends to focus on those cannabinoids occurring in the greatest abundance, due to availability of reference materials, regulatory environments, and ease of detection.[27] Namely, non-psychotropic cannabidiol (CBD) and psychotropic Δ9-tetrahydrocannabinol (Δ9-THC).[28,29] The molecular structures of Δ9-THC and CBD are shown in Figure 1.1.

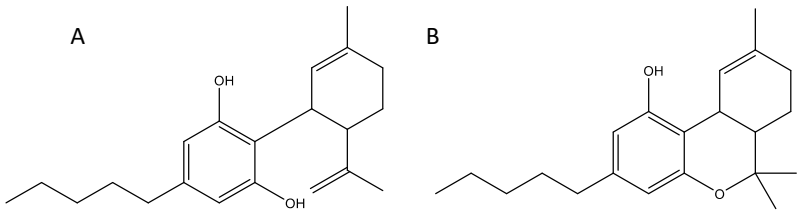

Figure 1.1.1: Molecular structures of A) non-psychotropic cannabidiol (CBD) and B) psychotropic Δ9-tetrahydrocannabinol (Δ9-THC).

The cannabis plant is notoriously complex, necessitating creative approaches to separation strategies.[30,31] Cannabis is a highly complex matrix that requires clean-up steps.[32] Cannabis samples used in this dissertation were cleaned using QuECHERS (Quick, Easy, Cheap, Rugged, Effective, and Safe) extraction, filtered through 0.2 µm polytetrafluoroethylene (PTFE), and where possible, diluted with neat solvent. The net impact of these clean-up steps is a lower signal-to-noise ratio, fewer interfering matrix components, and less complicated analysis.

This work initially sought to improve sensitivity and selectivity of HPLC separation to assay a greater number of cannabinoids than previously reported, using HPLC-QQQ.[15,33,34] This work then sought to further improve on existing methods by simultaneously analyzing work that

quantitatively separates cannabinoids and pesticides together. Increasing the number of measurable cannabinoids and identifying which matrices they are most abundant in, facilitates their eventual strategic isolation at the preparative scale.[35,36] A multi-dimensional approach to separation and isolation of cannabinoids and other molecules of interest such as pesticide contaminants is necessary to improve upon existing separation techniques and technologies.[37,38]

This work investigated two benchtop strategies for adsorptive separations of cannabinoids and pesticides within a variety of industrial processing sample types. The eventual goal of strategically isolating low-abundance cannabinoids or remediating pesticides from those same industrial matrices. This work seeks to improve on existing benchtop separation methods for a broad array of cannabinoids and pesticides, with the eventual goal of larger-scale isolations for remediation, industrial, or clinical applications. The following subsections present a summary of key topics necessary to understand the work herein reported.

1.2 Cannabinoids

Cannabinoids are a class of molecules that interact with the body's endocannabinoid system and are classified into three groups: endocannabinoids, phytocannabinoids, and synthetic cannabinoids.[39–41] *Endo*cannabinoids are naturally occurring molecules produced by the human body, *synthetic* cannabinoids are non-naturally occurring, and *phyto*cannabinoids are produced by plants.[42–44] Cannabinoids studied in this dissertation are specific to the cannabis plant and thus *phyto*cannabinoids, however, will be generally referred to as 'cannabinoids' for the purpose of colloquial simplicity. Cannabis-derived cannabinoids are enzymatically produced in the plant by a common pathway starting from olivetolic acid and geranyl pyrophosphate. Cannabinoids are predominately biosynthesized in trichomes in the female flowers and produced in the acid form.

Cannabinoid acids are then decarboxylated through non-enzymatic processes (heat, light), then further differentiated by oxidation and isomerization. Figure 1.2.1 demonstrates the synthetic pathways of cannabigerolic acid (CBGA), cannabigerol (CBG), Δ9-tetrahydrocannabinolic acid (THCA), cannabichromenic acid (CBCA), cannabidiolic acid (CBDA), cannabichromene (CBC), THC, CBD, and Δ8-tetrahydrocannabinol (Δ8-THC).

1.3 Pesticides

A primary concern for the cannabis industry is crop contamination with pesticides. [16–18] Despite clear and stringent pesticide regulations, it is still possible that unapproved pesticides may contaminate cannabis materials. This can be due to cross-contamination from adjacent fields or poor cultivation practices by growers.[45] Three examples of unapproved, contaminant pesticides evaluated in this work are boscalid, carbaryl, and diuron, their structures are shown in Figure 1.3.1. Six additional pesticides were evaluated in this work and will be discussed in Chapters 2 and 4.

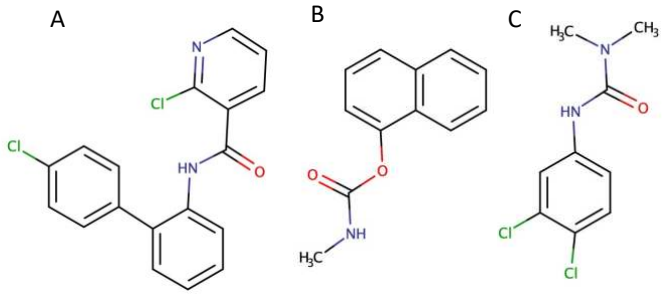

Figure 1.3.1: Molecular structures of pesticides A) boscalid, B) carbaryl, and C) diuron.

1.4 High-performance liquid chromatography

High-performance liquid chromatography (HPLC) is a benchtop-scale separation technique, where analytes are separated by selective partitioning between a solid stationary and

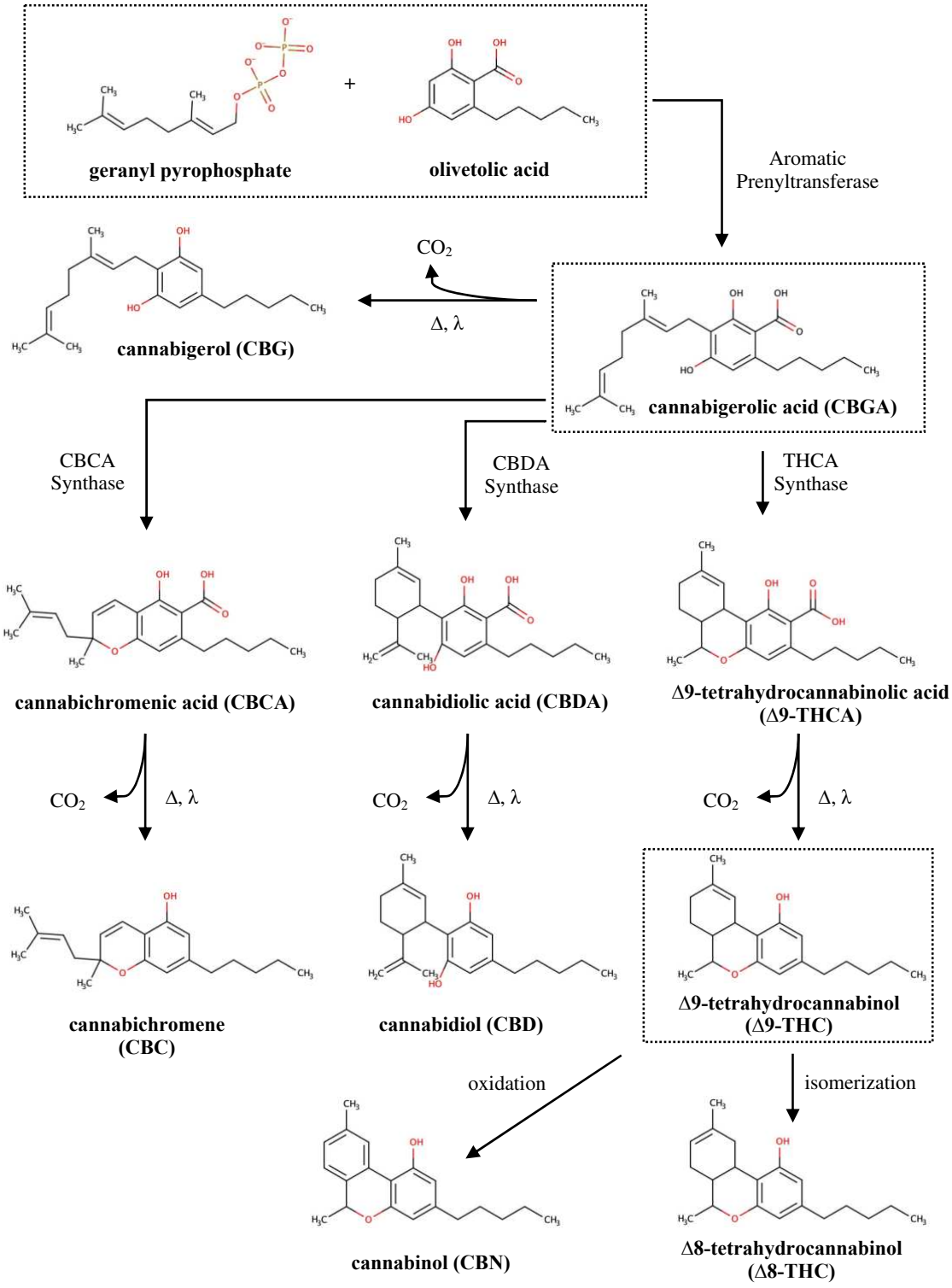

Figure 1.2.1: Synthetic pathway of cannabinoids CBGA, Δ9-THCA, CBCA, CBDA, CBG, CBC, CBD, Δ9-THC, CBN, and Δ8-THC.

liquid mobile phase.[46–49] Stationary phase is defined as an adsorptive material, such as octyldecylsilane, which is packed into a column. The stationary phase packing and particle size are highly regular throughout the column. A mobile phase is a fluid which carries aliquots of sample through the instrument and drives analytes across the column packed with stationary phase. Mobile and stationary phase compositions are critical parameters in HPLC method development. A basic instrument schematic is presented in Figure 1.4.1.

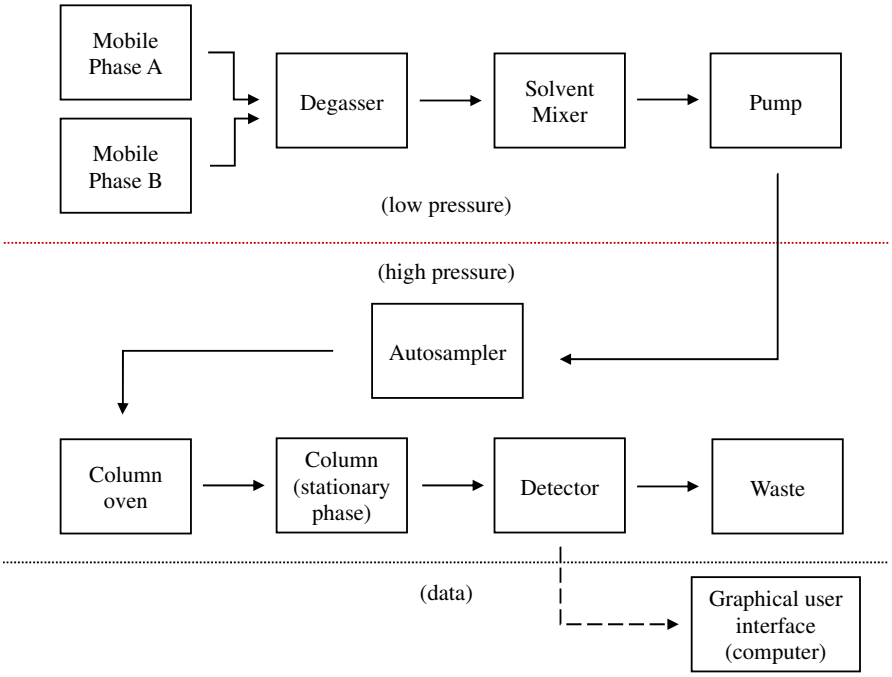

Figure 1.4.1: Basic schematic showing HPLC instrument flow path. A mobile phase of aqueous and organic fractions carries aliquots of sample across a stationary phase, then on to a detector and finally, waste. Detector data is compiled and analyzed by the chemist on a computer.

The mobile phase composition may stay the same throughout the analysis (isocratic) or change according to a pre-determined gradient.[50,51] HPLC separations reported in this dissertation were performed in the reverse-phase, and all methods reported in this work involved gradient separations. The general gradient strategy of reverse-phase HPLC is to equilibrate the column with a polar (aqueous) fraction and then increase the non-polar (organic) fraction.[52] Analyte partitioning is driven by the relative polarity of analytes, mobile phase, and stationary

phase.[53,54] For example, non-polar analytes will have greater affinity for the stationary phase when the polar mobile phase fraction is high, whereas more polar analytes will have greater affinity towards the mobile phase under the same conditions.[55,56] Analytes with greater affinity for the mobile phase will move more quickly through the column, and thus be detected early in the eluent.[55] The mobile phase composition changes toward 100% organic as the gradient proceeds, and analyte partitioning changes based on the composition.[57] More non-polar analytes begin to elute as the organic fraction increases, culminating in a 100% organic wash. The mobile phase composition is then returned to initial conditions and the column re-equilibrated prior to subsequent injection.

Separations reported in this dissertation utilized a compositional gradient of 0.1 % (v/v) phosphoric/formic acid in both water (mobile phase A, MPA) and ACN (mobile phase B, MPB). Acid selection will be discussed in section 1.3. The aqueous fraction of eluent was 40 % or lower and all separations occurred at pressures between 80-200 bar. Mobile phase pH is an important factor in analyte retention times in RP-HPLC because the protonation state/charge of analytes will be influenced by the solvent environment.[58] Within the scope of this dissertation, mobile phase pH is especially important for separation of cannabinoid acids containing a carboxylate motif. [59]

MPA and MPB are drawn into the instrument, passed through a degasser, mixed at a known ratio, then pumped at high pressure through a stainless-steel column packed with stationary phase.[60] After passing through the column, the mobile phase passes to a detector and then to waste.

Two HPLC detectors were used in this work and are described in detail in sections 1.5 and 1.6. In either case, the detector records a response relative to a baseline value that is

presented in a chromatogram and analytes appear as peaks in the chromatogram. An ideal peak will have gaussian shape with high symmetry.[64] The area bound by the baseline and absorbance signal is calculated by integration.[64] The baseline is defined as the average instrument response during normal operation in the absence of analyte, within 0.3 minutes of beginning and end points of peak integration. There will be some noise in the instrument signal and can be caused by a number of factors such as electronic fluctuations, minor variations in eluent composition, etc. The method sensitivity is defined by the ratio of signal to noise coming from the detector.

The peak area of the unknown sample is plotted along the external calibration curve to determine the concentration. The method is suitable for concentrations within the linear range. The linear range is the region where change in analyte concentration scales with peak area.[65] The upper bound is the limit of linearity.[65] There are two regions at the low end of the linear range: the limit of detection (LOD) and limit of quantitation (LOQ).[65] The LOD is defined as three times the signal-to-noise ratio of the baseline signal.[66] The LOQ is defined as ten times the signal-to-noise ratio.[66] Measurements made between the LOQ and LOD are considered qualitative rather than quantitative – in other words, "we know that it's there but we can't confidently say how much of it there is."

1.5 Diode array detection

Diode array detection (DAD) measures light absorbance through a flow cell over time.[61,62] The Agilent 1260 Infinity II (detector PN: G7115A) has two long-life deuterium lamps and can measure 190-950 nm.[63] The control software used in this dissertation was Agilent OpenLAB CDS Acquisition version 2.5.0.842, which allows for up to 8 individual wavelengths to be selected and full absorption spectra to be collected. The signal is zeroed at initial

conditions and plotted over time. This data is plotted as a chromatogram. An example chromatogram is presented in Figure 1.5.1. A single analyte with peak absorbance λ = 200 nm in isocratic conditions will appear as a "peak." Peak shape can be used as an indicator of column suitability.[64]

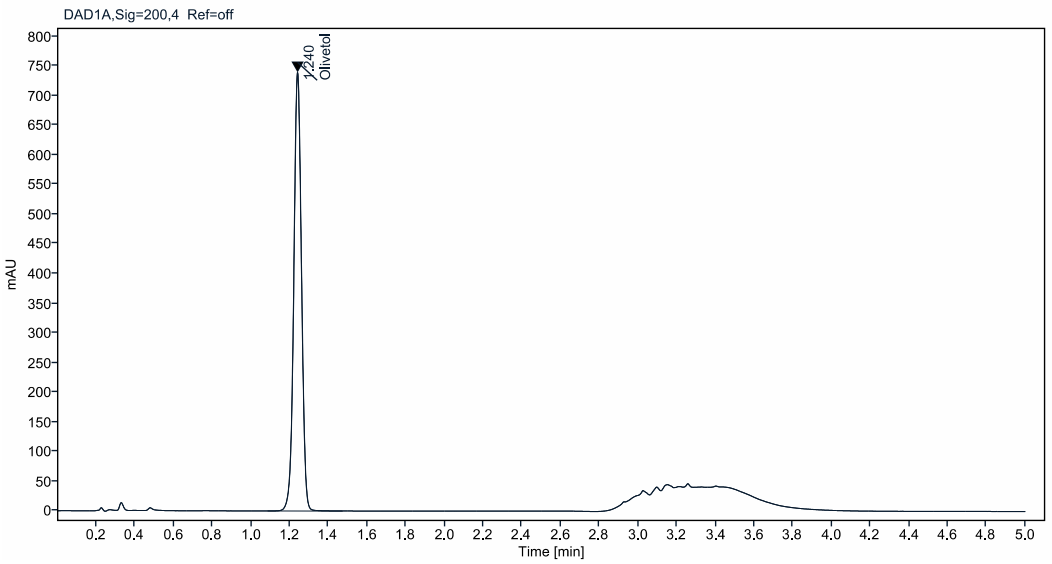

Figure 1.5.1: A representative chromatogram of a single-component solution.
Sample: 145 µg/mL olivetol.

The peak area of integration scales linearly with analyte concentration. Quantitative measurement of a known analyte with unknown concentration can be done in four ways: external calibration, standard addition, matrix spike, or internal standard.[62] Methods described in this dissertation used external calibration. A known amount of standard is diluted to produce a stock solution of known concentration, then diluted to produce multiple solutions of lower, known concentrations. Peak area for each standard solution is plotted against concentration. The trendline should be linear with square of the residuals (R^2) 0.999 or greater. This is a calibration curve; a representative calibration curve is presented in Figure 1.5.2.

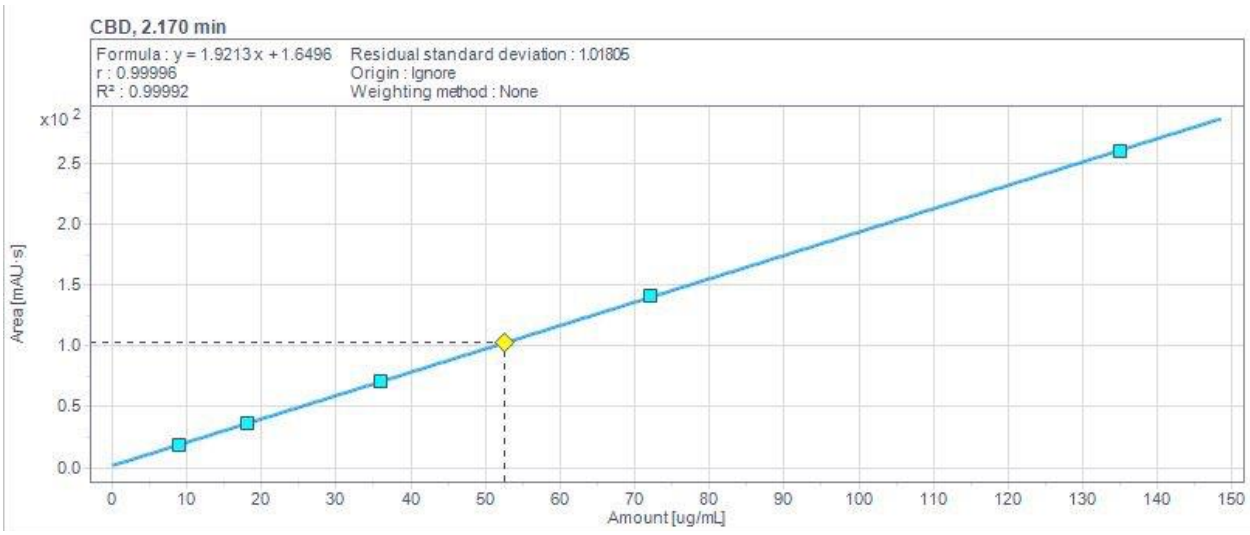

Figure 1.5.2: A representative five-level calibration curve. Calibration levels and a check standard are depicted with blue squares and a yellow diamond, respectively. Sample: CBD in ACN solution.

For separations involving two or more analytes, each analyte must elute separately before passing through the detector. Ideally, all chromatographic peaks will have baseline resolution. A representative chromatogram showing baseline resolution of two analytes is presented in Figure 1.5.3.

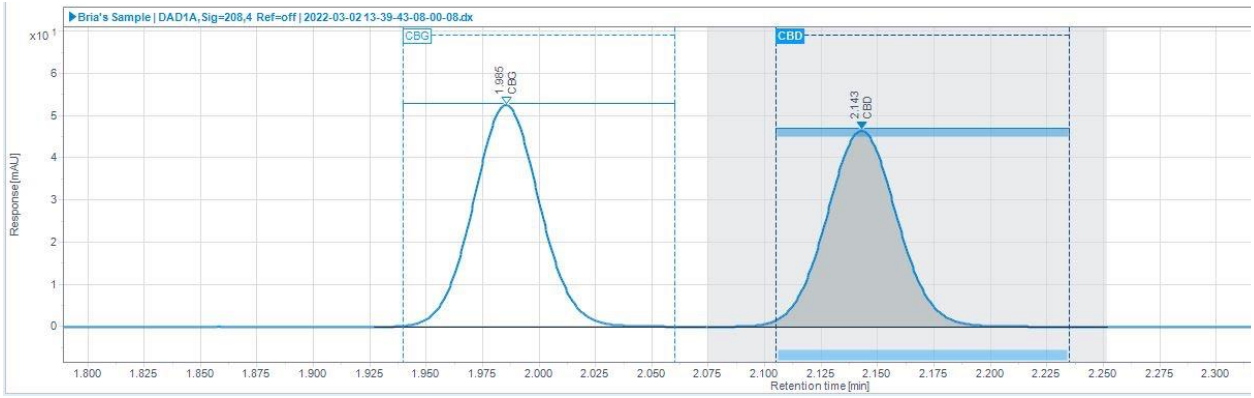

Figure 1.5.3: A representative chromatogram of a two-analyte solution, demonstrating baseline peak resolution. Sample: 5.1 µg/mL CBG and 5.0 µg/mL CBD in acetonitrile.

Unresolved peaks can be integrated by the area bound by the baseline, instrument signal, and the timepoint where the signal minimum occurs, but at a cost to accuracy. This is called drop integration. DAD is also limited to analytes with chromophores in the detector range.

Matrix interference can occur when background species with some absorbance at the analytical wavelength coelute with the analytes. For this reason, sample preparation must be considered during method development, and clean-up steps to remove interfering species may be needed.

1.6 Triple-quadrupole mass spectrometry

Triple-quadrupole mass spectrometry, also known as tandem mass spectrometry, resolves analytes by their mass-to-charge ratios (m/z) by passing them through a series of quadrupoles under vacuum.[67] The system used in this work ionized eluent via electrospray ionization, where the eluent is passed through a nebulizer and dried with hot nitrogen, which removes the solvent shell and effectively vaporizes analytes at ambient pressure. Separations in this dissertation were performed in acidic mobile phase so excess protons are also left behind when the solvent shell evaporates, giving the analytes a positive charge. The charged particles are then drawn into the detector at 90° and focused through an acceleration chamber. The ion stream and internal schematic of the detector are shown in Figure 1.6.1.

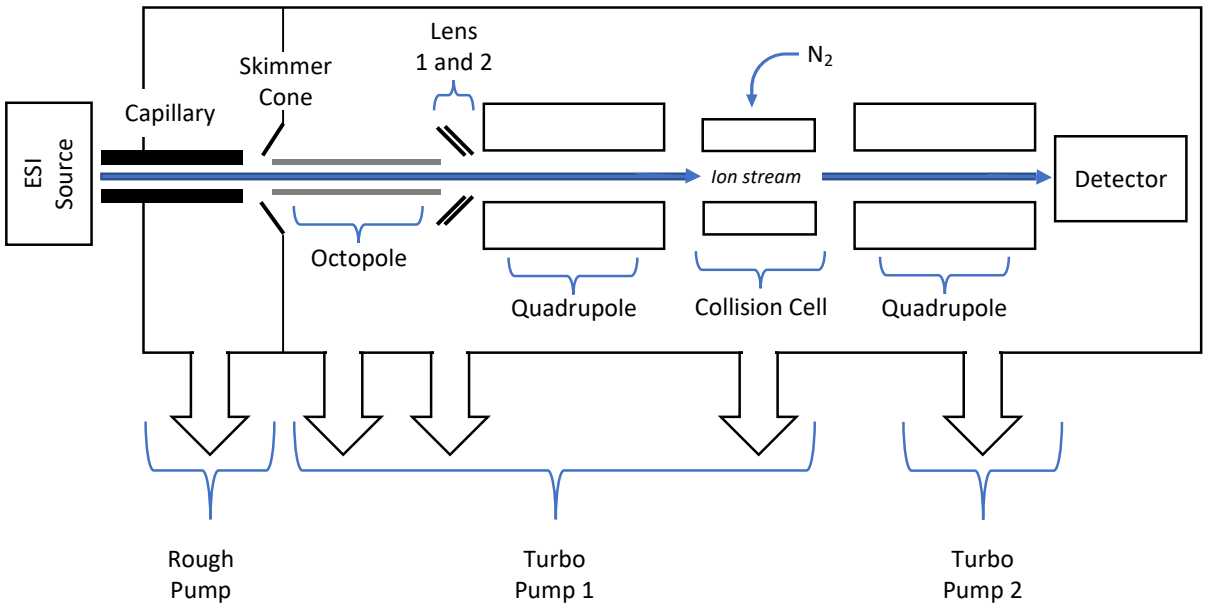

Figure 1.6.1: Instrument schematic showing the path charged ions take through the detector.

The benefit of using multiple quadrupoles is that it increases molecular specificity. Precursor ions of only a specific mass are drawn into the ion stream then obliterated with high temperature nitrogen in the collision cell. The product ions produced in the collision cell from a given precursor ion will occur in a predictable ratio, and the second quadrupole then selects for those specific product ions (previously optimized). The analyte is quantified using the product ion of highest abundance, and then confirmed by the ratio of secondary product ions also detected (qualifier ions). Figure 1.6.2A depicts two mass transitions of CBE (precursor m/z = 331.2). The highest abundance product ion has a mass-to-charge ratio of 109.1 and the qualifying product ion has a mass-to-charge ratio of 135.1. Figure 1.6.2B shows the mass spectrum of the CBE precursor and product ions reaching the detector.

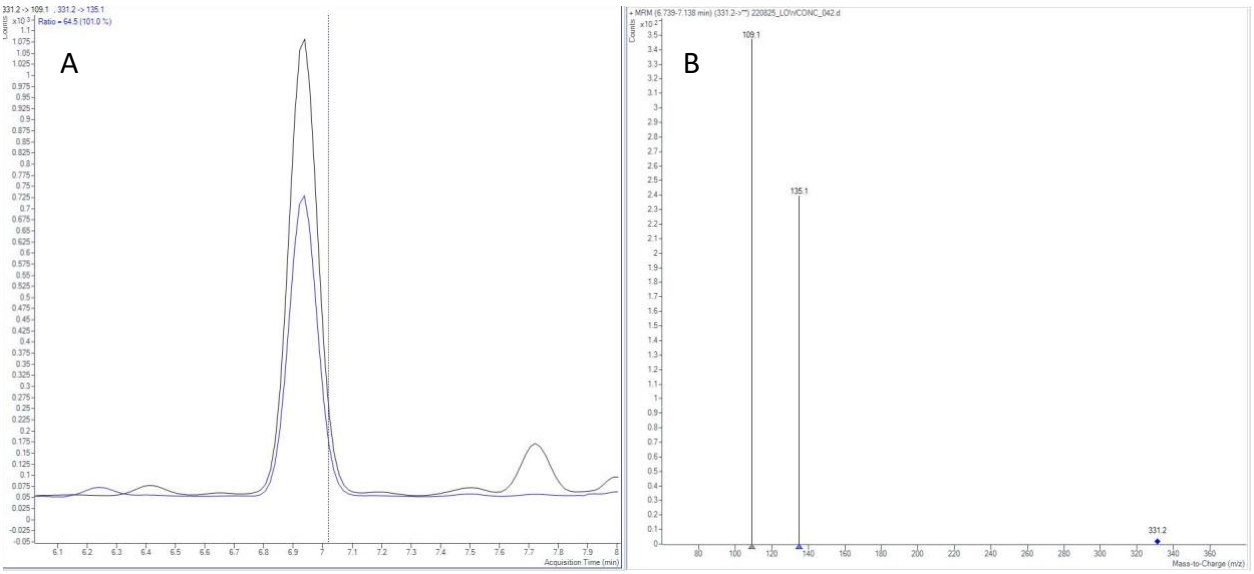

Figure 1.6.2: Tandem mass spectrometry data for CBE eluting at RT = 6.94 min. A) The black trace is the quantifying mass transition (331.2 to 109.1 m/z), and the blue trace is the qualifying mass transition (331.2 to 135 m/z). B) Mass spectrum of the integrated CBE peak. The 331.2 m/z precursor ion is represented with a blue diamond, and the 135.1 and 109.1 m/z product ions are indicated with blue triangles. The magnitude of the quantifying mass transition is greater than that of the qualifying mass transition.

1.7 Metal-organic frameworks

Metal-organic frameworks (MOFs) are a class of materials composed of metal ion nodes linked by organic molecules in an infinite array.[68] MOFs are highly tunable due to the broad variety of metals and organic molecules.[69] As of 2022, there were over 89,864 MOFs in the Cambridge Crystallographic Database (CCD).[70] MOFs are porous and notable for their characteristically high surface areas; many have hundreds or thousands of square meters per gram of material.[71] The highest reported surface area for MOFs are over 7000 m^2/g.[72] General MOF structure, as well as that of commercially available MOF MIL-53(Al), are presented in Figure 1.7.1.

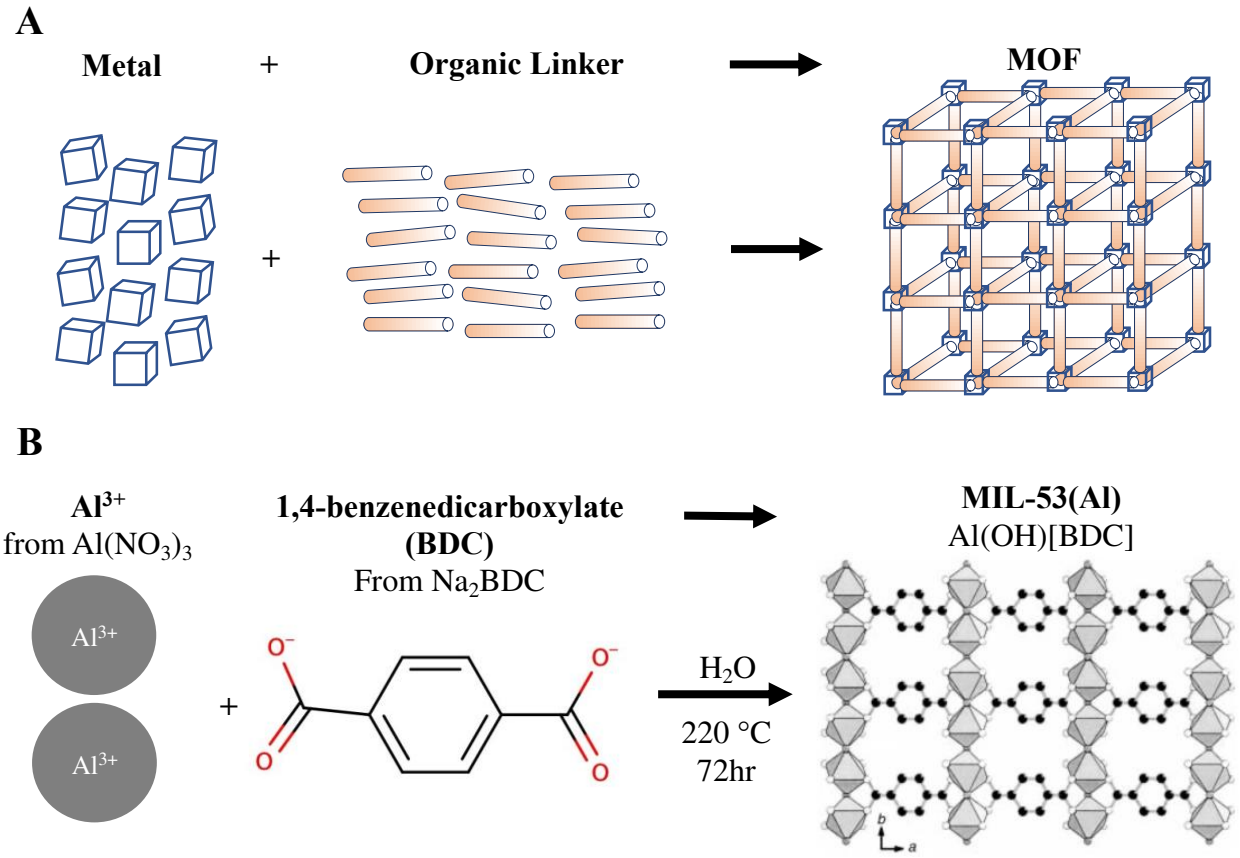

Figure 1.7.1 A) Metal-organic frameworks are self-assembling, repeating arrays of metal nodes connected by organic linker molecules. B) MIL-53(Al), sold commercially as Basolite A100, is a MOF discussed in detail in Chapter 3. Greyscale MIL-53(Al) framework adapted from Loiseau et al (2004).[73]

The high surface areas of MOFs make them potentially useful for adsorptive separations, where adsorption capacity corresponds to surface area.[74] Most of the MOF surface area is in the interior, and access to that surface is limited to molecules able to diffuse through the pores.[75] Solvent molecules are small enough to diffuse through the framework and fill internal pores as guest molecules. These guest molecules can interfere with surface area measurements, so samples must be activated under vacuum prior to analysis. The effect of guest molecules in the framework is to skew surface area measurements negatively. Solvent removal is aided by heat, but the framework can thermally degrade at high temperatures, so heat stability is an important consideration in method development. In a previous study, our group investigated the parameters affecting adsorption of the uremic toxin p-cresyl sulfate by a group of zirconium MOFs and MIL-100(Fe), and found poor correlation between adsorption and surface area or pore volume.[38] The presence of a solvation shell around adsorbates in the liquid phase may increase the effective adsorbate dimensions of the substrate and thus further limit diffusion into the MOF. For this reason, the utility of MOFs' high surface area may have an upper limit for adsorptive separations.

Chapter 3 will discuss the selection of the commercially available MIL-53(Al) in depth. Briefly summarized, MIL-53(Al) is composed of terephthalate linkers and Al^{3+} metal nodes.[24] MIL-53(Al) has the potential to improve upon commercially available stationary phases for adsorption-driven reverse phase liquid chromatographic separations, because MIL-53(Al) is unique among MOFs due to its stability in liquid water for at least 6 months and its reported stability between pH 2-12 over the same timeframe.[25–27] MIL-53(Al) has a reported Brunauer-Emmett-Teller (BET) surface area up to1706 m^2/g.[24,26–32] MIL-53(Al) has previously been used as a stationary phase in liquid chromatography to separate mixtures of phthalate acid esters.[37]

The stability in aqueous environments and across a wide pH range makes MIL-53(Al) a promising candidate for more generalized adsorptive separation applications in the liquid phase.

1.8 Brunauer-Emmett-Teller Surface Area

This dissertation reports MOF surface areas measured by Brunauer-Emmett-Teller (BET) analysis.[76,77] The general analytical flow was as follows. A sample tube was evacuated, then cooled to -77.4 K with liquid nitrogen and nitrogen gas was added back in known amounts.[78] The pressure in the tube is measured and related to amount of adsorbed nitrogen.[77] Pressure data is collected for both adsorption and desorption and is plotted as an isotherm. The surface area is calculated using the molecular dimensions of the adsorbing gas. The shape of the isotherm depends on the sample type. For example, type II isotherm is indicative of mesoporous sample with pore apertures 2 – 50 Å.[76] A representative type II isotherm is presented in Figure 1.8.1.

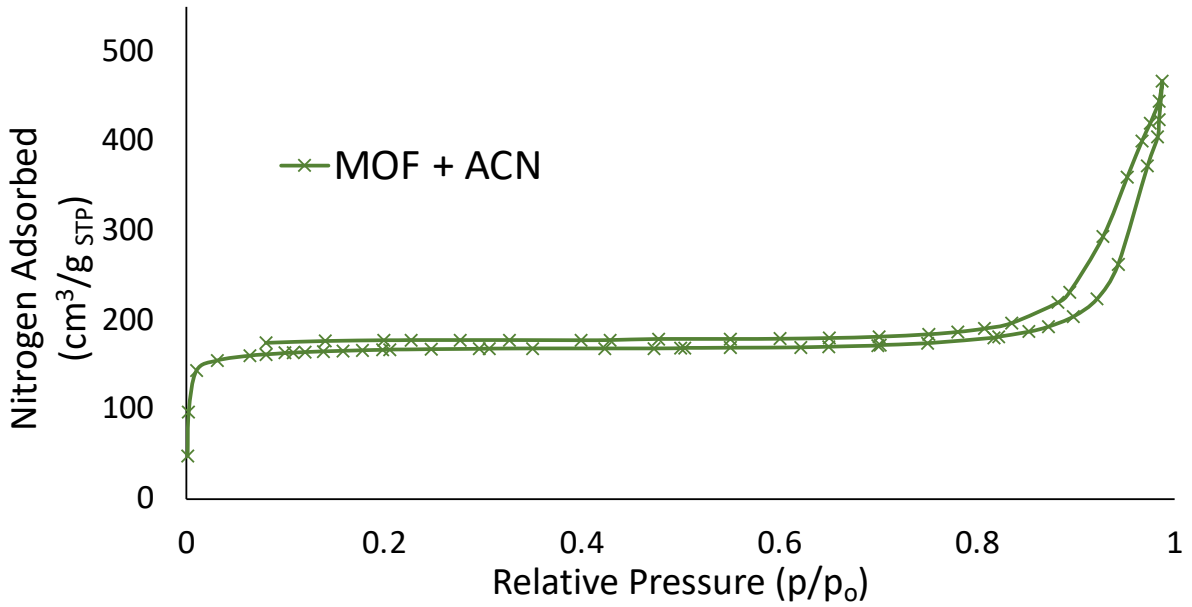

Figure 1.8.1: A representative Type II BET isotherm. Sample: MIL-53(Al) soaked in acetonitrile and degassed at ambient temperature.[78]

Type II isotherms have three characteristic regions. The first is a steep, positive slope at low partial pressures, and corresponds to formation of a monolayer on the sample surface.[77]

Second is a gentle, positive slope at middle partial pressures, corresponding to the formation of a multilayer.[77] Third is a steep, positive slope at high partial pressures, corresponding to adsorptive saturation.[77] The BET surface area is calculated from the slope of region one, at partial pressures $0.05 \leq p^o/p \leq 0.30$, ideally with at least 5 points.[76]

1.9 Dissertation outline

The following dissertation investigates adsorptive separations of cannabinoids and pesticides using a three-fold approach and advances the field of analytical separations by:

1. Increasing the number of simultaneous cannabinoids and pesticides measured by an HPLC-QQQ method.
2. Reports the first investigations into cannabinoid adsorption using a MOF.
3. Probes the suitability of preparative-scale chromatography for pesticide remediation and cannabinoid isolations using HPLC.

Chapter 2 describes a high selectivity method for simultaneous analysis of 25 cannabinoids and 9 pesticides using HPLC-QQQ. Analytes were calibrated using a six-level external calibration curve, each with $R^2 \geq 0.999$, and quantified in 6 different cannabis matrices. The matrices analyzed were raw flower, ethanolic crude extract, supercritical CO_2 crude extract, distillate, distillation mother liquor, and distillation bottoms. The method advances current methods by resolving Δ8- and 9Δ-THC in standard solution and increasing the number of simultaneous cannabinoids analyzed by 8 species as well as adding 8 pesticides. One challenge of accurate quantitation in cannabis samples is the lack of a suitable matrix blank. Chapter 2 reports on investigation of the suitability of extracted *Humulus lupulus* (common hops, var. Cascade), spiked with cannabinoids and pesticides, toward development and validation of an

advanced calibration matrix. Additionally, analyses of samples with different dilutions had problems with reproducibility. Chapter 2 discusses strategies to address these reproducibility issues as method optimization steps, although this work is ongoing. Finally, multiple peaks were observed in MRM data for some cannabinoid acids, and possible structural isomerism of the analytes is presented. Chapter 2 is currently in preparation for submission to the ACS journal *Analytical Chemistry*.

Chapter 3 investigates the use of a commercially available, high surface area MOF, MIL-53(Al), for adsorption capacity and selectivity of Δ9-THC, CBD, and CBN. These three cannabinoids were selected because they are produced in relatively large amount by the cannabis plant. This was the first reported study using a MOF for cannabinoid separations. This work challenges the assumption that the high surface area and solvent stability of MOFs are primary concerns for using a MOF as an adsorbent, by demonstrating access to the MOF interior is limited by the relative size of the pore window aperture to the adsorbate. This study used BET surface area, HPLC-DAD, HPLC-QQQ, and computational modeling as complementary methods to reductively eliminate competing adsorption hypotheses. This work suggested that cannabinoid adsorption to the MOF is size limited by the computed molecular radius of gyration (R_g) relative to the pore aperture. R_g of THC, CBD, and CBN = 4.1 Å, R_g of ACN = 3.3 Å, and the pore window R_1 of MIL-53(Al) = 4.0 Å. Thus, solvent (ACN) molecules are able to penetrate into the bulk of the MOF, but cannabinoids are size-excluded from accessing the MOF interior surfaces. Figure 1.9.1 graphically summarizes this finding. This work was published in *ACS Applied Materials* as an original research article.

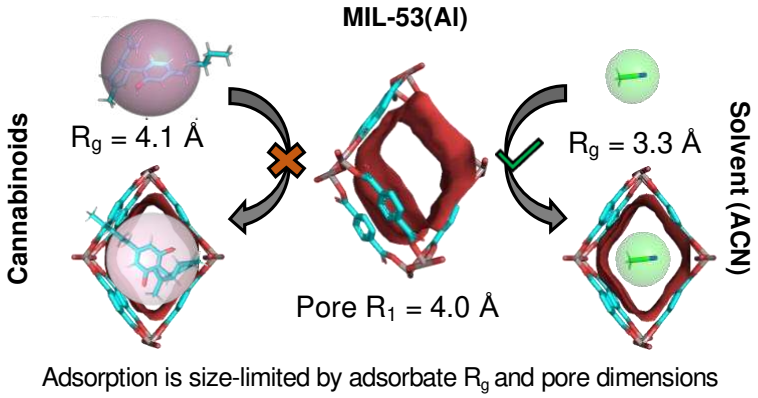

Figure 1.9.1: Cannabinoids have an R_g = 4.1 Å and cannot pass through the pore aperture (R_g = 4.0 Å). ACN solvent molecules have an R_g = 3.3 Å and can pass into the bulk MOF. This work indicates that access of an adsorbate to the interior surface area of a MOF is size-limited by the adsorbate radius of gyration relative to the pore aperture size.

Chapter 4 describes a benchtop gradient separation method to resolve 11 pesticides from 26 cannabinoids, and the precursor molecule olivetol in cannabis samples, with the aim of scale-up to a preparative scale separation. Chapter 4 includes a study on extraction efficiency of pesticides in the 6 sample types using the QuECHERS EN method. Clothianidin, imidacloprid, carbaryl, olivetol, diuron, Spinosad, and myclobutanil eluted in the first 3.6 minutes, and all cannabinoids (except for 7-OH-CBD) eluted in the final 12.6 minutes of the 19-minute gradient for all matrices evaluated. Thus, the present method is suitable for simple fractionation of 6/11 pesticides and 25/26 cannabinoids evaluated on 2.7 µm C18 Poroshell media. 7-OH-CBD, pyrethrins I and II, permethrin, and piperonyl butoxide will require additional purification steps beyond the present gradient. Preliminary benchtop separations using 10 µm C18 stationary phase are ongoing but require further optimization prior to method transfer. Carbaryl, boscalid, and Spinosad were spiked into six industrial cannabis processing matrices: flower, ethanol crude extract, CO_2 crude extract, distillate, distillation mother liquor, and distillation bottoms. Percent spike recoveries were calculated for all three pesticides, and it was observed that ethanolic crude extract had the largest recovery for all three pesticides, and the RSDs of spike recoveries of the

individual matrices were significantly smaller compared to all samples. A key finding is that matrix composition must be considered when extracting samples for pesticide remediation.

Key outcomes from this work were improvement in the number of cannabinoids detected by HPLC-QQQ, a method for simultaneous quantification of 25 cannabinoids and 10 pesticides, the first investigation of a MOF for cannabinoid separation and demonstrating that the adsorption-accessible surface area is size limited, that gradient elution of pesticide-contaminated cannabis materials through an on 2.7 µm C18 Poroshell column is sufficient to fractionate 6/11 pesticides, olivetol, and 25/26 cannabinoids, and indicates that preparative-scale liquid chromatography could be used to remediate or isolate those compounds of interest.

The field of cannabis chemistry will be advanced through future developments of the work presented herein in the following ways. The HPLC-QQQ method reported in Chapter 2 is validated in neat solvent, but additional sample clean up and development of a suitable calibration matrix are necessary prior to accurate quantitation and method validation for cannabis samples. Advancing adsorptive separation studies of cannabinoids or pesticides using MOFs reported in Chapter 3 will require a different MOF with larger pore aperture than MIL-53(Al). Ideally, a MOF with the same solvothermal stability as MIL-53(Al), which may require development of new synthetic methods in our research group. Preliminary experiments for benchtop-scale separations reported in Chapter 4 using 10 µm C18 stationary phase are ongoing but require further optimization prior to method transfer to preparative-scale.

CHAPTER 2[1] – SEPARATION AND QUANTITATION OF MINOR CANNABINOIDS AND PESTICIDES IN SIX EXTRACTION MATRICES

2.1 Summary

The purpose of this study was to develop a high-performance liquid chromatography-tandem mass spectrometry (HPLC-QQQ) method for simultaneous analysis of 25 cannabinoids and 9 pesticides in six cannabis sample matrices. The matrices evaluated were raw cannabis flower, CO_2 and EtOH crude extracts, distillation mother liquors, distillate, and distillation bottoms. This work advances the field of cannabis chemistry in five ways. First, to my knowledge, quantifying 25 cannabinoids in a single HPLC-QQQ method is more than has previously been reported, advancing the field of cannabis research. Second, this method simultaneously measures pesticides and cannabinoids in multiple sample types, addressing a primary concern for the cannabis industry. Third, this method improves the LOD and LOQ of HPLC-Diode Array Detection (HPLC-DAD) methods (neat solvent) by approximately 50-fold. Fourth, this method chromatographically resolves Δ8-tetrahydrocannabinol (Δ8-THC) and Δ9-THC, two cannabinoids with high structural similarity but different regulatory statuses. Fifth, this work reports preliminary investigations into the use of extracted hops flower as a calibration matrix. Additional sample clean up steps and validation of a suitable calibration matrix are still needed.

[1] Chapter 2 is adapted from a manuscript in preparation for submission to *ACS Analytical* Chemistry with coauthors Dr. James Baumgartner and Dr. Melissa Reynolds. Samples used in this work were provided by Panacea Life Sciences, Golden, CO.

2.2 Introduction

Cannabis sativa L. (cannabis) has been used for over 6000 years for medicinal, utilitarian, recreational, and religious purposes.[88,89] Cannabis produces a number of pharmacoactive compounds, including phytocannabinoids, terpenoids, flavonoids, and alkaloids.[1] Phytocannabinoids are terpenophenolic molecules; perhaps the best known are Δ9-tetrahydrocannabinol (Δ9-THC) and the non-psychoactive cannabidiol (CBD).[90] THC produces the recreational "high" associated with marijuana, and CBD is a non-psychoactive analog that is reported to have antiemetic, anti-seizure, and anti-inflammatory properties.[91] C. sativa can be broadly differentiated into two types: hemp and recreational or medicinal marijuana.[26,92] The distinction between marijuana and hemp is defined by the relative THC content on the dry weight basis. Hemp is characterized as having less than 0.3% (w/w) THC, whereas marijuana has THC in amounts above that threshold.[31,93,94] In general, hemp produces CBD in much greater amounts than marijuana, and is thus an important cash crop in the emerging cannabis industry.[23] The molecular structures of Δ9-THC and CBD are shown in Figure 2.2.1.

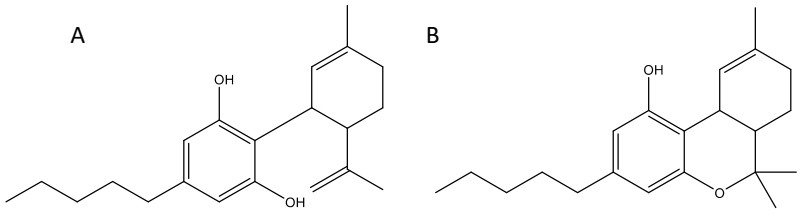

Figure 2.2.1: Molecular structures of A) CBD and B) Δ9-THC, two high value cannabinoids that are produced in high abundance in the cannabis plant.

Pesticide contamination of cannabis source material is a primary concern in the production of cannabis products, and acceptability criteria for the presence of pesticides are regulated by state agencies.[19] Although direct use of pesticides on hemp products is regulated, occasionally the plants are indirectly exposed to banned pesticides. Cannabis is a hyperaccumulator; therefore, trace contamination of biomass is an issue when grown next to

other crops.[38,95] For example, hemp grown in proximity to other commodity crops can be contaminated by pesticides from those adjacent fields.[96] This becomes problematic when the pesticides used are not accepted by commercial cannabis regulations and drift to the hemp crop. Carbaryl, boscalid, Spinosad, imidacloprid, clothianidin, diuron, myclobutanil, piperonyl butoxide, pyrethrins I and II, and permethrin are a representative group of pesticides banned from use in cannabis products.[21] Their structures are presented in Figure 2.2.2.

The purpose of this study was to develop a HPLC-QQQ method for simultaneous analysis of 25 cannabinoids and 9 pesticides in 6 cannabis sample matrices. The matrices evaluated were raw cannabis flower, CO_2 and EtOH crude extracts, distillation mother liquors, distillate, and distillation bottoms. This work advances the field of cannabis chemistry in five ways. First, to my knowledge, quantifying 25 cannabinoids in a single HPLC-QQQ method is more than has previously been reported, advancing the field of cannabis research. Second, this method simultaneously measures pesticides and cannabinoids in multiple sample types, addressing a primary concern for the cannabis industry. Third, this method improves the LOD and LOQ of HPLC-DAD methods (neat solvent) by approximately 50-fold.[97–99] Fourth, this method chromatographically resolves Δ8-THC and Δ9-THC, two cannabinoids with high structural similarity but different regulatory statuses. Fifth, this work reports preliminary investigations into the use of extracted hops flower as a calibration matrix.[25]

In an analytical context, the matrix is defined as the analyte and all concomitant species in the sample. Calibration via the external standard method assumes that the same instrument response will be observed in the standards as the sample. An ideal calibration matrix is identical to the analytical matrix, minus analytes. Calibration in solvent, as is reported in this chapter, is not an ideal matrix because it lacks the concomitant species present in an extracted cannabis

sample. Preparation of an ideal cannabis-based calibration matrix was not possible, which motivated investigation into use of hops as a stand-in. Additional injections can be made to eliminate potential interferences from solvent or reagents present in the samples. For example, acetonitrile was used as the sample extraction solvent, so solvent blanks were analyzed at the start of chromatographic sequences to demonstrate non-interference prior to analysis. Reagent blanks, which ideally contain all reagents plus solvent used, were also analyzed to demonstrate non-interference. The reagent blank is not a matrix blank because it doesn't contain the sample matrix.

It should be emphasized that the acetonitrile solvent and the reagent blanks are *not* the matrix. The analytical matrix incorporates all constituents of the sample, which are not present in the reagent or solvent blanks. Under certain other circumstances, the solvent or reagent blank may be considered a matrix. For example, a QC assay method evaluating the purity of a raw material, where the raw material (100% theoretical purity) is dissolved in mobile phase. An external calibration using known amounts of reference material is dissolved in mobile phase and analyzed using the same method as the sample. The matrix in this example is the mobile phase diluent and the analyte and is present in both the standard and sample preparations. A solvent blank composed of mobile phase is an ideal matrix blank because it contains all concomitant species besides the analyte. For the purpose of work described in this dissertation, however, an analogous blank would be a solvent or reagent blank and is not congruent with the sample matrix.

An alternative to external standard calibration in the absence of an ideal matrix blank is to use the standard addition method. Standard addition evaluates changes in instrument response according to addition of known amounts of standard to the sample matrix. This approach

eliminates the need for preparation of an ideal matrix blank. Standard addition calibration was not used in the scope of work reported in this dissertation because I wanted to build stepwise from external calibration methods I'd found reported in the literature. The body of data reported in this chapter does not support the use of an external calibration prepared in solvent or reagent blank matrices, and future experiments should be undertaken to incorporate standard addition calibration into the method.

HPLC methods to quantify cannabinoids and pesticides have been reported in the literature using a variety of detectors. Tandem mass spectrometry is preferable over diode array detection (DAD) to the higher selectivity and sensitivity of the detector.[22] DAD methods operate on the basis of light absorption or refraction through the mobile phase and have limits of quantitation (LOQ) on the order of 500 ng/mL.[97,100,101] QQQ first selects only those species of a pre-programed mass-to-charge ratio at a given retention time, then counts the number of product ions produced following collision with high-energy N_2.[67] The product ion spectrum occurs in predictable ratios and allows for secondary qualitative identification of detected analytes. This is particularly useful for analyzing groups of cannabinoids with the same precursor masses, which have different product ion spectra. QQQ has the advantage of resolving coeluting analytes with different precursor mass-to-charge ratios, resulting in a greater detection specificity over DAD and RI methods. The method LOQ is lower in QQQ methods compared to light-based methods because only those species with pre-programmed mass transitions reach the detector, resulting in a lower signal-to-noise ratio. The LOQ of the present method in ACN is 10 ng/mL, which is a

50-fold sensitivity increase over DAD methods.[97,100,101] Representative LOQs of other QQQ methods reported 0.1-1 ng/mL.[102,103]

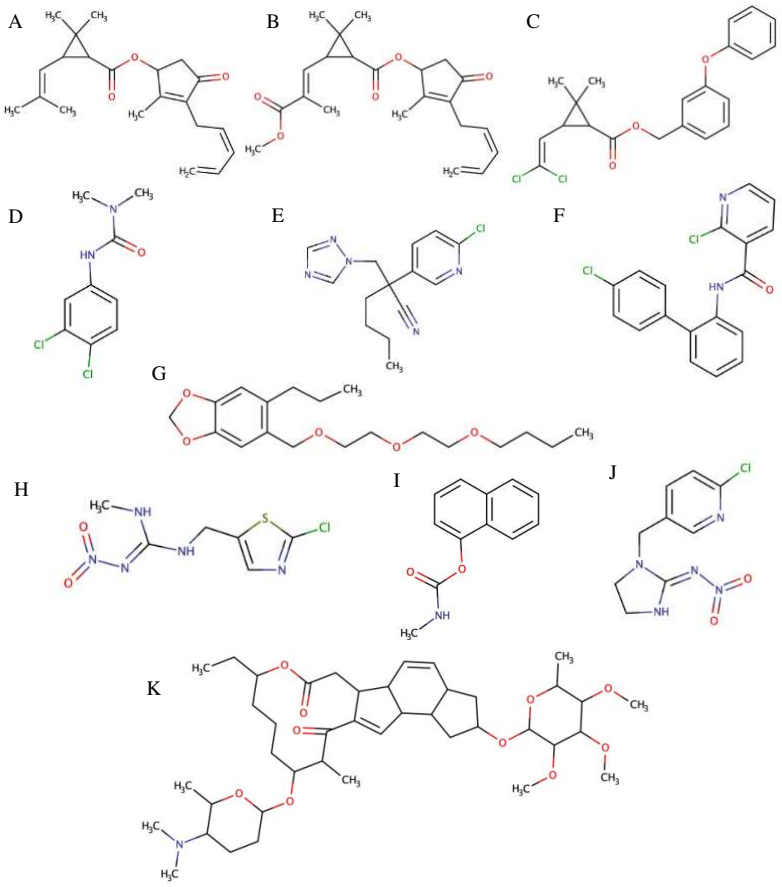

Figure 2.2.2: Structures of pesticides investigated for the present HPLC-QQQ method. A) pyrethrin I, B) pyrethrin II, C) permethrin, D) diuron, E) myclobutanil, F) boscalid, G) piperonyl butoxide, H) clothianidin, I carbaryl), J) imidacloprid, K) Spinosad A.

Cannabinoids Δ8- and Δ9-THC produce similar psychotropic effects in the body but have different regulatory statuses.[104] Chromatographic resolution of the two cannabinoids is made difficult by their high structural similarity. Coelution of Δ8-and Δ9-THC skews quantitation of schedule I Δ9-THC high. The present instrument method was able to resolve Δ8- and Δ9-THC across all six calibration levels, facilitating quantitation of each.

A key challenge of developing this method was that the cannabis matrix is notoriously complex and can interfere with detector sensitivity. Previous methods have sought to work

around this problem by preparing calibration levels in neat solvent, then applying the calibration to samples. This technique has the advantage of high analyte linearity but the disadvantage of not taking matrix interference into consideration. Mass spectra of extracted cannabis samples are inherently noisier than spectra in neat solvent, which can lead to integration errors and increase the LOD/LOQ. I have collected preliminary data spiking all 34 analytes into extracted *Humulus lupulus L.* (common hops) with the goal of validating a suitable calibration matrix. Hops were selected for their close taxonomic relation to cannabis – both belong to the *Cannabaceae* family – and because they do not produce of cannabinoids.[105,106] In this report, spike/recovery values are reported for hops calibration levels. Although this approach may limit instrumental error from matrix inferences, additional work is needed before validation can be completed. An alternative approach would be to use internal standards. The use of phenanthrene, isoprocarb, and deuterated cannabinoid standards has been reported in the literature.[102,107–109]

Samples used in this study represented a variety of industrial cannabis sample types: raw flower, crude CO_2 extract, crude EtOH extract, distillate, distillation mother liquor, and distillation bottoms. Following literature precedent, I applied the neat calibration method to extracted cannabis samples for quantification.[100] An ongoing challenge of this method is that assay values of both the low- and high-abundance cannabinoids have poor reproducibility. This is likely due to integration errors caused by matrix interference and indicates that a more robust calibration method than using only neat solvent alone is needed. The cannabinoid profiles of each of these sample types were unique and the concentrations of some cannabinoids occurred in much higher abundance than others. To account for this difference, analytical samples were prepared with two dilution schemes and high- and low-abundance cannabinoids detected separately. The high-abundance method looked specifically at CBD, CBDA, CBG, CBGA, Δ9-

THC, and CBGVA. It was unexpected that Δ9-THC should be detected in high quantities in hemp-type cannabis, but it was added to the high-abundance method following preliminary experiments. The low-abundance method evaluated all other analytes.

2.3 Materials and methods

2.3.1 Materials

LC-MS grade acetonitrile (PN: A955-4) and LC-MS grade formic acid (PN: A117-50) were purchased from Fisher Scientific. A Sigma Millipore Direct-Q 5 water filtration system was used to deliver 18.0 mΩ•cm water.

Reference materials of Δ8-tetrahydrocannabinol (Δ8-THC; PN: ISO60158), Δ9-tetrahydrocannabinol (Δ9-THC, PN: ISO60157), Δ9-Tetrahydrocannabinolic acid (Δ9-THCA; PN: 33448), Δ9-tetrahydrocannabutol (Δ9-THCB; PN: 33078), Δ9-tetrahydrocannabihexol (Δ9-THCH; PN: 33352), Δ9-tetrahydrocannabiphorol (Δ9-THCP; PN: 30171), Δ9-tetrahydrocannabivarin (Δ9-THCV; PN: 18091), Δ9-tetrahydrocannabivarinic acid (Δ9-THCVA; PN: 21259), 7-OH-cannabidiol (7-OH-CBD; PN: 36517), cannabichromene (CBC; PN: 26252), cannabichromeorcin (CBCO; PN: 21742), cannabichromevarin (CBCV; PN: 21974), cannabichromevarinic acid (CBCVA; PN: 32718), cannabidiol (CBD; PN: 21259), cannabidiolic acid (CBDA; PN: 18090), cannabidiolic acid methyl ester (CBDA-ME; PN: 28347), cannabidiphorol (CBDP; PN: 30169), cannabidivarin (CBDV; PN: 20165), cannabielsoin (CBE; PN: 21092), cannabigerol (CBG, PN: 20164), cannabigerolic acid (CBGA PN: 20019), cannabigerol quinone acid (CBGAQ, PN: 31772), cannabigerovarin (CBGV PN: 29117), cannabigerovarinic acid (CBGVA; PN: 25469), cannabicyclol (CBL; PN: 22036), cannabinol

(CBN; PN: 25495), and cannabicitran (CBT; PN: 21295) were purchased from Cayman Chemical.

Cascade hops (PN: HCASW1LB) were purchased from MoreFlavor!, Inc. Cannabis samples used were acquired from Panacea Life Sciences between November 2020 and January 2022. Cannabis flower, hops, and cannabis samples were stored at 5 °C.

2.3.2 Instrument Methods

An Agilent 1290 Infinity II ultra-high performance liquid chromatograph coupled with Agilent 6460 triple quadrupole mass spectrometer with a Jetstream electrospray ionization source (ESI-HPLC-QQQ) was used. Agilent Masshunter Acquisition software was used for data collection, and Agilent Masshunter Quantitation was used for data analysis. Ion transitions and detector parameters were optimized using Agilent Optimizer software and reported in table 2.2.1.

LC separations were performed on an Agilent Poroshell 120 C18-EC (PN: 695975-902) column, with a flow rate of 0.75 mL/min. The column temperature was 50 °C. The autosampler temperature was set at 5 °C. Mobile phase A (MPA) was 0.1 % formic acid in 18.0 mΩ•cm water. Mobile phase B (MPB) was 0.1% formic acid in acetonitrile. The gradient used was 0 min, 60 % MPB; 1 min, 60 % MPB; 8 min, 80 % MPB; 13 min, 100 % MPB; 15 min, 100 % MPB; 15.01 min, 60 % MPB. The total injection runtime was 17.5 min. Separation was performed using a 100 x 4.6 mm Agilent Poroshell 120 EC-C18 column, with particle size 2.7 µm. Data was quantified in this chapter as integrated peak area of each analyte. Units of measurement were counts*time. Samples were quantified using an external calibration of standards dissolved in acetonitrile. Standard preparation is described in section 2.3.4.

A pre-injection program was used to eliminate sample carryover. The program drew 6 µL methanol (MeOH) into the injection needle, which was then ejected to waste. The MeOH rinse was repeated three times. The program drew 6 µL isopropanol (IPA) into the injection needle, which was then ejected to waste. The IPA rinse was repeated three times. Then, 6 µL ACN was drawn into the injection needle and ejected to waste. ACN rinse was repeated three times. Residual solvent was removed from the injection needle by drawing 12 µL air and then ejecting to waste. All rinse steps were repeated three times in sequence, drawing up at default speed and ejecting at maximum speed. Once the pre-injection program was completed, 2 µL of sample were drawn up, and the needle rinsed with LCMS-grade MeOH for 3 seconds prior to injection.

The ion source was an Agilent Jet Stream Electrospray Ionizer, with a cycle time of 1000 ms in the MRM mode. All measurements were made in the positive ion mode. The gas flow rate was 13 L/min at a temperature of 250 °C. Nebulizer pressure was 30 psi. The sheath gas flow rate was 11 L/min at a temperature of 305 °C. The detector passed a check tune each day prior to analysis.

Due to differences in observed relative abundances of cannabinoids in samples, two instrument methods were needed for high- and low-abundance cannabinoids. The high-abundance method detected CBD, CBDA, CBG, Δ9-THC, CBGA, and CBGVA. The low abundance method detected all other analytes. Calibration levels, low-abundance samples, and high-abundance samples were bracketed by ACN blanks.

2.3.3 Experimental systems

The work described in this chapter includes three systems. The first is described in sections 2.4.1-2.4.2 and is comprised of commercially available standards dissolved in acetonitrile. Standard preparations are described in section 2.3.4. The second system is described in section 2.4.3. System two is comprised of standards in acetonitrile as well as six cannabis processing matrices extracted in acetonitrile: raw flower, CO_2 and EtOH crude extracts, distillate, distillation mother liquor, and distillation bottoms. Sample preparations are described in sections 2.3.5. The second system was quantified using the calibration produced by measurements of the first system. The third system is described in section 2.4.4 and is comprised of common hops flower extracted in acetonitrile, spiked with aliquots of standards in ACN. Sample preparation for the third system is reported in section 2.3.6.

2.3.4 Standard preparation

Certified reference materials were quantitatively transferred to 10.0 mL class A volumetric glassware and brought to volume with acetonitrile. For reference materials in solution, the lab temperature at time of transfer was recorded, and concentrations of the standard solutions were calculated taking CRM solvent (MeOH or ACN) density into consideration. Individual standards were transferred to scintillation vials and stored at -20 °C.

A stock standard was prepared by combining individual standards of all analytes and brought to 10.0 mL final volume, such that the final concentration of each analyte was 2 µg/mL. The strategy of preparing a stock standard with uniform analyte concentration was selected to limit dilution biases in the stock.

Six calibration levels were prepared by serial dilution of the stock in ACN. Level concentrations were from 10 – 2000 ng/mL for all analytes except carbaryl. Carbaryl response was past the limit of linearity at 2000 ng/mL, and thus level six was excluded for that analyte. The calibration curve was run in triplicate and the average measurement per calibrant level (n=3) was used. The purpose of this calibration method was to normalize instrumental variation. The fit of all calibrants had $R^2 \geq 0.999$ or greater.

2.3.5 Sample preparation

Samples were prepared in 50 mL falcon tubes and placed as near the tube bottom as possible. Sample masses used were as follows: 190 ± 10 mg for flower and hops; 80 ± 10 mg for crude extracts, distillate, mother liquor, and distillation bottoms. 10 mL ACN and a ceramic homogenizer were then added to the tubes. Tubes were capped and vortexed at 3000 RPM for 60 seconds each. Samples were allowed to sit on the benchtop for 30 minutes, vortexed for 60 seconds, then left on the benchtop for another 30 minutes (60 minutes total). Next, 10 mL water and 6.5 g QuECHERS salts were added. Tubes were capped and vortexed at 3000 RPM for 60 seconds each, followed immediately by centrifugation at 2500 RPM for 5 minutes. The top (ACN) layer was decanted off and filtered through 0.2 µm PTFE into 1.5 mL HPLC vials, and stored at 5 °C.

The sample filtrate was diluted in ACN to prepare analytical samples. Low-abundance samples were diluted 1/100. High-abundance samples were then prepared by 1/40 serial dilution to produce a total dilution of 1/4000. Samples were prepared in triplicate, and results are reported as the average ± relative standard deviation. A representative photo of extracted samples is shown in figure 2.3.1.

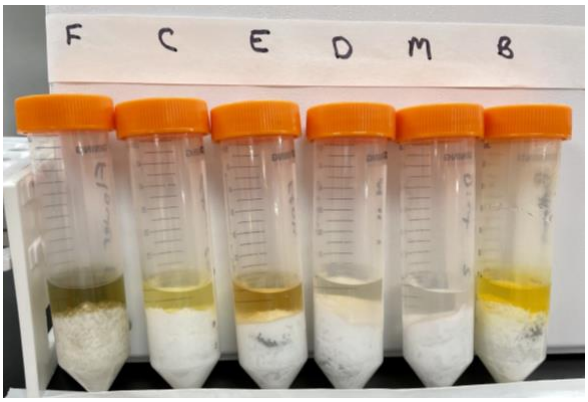

Figure 2.3.1: Representative image showing extracted samples. The top (ACN) layer was sampled for analysis and the bottom (aqueous, salts) layer was discarded. F) raw flower; C) CO_2 crude; E) EtOH crude; D) distillate; M) distillation mother liquor; B) distillation bottoms.

2.3.6 Calibration spikes in hops

A mass of 190 ± 10 mg hops was transferred to a 50 mL falcon tube and placed as near the tube bottom as possible. Then 10 mL ACN and a ceramic homogenizer were added. The tube was capped and vortexed at 3000 RPM for 60 seconds. Sample was allowed to sit on the benchtop for 30 minutes, vortexed for 60 seconds, then left on the benchtop for another 30 minutes (60 minutes total). Next, 10 mL water and 6.5 g QuECHERS salts were added. The tube was capped and vortexed at 3000 RPM for 60 seconds each, followed immediately by centrifugation at 2500 RPM for 5 minutes. The top (ACN) layer was decanted off, and filtered through 0.2 µm PTFE into 1.5 mL HPLC vials, and stored at 5 °C.

An intermediate hops stock was prepared by diluting the sample filtrate 1:9 in ACN. All 34 analytes plus intermediate stock were added to an HPLC vial then diluted in ACN such that the final analyte concentration was approximately 1900 ng/mL and the hops matrix present in a 1:99 ratio with ACN. This was the working standard. Subsequent levels were prepared by serial dilution of the working standard with ACN.

Table *2.2.1*: Detection parameters for cannabinoids and pesticides analyzed in this study. Includes quantifier and qualifying transitions, fragmentation voltage, cell energy, cell acceleration voltage, retention times. All measurements were made in the positive mode. Quantifying transitions are represented with bold text. Qualifying peak acceptability was set at ± 20% optimized values.

Name	Precursor Ion	Product Ion	Fragmentation Voltage (V)	Collision Energy (V)	Cell Accel. Voltage (V)	Retention Time (min)	ISTD?
7-OH-CBD	**331.2**	**105.1**	**78**	**42**	**4**	**3.52**	**No**
7-OH-CBD	331.2	77.1	78	94	4	3.52	No
Boscalid	**343**	**271.1**	**123**	**38**	**4**	**3.59**	**No**
Boscalid	343	112	123	54	4	3.59	No
Carbaryl	**202.1**	**127.1**	**75**	**30**	**4**	**2.27**	**No**
Carbaryl	202.1	115.1	75	46	4	2.27	No
CBC	**315.2**	**193.1**	**108**	**30**	**4**	**12.83**	**No**
CBC	315.2	123.1	108	30	4	12.83	No
CBC	315.2	81.1	108	30	4	12.83	No
CBCO	**259.2**	**137**	**72**	**30**	**4**	**7.1**	**No**
CBCO	259.2	69.2	72	30	4	7.1	No
CBCVA	**331.2**	**191**	**87**	**30**	**4**	**9.9**	**No**
CBCVA	331.2	69.1	87	38	4	9.9	No
CBD	**315.2**	**193.1**	**111**	**24**	**4**	**8.01**	**No**
CBD	315.2	123.1	111	40	4	8.01	No
CBDA	**359.2**	**341.2**	**81**	**30**	**4**	**7.2**	**No**
CBDA	359.2	219.1	81	38	4	7.2	No
CBDA-ME	**373.2**	**341.2**	**84**	**30**	**4**	**11.6**	**No**
CBDA-ME	373.2	219.1	84	38	4	11.6	No
CBDP	**343.3**	**123.1**	**129**	**42**	**4**	**10.2**	**No**
CBDP	343.3	91.1	129	66	4	10.2	No

Table 2.2.1 (continued)

Name	Precursor Ion	Product Ion	Fragmentation Voltage (V)	Collision Energy (V)	Cell Accel. Voltage (V)	Retention Time (min)	ISTD?
CBDV	**287.2**	**165.1**	**96**	**30**	**4**	**5.96**	**No**
CBDV	287.2	77.1	96	86	4	5.96	No
CBE	**331.2**	**135.1**	**105**	**26**	**4**	**6.97**	**No**
CBE	331.2	109.1	105	22	4	6.97	No
CBG	**317.2**	**193.1**	**84**	**30**	**4**	**7.78**	**No**
CBG	317.2	123.1	84	38	4	7.78	No
CBGA	**361.2**	**219.1**	**78**	**30**	**4**	**7.46**	**No**
CBGA	361.2	149	78	46	4	7.46	No
CBGQA	**375.2**	**235.1**	**93**	**22**	**4**	**6.42**	**No**
CBGQA	375.2	81.1	93	50	4	6.42	No
CBGV	**289.2**	**165.1**	**87**	**30**	**4**	**5.93**	**No**
CBGV	289.2	123.1	87	34	4	5.93	No
CBGVA	**333.2**	**191**	**75**	**30**	**4**	**5.89**	**No**
CBGVA	333.2	91.1	75	70	4	5.89	No
CBN	**311.2**	**293.2**	**138**	**16**	**4**	**9.58**	**No**
CBN	311.2	223.1	138	20	4	9.58	No
CBTC	**315.2**	**193.1**	**135**	**30**	**4**	**11.3**	**No**
CBTC	315.2	123.1	135	42	4	11.3	No
Clothianidin	**250**	**132**	**78**	**22**	**4**	**1.5**	**No**
Clothianidin	250	113	78	30	4	1.5	No
Clothianidin	250	110.1	78	30	4	1.5	No
Δ8-THC	**315.2**	**123**	**99**	**38**	**4**	**10.49**	**No**
Δ8-THC	315.2	77.1	99	82	4	10.49	No

Table 2.2.1 (continued)

Name	Precursor Ion	Product Ion	Fragmentation Voltage (V)	Collision Energy (V)	Cell Accel. Voltage (V)	Retention Time (min)	ISTD?
Δ9-THC	**315.2**	**123.1**	**117**	**40**	**4**	**10.64**	**No**
Δ9-THC	315.2	193.1	117	24	4	10.64	No
Δ9-THC	315.2	93.1	117	28	4	10.64	No
Δ9-THCA	**359.2**	**341.1**	**69**	**30**	**4**	**11.47**	**No**
Δ9-THCA	359.2	219	69	38	4	11.47	No
Δ9-THCB	**301.2**	**179.1**	**78**	**30**	**4**	**9.35**	**No**
Δ9-THCB	301.2	123	78	38	4	9.35	No
Δ9-THCH	**329.2**	**123**	**129**	**42**	**4**	**11.5**	**No**
Δ9-THCH	329.2	77.1	129	82	4	11.5	No
Δ9-THCP	**343.3**	**123**	**90**	**38**	**4**	**12.4**	**No**
Δ9-THCP	343.3	77.1	90	90	4	12.4	No
Δ9-THCV	**287.2**	**165**	**117**	**30**	**4**	**8.11**	**No**
Δ9-THCV	287.2	123.1	117	38	4	8.11	No
Δ9-THCV	287.2	77.1	117	82	4	8.11	No
Δ9-THCVA	**331.2**	**313.1**	**75**	**30**	**4**	**9.24**	**No**
Δ9-THCVA	331.2	191	75	34	4	9.24	No
Diuron	**233**	**160**	**87**	**30**	**4**	**2.4**	**No**
Diuron	233	74.1	87	98	4	2.4	No
Diuron	233	72.1	87	30	4	2.4	No
Imidacloprid	**256.1**	**209**	**81**	**30**	**4**	**1.5**	**No**
Imidacloprid	256.1	175.1	81	30	4	1.5	No
Imidacloprid	256.1	78.1	81	74	4	1.5	No

Table 2.2.1 (continued)

Name	Precursor Ion	Product Ion	Fragmentation Voltage (V)	Collision Energy (V)	Cell Accel. Voltage (V)	Retention Time (min)	ISTD?
Myclobutanil	**289.1**	**125**	**102**	**42**	**4**	**3.3**	**No**
Myclobutanil	289.1	89.1	102	82	4	3.3	No
Myclobutanil	289.1	70.1	102	30	4	3.3	No
Pyrethrin I	**329.2**	**128.1**	**84**	**42**	**4**	**9.3**	**No**
Pyrethrin I	329.2	105.1	84	38	4	9.3	No
Pyrethrin I	329.2	77.1	84	70	4	9.3	No
Pyrethrin II	**373.2**	**105.1**	**90**	**46**	**4**	**11.7**	**No**
Pyrethrin II	373.2	91.1	90	78	4	11.7	No
Pyrethrin II	373.2	77.2	90	90	4	11.7	No
Spinosad	**732.5**	**142.1**	**162**	**30**	**4**	**2.2**	**No**
Spinosad	732.5	98.1	162	90	4	2.2	No

2.4 Results and discussion

2.4.1 Method development

Analyte specificity was established through both chromatographic and mass spectrometric detection. Most analytes in this study have different precursor ion masses and can be resolved by the QQQ detector, but some sets of cannabinoids sharing the same precursor mass had similar transitions and required separation with HPLC prior to detection. Table 2.4.1 shows the retention times of each analyte. The first set with the same precursor mass consisted of CBC, CBD, Δ8-THC, Δ9-THC, and CBTC; all have precursor ions of 315.2 m/z and transition to 193.1 and 123.1 m/z. Individual standard injections were necessary to identify retention times for these cannabinoids, and reproducible baseline resolution was paramount for reliable quantitation. This was particularly important for Δ8-THC and Δ9-THC due to their high structural similarity and similar retention times. The second set of analytes with identical precursor ions was 7-OH-CBD, CBCVA, CBE, and Δ9-THCVA with an initial mass-to-charge ratio of 331.2 m/z. However, each of the analytes in the second set had at least one unique product ion and retention times, which lead to simpler chromatography. The third set consisted of Δ9-THCH and pyrethrin I, which had precursor mass-to-charge ratios of 329.2 m/z, however these two analytes had unique mass transitions. The fourth set was Δ9-THCP and CBDPA, which have precursor ion mass-to-charge ratios of 343.3 m/z. The fifth set was Δ9-THCA and CBDA, which have precursor ion mass-to-charge ratios of 359.2 m/z. Baseline resolution was also paramount for sets four and five due to the high structural similarity of the analytes and the fact that there were no unique mass transitions. Finally, CBDA-ME and pyrethrin II both had initial mass-to-charge ratios of 373.2 m/z but had unique product ions. Ion transitions and detector parameters for each

cannabinoid and pesticide are reported in Table 2.2.1. For all analytes, qualifying peak acceptability was set at ± 20% optimized values.

Table 2.4.1: Retention times of cannabinoids and pesticides detected in the present method, organized alphabetically and by retention time.

	Analyte (Alphabetically)	*Retention Time (min)*	*Analyte (Elution order)*	*Retention Time (min)*
1	Δ8-THC	10.49	Clothianidin	1.5
2	Δ9-THC	10.64	Imidacloprid	1.5
3	Δ9-THCA	11.47	Spinosad	2.2
4	Δ9-THCB	9.35	Carbaryl	2.27
5	Δ9-THCH	11.5	Diuron	2.4
6	Δ9-THCP	12.4	Myclobutanil	3.3
7	Δ9-THCV	8.11	7-OH-CBD	3.52
8	Δ9-THCVA	9.24	Boscalid	3.59
9	7-OH-CBD	3.52	CBGVA	5.89
10	Boscalid	3.59	CBGV	5.93
11	Carbaryl	2.27	CBDV	5.96
12	CBC	12.83	CBGAQ	6.42
13	CBCO	7.1	CBE	6.97
14	CBCVA	9.9	CBCO	7.1
15	CBD	8.01	CBDA	7.2
16	CBDA	7.2	CBGA	7.46
17	CBDA-ME	11.6	CBG	7.78
18	CBDP	10.2	CBD	8.01
19	CBDV	5.96	Δ9-THCV	8.11
20	CBE	6.97	Δ9-THCVA	9.24
21	CBG	7.78	Pyrethrin I	9.3
22	CBGA	7.46	Δ9-THCB	9.35
23	CBGAQ	6.42	CBN	9.58
24	CBGV	5.93	CBCVA	9.9
25	CBGVA	5.89	CBDP	10.2
26	CBN	9.58	Δ8-THC	10.49
27	CBTC	11.3	Δ9-THC	10.64
28	Clothianidin	1.5	CBTC	11.3
29	Diuron	2.4	Δ9-THCA	11.47

Table 2.4.1 (*cont'd*):

	Analyte (Alphabetically)	*Retention Time (min)*	*Analyte (Elution order)*	*Retention Time (min)*
30	Imidacloprid	1.5	Δ9-THCH	11.5
31	Myclobutanil	3.3	CBDA-ME	11.6
32	Pyrethrin I	9.3	Pyrethrin II	11.7
33	Pyrethrin II	11.7	Δ9-THCP	12.4
34	Spinosad	2.2	CBC	12.83

The method sensitivity in neat solvent was demonstrated between 10 – 2000 ng/mL. The LOQ was estimated around 9-10 ng/mL, and the LOD was estimated around 3 ng/mL. Additionally, a quality control standard (calibration level 4 in neat solution) bracketed sample analyses every 12 injections, followed by an ACN blank. The method sensitivities for standards in neat solution and samples were slightly different due to matrix interference in the cannabis samples. The complex nature of cannabis matrix that persisted after sample clean up and dilutions ≥ 100x caused noisy baselines that impacted quantitative-qualitative transition ratios. Additional sample preparation, such as clarification with solid-phase extraction prior to analysis could reduce the signal-to-noise ratios observed. Additional experiments are necessary to identify the specific interfering species concomitant in the sample matrices, but potential targets are chlorophylls, proteins, nucleic acids, carotenoids, flavonoids, sesquiterpenes, or cholesterols which may not be completely extracted into the aqueous phase during QuECHERS sample prep. Sample preparation parameters are reported in section 2.3.4-2.3.5.

One cannabinoid and two pesticides were ruled out during method detection due to difficulties during optimization and calibration. Cannabicyclol (CBL), piperonyl butoxide, and permethrin could not be optimized in the positive mode and were excluded from study. This was possibly due to the ability of these analytes to accept charge during electrospray ionization,

preventing them from being drawn into the detector. McRae (2020) reported analysis of CBL and cannabicyclolic acid (CBLA) in the positive mode, but this result was not reproducible in this system.

2.4.2 Cannabinoid and pesticide resolution

Δ8-THC and Δ9-THC are structurally identical with exception of the direction of the double bond in the non-aromatic six-member ring from the geranyl motif. Resolution of these two species is of interest to the broader community largely due to regulatory considerations. Both molecules are psychoactive and produce the recreational high associated with cannabis use, however Δ9-THC has strict limits to potency. The two analytes have identical qualifying peak transitions, which prevents their resolution in the mass detector. Under the method conditions presented in this Chapter, Δ8-THC and Δ9-THC are chromatically resolved and have retention times differing by 0.32 minutes. A representative chromatogram with resolution of 1.6 is shown in Figure 2.4.3. Calibrants in neat solution for these two species were baseline resolved, however it was observed that they coeluted during sample analyses. It is expected that this was the result of matrix interferences in the sample; however, the exact interferents have not been identified.

The quantitative-qualitative mass transition ratio of CBGVA in neat solvent was 11.3. It was not detected in ACN blank. A small signal was detected for the 333.2 to 191.0 m/z transition at 5.79 min in the hops extract but with a qualifier ratio of 238.1. Signal counts of the quantifying transition did not surpass the qualifying transition signal baseline, and this measurement occurs very near the theoretical local LOD. CBGVA signal differences between ACN and hops blanks

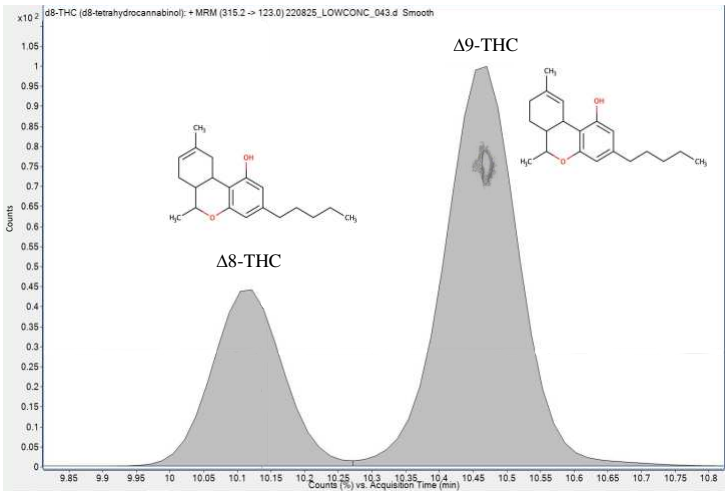

Figure 2.4.3: Representative chromatogram showing Δ8- and Δ9-THC peaks with resolution of 1.6. The two cannabinoids are difficult to resolve chromatographically due to their high structural similarity.

are representative of the noise introduced by the hops extraction matrix to the method and indicate the need for further optimization in sample clean up. The calibration in neat solvent will have a lower LOD/LOQ than one prepared in a more complex matrix like extracted sample and could produce false positive measurements and integration errors at low concentrations. The CBGVA signal qualifying ratio in extracted cannabis flower was 3160. Representative chromatograms of CBGVA mass transitions in neat solvent, hops, sample, and ACN blank are shown in Figure 2.4.4.

A measurement with no matrix interference should have the same relative ratio of counts for 333.2 -> 191.0 m/z and 333.2 -> 91.1 m/z mass transitions in ACN vs extracted flower. The representative chromatograms in figures 2.4.4.c and 2.4.4.d instead show an approximately 277-fold increase in the relative 333.2 -> 91.1 m/z abundance. This change is indicative of a matrix interference that is observed as a change in relative abundance in the 333.2 ->91.1 m/z mass transition. The relative increase in 333.2 -> 91.1 m/z could indicate coeluting species that also undergo this mass transition. Functionalization and internal rearrangements are responsible for the diversity of cannabinoid species, and it is possible that unresolved molecules are interfering

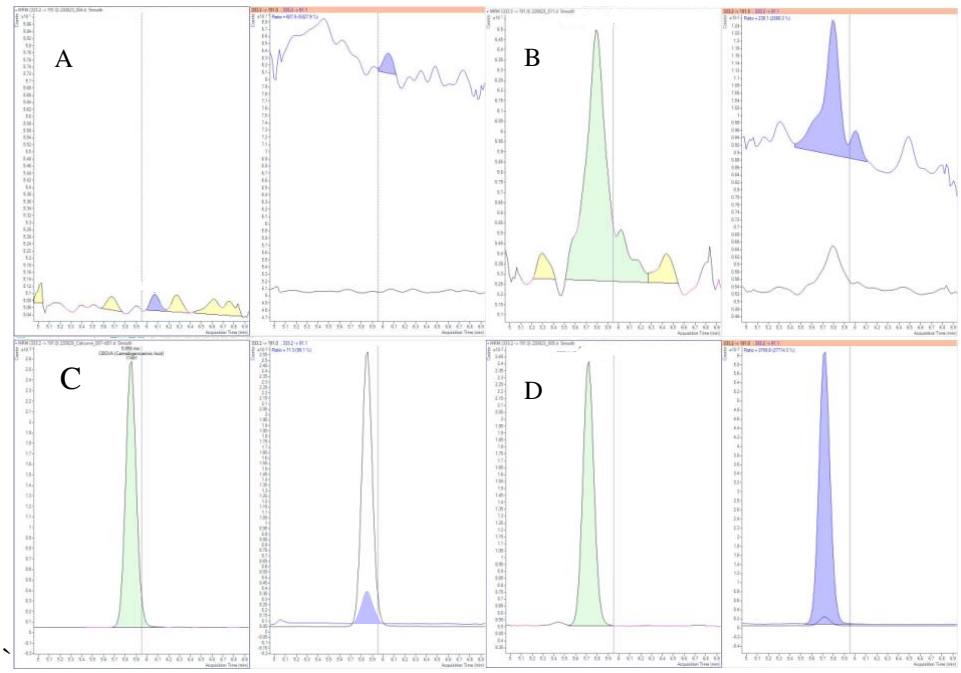

Figure 2.4.4: Representative chromatograms showing quantifying (333.2-> 191.0 m/z; left panes) and qualifying (333.2 -> 91.1 m/z; right panes) mass transitions for CBGVA. Samples: A) ACN solvent blank, B) extracted hops, C) CBGVA in ACN, and D) extracted cannabis flower.

with detection. CBG species occur with similar motifs to CBD and THC but have mass-to-charge ratios 2 Da greater. Similar to how CBD, Δ8-THC, Δ9-THC, CBC, and CBTC have the same precursor and qualifying ion transitions due to structural similarity, it may be the case that interfering sample species coelute with CBGVA and cause false negative qualitative detection.

Unidentified peaks with similar retention times were observed in standards of CBGA and boscalid. In both cases, the two peaks share mass transitions and elute at very similar retention times. It is possible that these minor peaks are isomers of the primary peak. Small rearrangements would produce a molecule with identical precursor mass, different chromatographic resolution, and likely similar mass transitions. In boscalid, the sp^3-hybridized nitrogen is chiral, and thus the eluents may be enantiomers of each other. The two eluents observed in CBGA may indicate structural isomers, in which the geranyl motif is placed in the 5, rather than the 3, position around the aromatic ring in the olivetolic acid motif. For the purpose

of this dissertation, the potential structural isomer will be identified as “CBGA-B”. The structure of “CBGA-B” is unconfirmed at this time. Figure 2.5.5 shows a representative chromatogram and expected structure of CBGA, as well as the hypothesized structure of CBGA-B are presented in Figure 2.4.5.

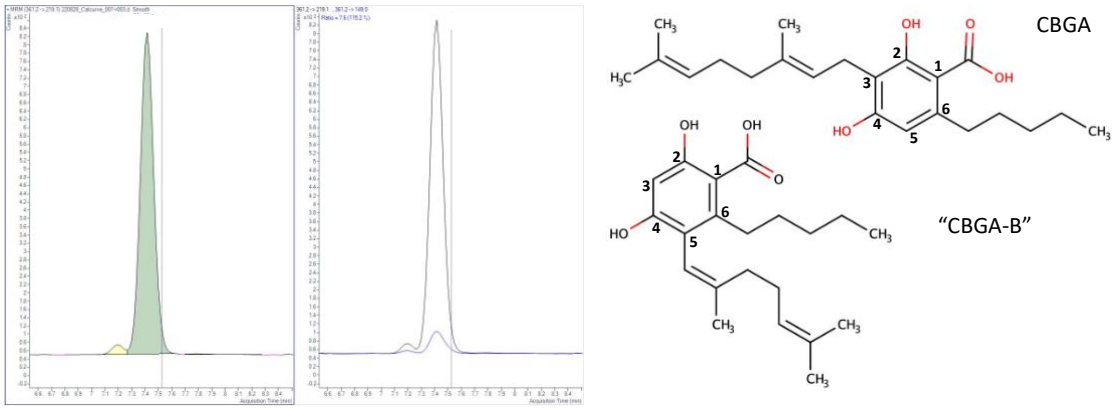

Figure 2.4.5: (Left) representative chromatograms showing quantifying and qualifying peaks of CBGA standard in ACN. (Right, top) structure of CBGA and (right, bottom) a potential structural isomer, “CBGA-B”.

2.4.3 Cannabinoid concentrations in the different matrices

The neat calibration was applied to the six matrix samples, but the measurements are unreliable at the time of submission of this dissertation. This evaluation is based on the average RSDs of all analytes (n = 31) in each matrix. The mean RSDs of each matrix are as follows: bottoms, 106%; CO_2 extract, 97.4%; distillate, 95.9%; EtOH extract, 104.4%; raw flower, 102.3%; mother liquor, 95.0%. This high variability indicates that, despite being highly linear, the calibration in neat solvent does not translate well to sample analysis. The LOD and LOQ of the method in extracted samples is different than that estimated from the neat calibration and is discussed further in section 2.4.4. Additional method development is needed to accurately quantify analytes in these six sample matrices. Dilution-corrected measurements (n = 3) and RSDs for the 25 cannabinoids and 9 pesticides in CO_2 sample are reported in table 2.4.2 and are

representative of the data set. ACN and extracted hops blanks (n = 1) are also presented for comparison. Data for flower, EtOH extract, distillate, mother liquor, and distillation bottoms samples can be found in appendix A. Measurements not detected are reported as ND.

Table 2.4.2: Dilution-corrected assay for cannabinoids and pesticides, detected using the present instrument method. ACN and hops blanks (n = 1), CO_2 sample (n = 3), and CO_2 RSD are presented as representative data. The high sample RSD indicates that these results are not suitable and further optimization is necessary for accurate quantification.

Analyte	*ACN Blank (ng/mL)*	*Hops (ng/mL)*	*CO_2 (ng/mL)*	*CO_2 RSD*
7-OH-CBD	ND	78	2965	125
Boscalid	ND	44	45	7
Carbaryl	ND	ND	OQ	OQ
CBC	ND	1664	11984	135
CBCO	ND	ND	860	133
CBCVA	ND	2144	29	173
CBD	OQ	OQ	7037738	9
CBDA	OQ	OQ	OQ	OQ
CBDA-ME	ND	26	65	101
CBDP	ND	240	247	133
CBDV	ND	46	5962	116
CBE	ND	635	43432	97
CBG	ND	ND	297312	5
CBGA	ND	ND	OQ	OQ
CBGQA	ND	125	691	166
CBGV	ND	3	80	114
CBGVA	ND	214	OQ	OQ
CBN	ND	270	22744	121
CBTC	ND	4351	90005	76
Clothianidin	ND	0	ND	ND
Δ8-THC	ND	117	18371	122
Δ9-THC	ND	511	51684	118
Δ9-THCA	ND	79219	13800	124
Δ9-THCB	ND	82	82	5
Δ9-THCH	ND	9644	930	103
Δ9-THCV	ND	7	219	126
Δ9-THCVA	ND	28	41	141
Diuron	ND	ND	ND	ND
Imidacloprid	ND	ND	ND	ND
Myclobutanil	ND	8	11	24
Pyrethrin I	ND	2089	7045	105

Table 2.4.2 (*cont'd*):

Analyte	ACN Blank (ng/mL)	Hops (ng/mL)	CO2 (ng/mL)	CO2 RSD
Pyrethrin II	ND	122	176	55
Spinosad	ND	ND	ND	ND

Although imprecise, some qualitative observations can be made from the HPLC-QQQ data. Acid-form cannabinoids are observed in the highest concentrations in the raw flower sample. A decrease in acid-form cannabinoids from raw flower to extract to mother liquor/distillate/bottoms is consistent with the expectation that cannabinoids will be decarboxylated with heat. Additional clean-up steps during sample preparation may facilitate less noisy, higher precision measurements. Alternatively, a more suitable calibration matrix may also help eliminate matrix interference of samples. Preliminary investigation into the use of hops flower as calibration matrix is discussed in the following section.

2.4.4 Preliminary study of hops as a calibration matrix

To establish the potential of hops as an external calibration matrix, neat standard was spiked into sample of extracted hops. Figure 2.4.6 shows the percent recoveries of calibration spikes for all analytes at six levels. Detection was negatively affected at low concentrations by noisy baselines. 14/34 analytes were not detected at 18 ng/mL, and 7/34 analytes were not detected at 90 ng/mL. The RSD of all measurements (n = 196) was 709, and of analytes detected at 90 ng/mL and greater (n = 165) was 137. Level 1 in Figure 2.4.6 is un-spiked extracted hops sample. Despite high RSDs, all analytes had $R^2 \geq 0.999$ except CBGQA (0.998), CBTC (0.997), and clothianidin (0.996). Further optimization is necessary prior to suitable use of hops as an external calibration matrix.

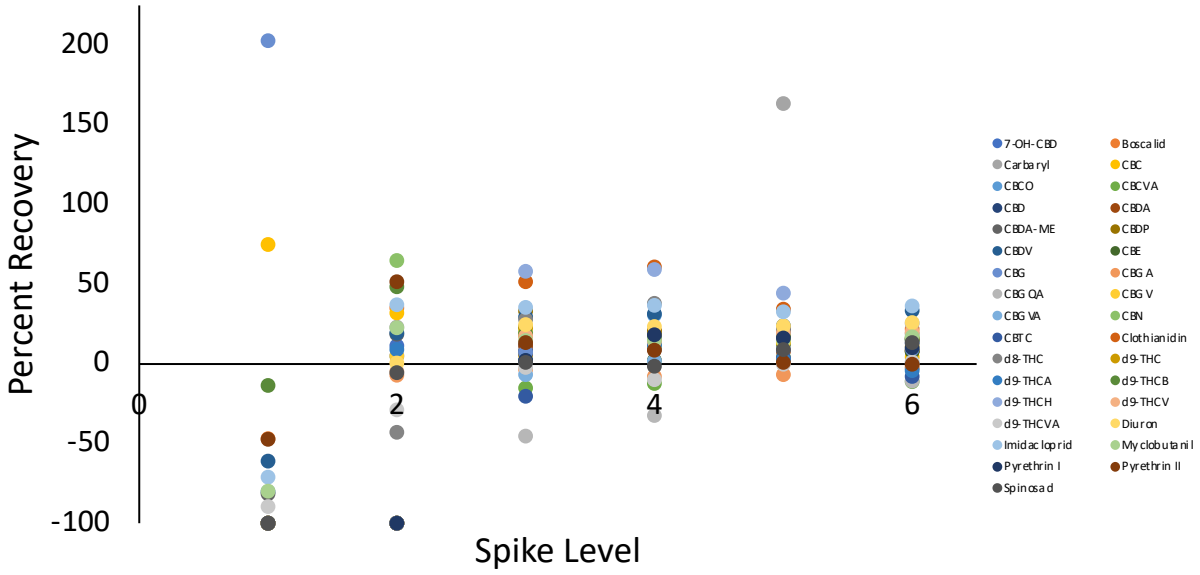

Figure 2.4.6: Percent recoveries of 25 cannabinoids and 7 pesticides spiked into extracted hops flower (levels 2-6), and hops matrix blank (level 1).

The LOD/LOQ of the method in extracted samples can be estimated using the above spiking data and is not the same for all analytes. 20/34 analytes were detected at 18 ng/mL, and their LOQs can be estimated around 60 ng/mL. 7 more analytes were detected at 90 ng/mL, and their LOQs can be estimated around 300 ng/mL. The remaining 7 analytes were detected between 90-180 ng/mL, and their LOQs can be estimated around 600 ng/mL. For reasons already discussed in this chapter, these sensitivities are above an order of magnitude greater than desired for a HPLC-QQQ method. External calibration in neat solvent or extracted hops may be less functional than calibration using standard addition.

2.5 Conclusions

The present method was demonstrated to have high reproducibility and linearity for cannabinoids and pesticides in neat solvent. A key success of the method was the resolution of Δ8- and Δ9-THC. It was observed that the qualifier transition for CBGVA increased by a factor of 280 between neat solvent and sample, indicating matrix interference from the sample.

Additionally, a side peak was observed in the CBGA neat standard and hypothesized to be a structural isomer, which for the purpose of this dissertation has been identified as “CBGA-B”. The structure of “CBGA-B” is unconfirmed at this time. The neat calibration was applied to six matrix samples: raw flower, CO_2 and EtOH extract, mother liquor, distillate, and distillation bottoms, and the measurements were unsuitable due to high RSDs. Extracted hops flower was investigated as a potentially suitable matrix blank but detection was significantly affected at low concentrations by noisy baselines. Calibration sensitivity may be greatly improved by the use of a standard addition calibration rather than external standard prepared in either ACN or extracted hops.

CHAPTER 3 – EVALUATION OF ADSORPTION-ACCESSIBLE SURFACE AREA OF MIL-53(Al) USING CANNABINOIDS IN A CLOSED SYSTEM[2]

3.1 Summary

Cannabinoids are important industrial analytes commonly assayed with High Pressure Liquid Chromatography (HPLC). The purpose of this study was to evaluate the suitability of MIL-53(Al), a commercially available MOF as a stationary phase for cannabinoid separations. The suitability of a MOF for a given separation is hypothesized to be limited by the ability of a given molecule to enter the pore of the MOF. To evaluate the extent of possible adsorptive interactions between cannabinoids and the interior surface area of MIL-53(Al), the Radii of Gyration (R_g) and Solvent Accessible Surface Areas (SASAs) were calculated for three cannabinoids: cannabidiol (CBD), cannabinol (CBN), and Δ9-tetrahydrocannabinol (THC), as well as the MOF. These values were used to calculate the theoretical adsorption capacity of the MOF, using four competing adsorption models. The R_g of cannabinoids (4.1 Å) is larger than one MOF pore aperture dimension (4.0 x 5.0 Å). The adsorption capacity was measured by relating a decrease in cannabinoid concentration in acetonitrile when exposed to 100 mg MOF. Cannabinoid uptake by the MOF was estimated using the relative standard deviation (RSD) of the soaking solution assay, as the Decomposition-Corrected RSD as Uptake (DCRU). The

---

[2] This dissertation chapter was adapted with permission from Cuchiaro, H.; DeRoo, J.; Thai, J.; Reynolds, M. M. Evaluation of Adsorption-Accessible Surface Area of MIL-53(Al) using Cannabinoids in a Closed System. *ACS Appl. Mater. and Interfaces.* **2022**, 14, *10*, 12836 - 12844. Copyright 2022 American Chemical Society. This work was supported by the Panacea Life Sciences Cannabinoid Research Center at Colorado State University. Thank you to Jacob DeRoo for help modeling the MOF framework and performing computational experiments. Thank you to Jon Thai for help with collecting scanning electron microscope images.

DCRU was calculated as 0.007 ± 0.004 $\mu g_{cannabinoids}/mg_{MOF}$. These findings indicate that most of the MOF surface area was inaccessible for adsorption by cannabinoids due to size-exclusion effects. The implication of this work is that the suitability of a MOF for adsorptive separations, such as liquid chromatography, must have an upper limit for size of the analyte. Additionally, MOFs may generally be more suitable for separations in the gas phase, where adsorbates are not hindered by the presence of a solvation shell.

3.2 Introduction

The Cannabis (hemp) plant is an important industrial crop that contains a range of useful phytomolecules known as cannabinoids.[26,94,110–112] Cannabinoids are a class of small molecules that require separation from the plant biomass for use; notably, CBD, THC, and CBN (Figure 1).[1113–115] Standard assay methods use High Pressure Liquid Chromatography (HPLC) to separate and quantify cannabinoids from plant sources in acidic conditions.[116] Distinction between drug-type and fiber-type cannabis are classified based on the amount of THC. Drug-type Cannabis has greater than 0.3% THC on a dry weight basis, and fiber-type tends to have a higher CBD content on the dry weight basis. [31,94] CBN is the oxidative decay product of THC. [94,117] The structures of THC, CBD, and CBN are shown in Figure 3.2.1.

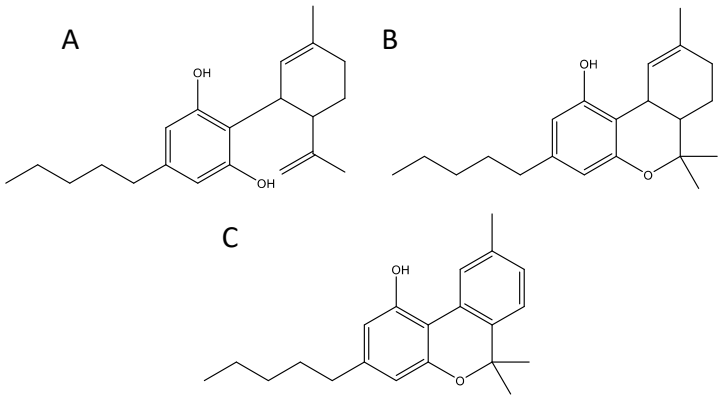

Figure 3.2.1: Structures of A) CBD, B) THC, and C) CBN.

Metal-organic frameworks (MOFs) are highly porous and feature high surface areas per volume in comparison to other solids, making them ideal candidates for adsorption-based applications.[74,118] The high adsorptive capacity of MOFs is well documented for gas storage and heavy metal capture.[71,119–122] MOFs are composed of organic linker molecules coordinated to metal nodes in a repeating array, and have been used as stationary phase in interface separations in gas, liquid, and size exclusion chromatography. [69,71,119–122] MOFs offer unparalleled tunability in comparison to other solid-state materials such as zeolites due to the broad variety of metal and organic units that can be used.[69,123] The high tunability of MOFs is advantageous because it allows for application-specific material properties such as pore size, aperture, and surface area. As of 2019, there were more than 82,600 known MOFs in the Cambridge Structural Database compared to just 248 zeolites in the Database of Zeolite Structures.[124,125]

MIL-53(Al) (Figure 3.2.2) is a commercially available MOF composed of terephthalate linkers and Al^{3+} metal nodes.[73] MIL-53(Al) has the potential to improve upon commercially available stationary phases for adsorption-driven reverse phase liquid chromatographic separations, because MIL-53(Al) is unique among MOFs due to its stability in liquid water for at least 6 months and its reported stability between pH 2-12 over the same timeframe.[76–78] MIL-53(Al) has a reported Brunauer-Emmett-Teller (BET) surface area of 904-1706 m^2/g.[73,77–83] It is important to note that the framework dimensions can fluctuate depending on changes in the solvation environment, temperature, pressure, and guest molecule adsorption state.[73,126–129] Upon hydration, the pore volume of MIL-53(Al) decreases significantly in a reversible process from 1440 $Å^3$ to 1012 $Å^3$, and is thus expected to be in the constricted conformation in an aqueous (reverse phase) environment.[73,128] MIL-53(Al) has previously been used as a stationary phase in liquid chromatography to separate mixtures of phthalate acid esters.[84] The stability in aqueous

environments and across a wide pH range makes MIL-53(Al) a promising candidate for more generalized adsorptive separation applications in the liquid phase.

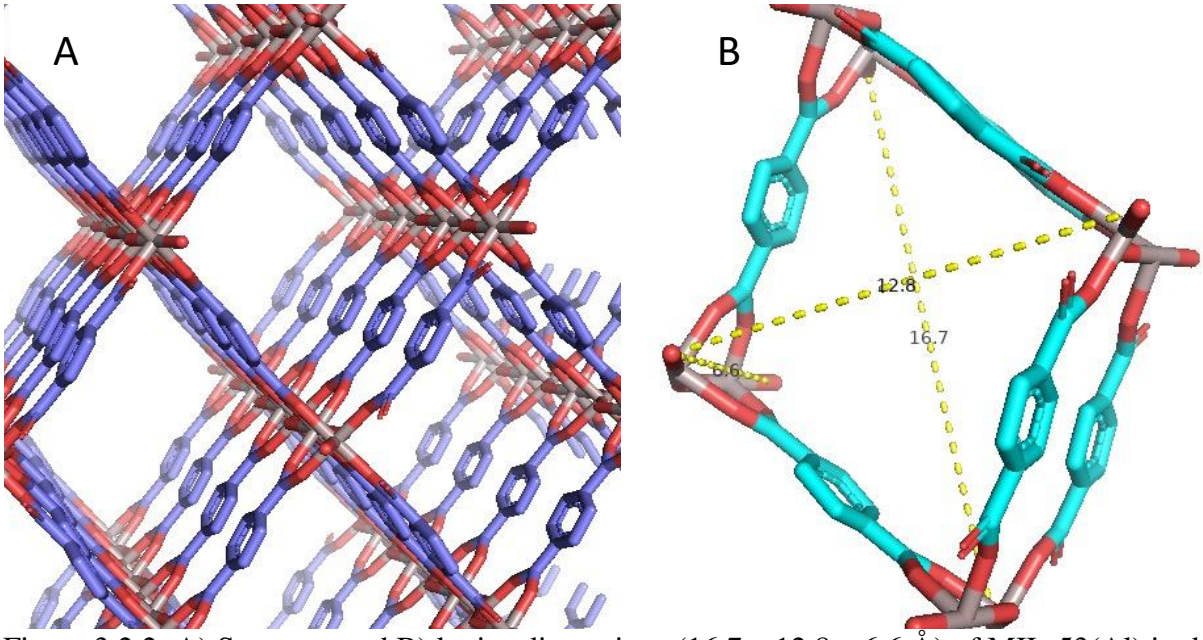

Figure 3.2.2: A) Structure and B) lattice dimensions (16.7 x 12.8 x 6.6 Å) of MIL-53(Al) in the open (activated) configuration.

Although the high surface area of MOFs is potentially advantageous for interface separations, it is unclear whether the bulk of the surface area is accessible for adsorption. In a previous study, our group investigated the parameters affecting adsorption of the uremic toxin p-cresyl sulfate by a group of zirconium MOFs and MIL-100(Fe), and found poor correlation between adsorption and surface area or pore volume.[68] We hypothesized that adsorbate diffusion into a MOF is size-limited by the pore aperture, whereby the bulk of adsorptive interactions of a molecule with dimensions greater than the pore aperture occur at or near the exterior surface of a MOF particle. This means that although the MOF provides a high-level of surface area, most of it is not accessible to the substrate due to the molecule being too large to enter the pore. The presence of a solvation shell in the liquid phase may increase the effective adsorbate dimensions of the substrate and thus further limit diffusion into the MOF. For this reason, the utility of MOFs' high surface area may have an upper limit for adsorptive separations.

The objective of this work is to measure adsorptive uptake of CBD, THC, and CBN by MIL-53(Al) in a closed system and evaluate the adsorption-accessible surface area compared with theoretical models. It was hypothesized that CBD, THC, and CBN would interact with MIL-53(Al) via non-polar interactions between the benzene moiety of the terephthalate linker molecules in the MOF and the pentylbenzene moiety of all three cannabinoids, as well as the methylbenzene moiety of CBN. Adsorption effects at the MOF metal nodes are expected to be limited due to steric effects. Adsorption at the aromatic benzene motif of the terephthalate linker is also expected to dominate because of the overall non-polar nature of the cannabinoids. Theoretical cannabinoid adsorption capacities by MIL-53(Al) were computed using three competing models: first, where the total BET surface area of the MOF is accessible; second, where cannabinoid adsorption occurs uniformly (a saturated monolayer of cannabinoids) across a spherical MOF particle congruent to the average particle diameter; third, where adsorption occurs non-uniformly across a sphere congruent to the average particle diameter and is limited to one cannabinoid per terephthalate linker. Each model is likely an overestimation of adsorptivity because they assume 100% loading of cannabinoids, and don't account for interference by solvation shells around the adsorbates. Still, this approach is useful for eliminating competing models based on difference in magnitudes of theoretical adsorption as well as experimental observations. CBD, THC, and CBN are ideal adsorbates to evaluate these competing hypotheses because they are dimensionally larger than the pore aperture of MIL-53(Al), possess high structural similarities, and high theoretical affinity for the MOF.

Herein, cannabinoid adsorption to the MOF was evaluated by soaking activated MOF in cannabinoid solution. Previous studies have used diode array detection to quantify adsorbate concentrations in the soaking solution, then deducing adsorptive uptake as the concentration

difference relative to a reference with high pressure liquid chromatography-diode array detection (HPLC-DAD).[130] In this work, we have expanded on this methodology by digesting the MOF in 3M HCl to release adsorbed cannabinoids back into solution to detect them directly by high pressure liquid chromatography-triple quadrupole mass spectrometry (HPLC-QQQ). The high sensitivity and specificity of HPLC-QQQ facilitated quantification of cannabinoids at lower concentrations than HPLC-DAD with high confidence. Electrospray ionization (ESI) was used for introducing sample into the detector because it preserves the molecular integrity of the analytes, thus maximizing the number of precursor ions and detector signal in contrast to more destructive "hard" ionization techniques such as atmospheric pressure chemical ionization.[131] This means more of the parent ion is introduced into the detector, which produces a stronger signal.

3.3 Materials and Methods

3.3.1 Materials

MIL-53(Al) (688738) was purchased from Sigma Aldrich. Acetonitrile, >99% (A998-4); methanol, >99.8% (A412-4); formic acid, >88% (A118P-500); hydrochloric acid, 33-38% (A142-212) were purchased from Fisher Scientific. Certified reference standards (1.0 mg/mL) of cannabidiol (ISO60156), cannabinol (ISO60183), and Δ-9-tetrahydrocannabinol (ISO60157) were purchased from Cayman Chemical. High purity water was purified by a Millipore Direct-Q water purification system to 18.2 MΩ cm resistivity prior to use.

3.3.2 Solution and sample preparation

MIL-53(Al) was gently ground by mortar and pestle, then physically separated using electroformed sieves between 112 – 125 µm. The MOF was then activated under vacuum at 200 °C overnight prior to use.

Analytical standards (HPLC-DAD): 1 mL each of 1.0 mg/mL CBD, CBN, THC certified reference standards were transferred to 20.0 mL class A volumetric glassware and brought to volume in acetonitrile to produce a stock concentration of 50 µg/mL per cannabinoid. Flasks were vortexed for 30 s. Subsequent standards of 10, 5, 1, 0.5 µg/mL per cannabinoid were prepared by serial dilution of the stock in acetonitrile in 1.5 mL HPLC vials. HPLC vials were vortexed 30 s between dilutions.

Analytical standards (HPLC-QQQ): 1 mL each of 1.0 mg/mL CBD, CBN, THC certified reference standards were transferred to 20.0 mL class A volumetric glassware and brought to volume in acetonitrile to produce a stock concentration of 50 µg/mL (50,000 ng/mL) per cannabinoid. Subsequent standards of 2500, 500, 100, 20, 4, and 2 ng/mL per cannabinoid were prepared by serial dilution of the stock in methanol in 1.5 mL HPLC vials. HPLC vials were vortexed 30 s between dilutions.

Cannabinoid sample solution: 1 mL each of 1.0 mg/mL CBD, CBN, and THC certified reference standards were transferred to 25.0 mL class A volumetric glassware and brought to volume in acetonitrile to produce a concentration of 40 µg/mL per cannabinoid in HPLC vials. HPLC vials were vortexed 30 s between dilutions.

Cannabinoid Adsorption: 100 mg activated MIL-53(Al) was combined with 2.5 mL cannabinoid sample solution in 3.5 mL sample vials, then covered with foil and gently vortexed for 2 days at room temperature, at 2500 RPM. Vials were then centrifuged, and the supernatant

filtered through 0.2 µm PTFE into 1.5 mL HPLC sample vials and stored at -20 °C. The MOF solids were retained and then dried under vacuum overnight at room temperature.

Acid Digestion: 95 mg dried MIL-53(Al) solids, recovered from cannabinoid adsorption method, were transferred to fresh 3.5 mL sample vials and combined with 2.5 mL 3N HCL. Vials were covered in foil and gently vortexed for 1 hr. Vials were then centrifuged and filtered through 0.2 µm PTFE. 500 µL of the filtrate were transferred to fresh 1.5 mL HPLC vials and dried under a constant flow of nitrogen at room temperature, then reconstituted in 250 µL MeOH and stored at -20 °C.

All measurements were run in triplicate and the average and standard deviations are reported.

3.3.3 Instrumentation and Methods

Brunauer-Emmett-Teller (BET) adsorption was measured using a Micromeritics ASAP 2020 adsorption apparatus and software version V4.03 H. Samples were degassed under ambient conditions overnight under vacuum in sample vials before transfer to the instrument. The MOF starting material was degassed at 525 K, and the cannabinoid-exposed MOF was degassed at ambient conditions on instrument. Analyses were initiated when the pressure in the sample tube was stable below 5 µmHg. Isotherms were collected at 77 K, using N_2 as the adsorptive gas. Adsorption data was collected at absolute pressures between 0.00989 – 633 mmHg. The BET surface areas were calculated using the slope of monolayer formation at partial pressures of 0.05-0.15 P/P_o.

Fourier-transform infrared (FTIR) spectra were collected using a Thermo-Nicolette 6700 equipped with KBr beam splitter and diamond attenuated total reflectance crystal. Background

and analytical spectra were compiled from 128 scans. Samples were analyzed from 650-4000 cm^{-1}.

SEM imaging was performed using a JEOL JSM-6500F microscope. An accelerating voltage of 3.0 kV and a working distance of 10.2-10.3 mm were used. All samples were placed under vacuum and coated with 20 nm of gold prior to imaging. Three to four representative images were taken at three different magnifications for each sample.

DLS was performed on a Zetasizer Nano-ZS using a quartz cuvette. Samples were dispersed in 20 °C acetonitrile and equilibrated for 2 minutes prior to analysis. A refractive index of 1.344, viscosity of 0.35 cP, and 173° backscatter angle were used.

Adsorption capacities were calculated assuming an equally distributed monolayer adsorbed to the MOF surface. Solvent accessible surface areas (SASAs) were calculated using the MSMS and Hollow packages.[132,133] The SASA is computed by rolling a sphere of radius r across the surface of the molecule and the accessible area quantified. Cannabinoid SASAs were calculated using an r value of 3.26 Å (equal to radius of ACN), and visualizations performed in PyMOL.[133–135] The surface-limited MOF particles was modeled assuming a spherical particle morphology, uniform framework dimensionality, and that occupied and vacant space are stoichiometrically distributed according to the unit cell composition. The effective cannabinoid surface area was calculated as the average cannabinoid SASA. In the surface-limited models, the effective cannabinoid surface area was divided by 2, to account for adsorbate surface area oriented away from the MOF substrate.

Cannabinoids were separated prior to quantification using high performance liquid chromatography (HPLC). Analyses of the retained MOF soaking solution were carried out on an Agilent Infinity II 1260 HPLC with a diode array detector (HPLC-DAD). The detection

wavelength was 220 nm. Analysis of the reconstituted acid-digestion samples were carried out on an Agilent Infinity II 1290 HPLC equipped with electrospray ionization and triple quadrupole (HPLC-QQQ) mass spectrometer. The HPLC instrument method and mobile phases were the same for HPLC-DAD and HPLC-QQQ detection. Cannabinoids were separated on an Agilent InfinityLab Poroshell 120 EC-C18 3.0 x 50 mm column with 2.7 μm particle diameter (699975-302), using a binary gradient. Mobile phase A was 0.1% (v/v) formic acid in water. Mobile phase B was 0.05% (v/v) formic acid in methanol. The injection volume was 5 μL. The method gradient was 60% B, 0 min; 80% B, 8 min; 100% B, 9min; 10.5 min runtime; 2 min post time. The method was calibrated using the analytical standard solutions ($R^2 > 0.999$, all cases). HPLC data was quantified using external calibrations of analytical standards dissolved in acetonitrile. Instrument response used in quantification was defined as the integrated peak area of counts over time (QQQ), and integrated peak area of absorbance over time (DAD). The units of measurement were counts*time (QQQ) and mAU*time (DAD).

3.3.4 Experimental systems

The research described in this chapter evaluates an overarching system through a series of 1 system broadly defined, and 5 subsystems individually analyzed. Section 3.4.1 describes a series of cannabinoid adsorption models that would then be experimentally eliminated through analyses of experimental systems. The overarching system has two components: activated MIL-53(Al), which was then soaked in cannabinoid solution. Sample preparations for this system are described in section 3.3.2. The soaked MOF solids were recovered from solution to allow for separate analyses of subsystems using a variety of analytical techniques. The first subsystem is comprised of recovered MOF solids from acetonitrile and cannabinoid solution in acetonitrile

and these analyses are reported in section 3.4.2. Recovered solids were dried, and surface area measured with isothermal N_2 adsorption during BET analysis, and then subsequently infrared absorption spectra collected on the dried solids. The second subsystem is defined as recovered cannabinoid-exposed MOF solids suspended in acetonitrile, then analyzed by DLS. Analytical results for the second subsystem are reported in section 3.4.3. A third subsystem is described in section 3.4.4, and is comprised of computational renderings of CBD, CBN, Δ9-THC, MIL-53(Al), and ACN. A fourth subsystem is described in section 3.4.5 and is the recovered MOF soaking solution and a reference soaking solution from the same stock. A fifth subsystem is described in section 3.4.6 and is comprised of recovered MOF decomposed in 3 N HCl, with acid removed and then reconstituted in methanol. Additionally, subsystem 5 included calibration standards which were prepared in acetonitrile. Sample and standard preparation for each system is reported in section 3.3.2 and instrument parameters are reported in section 3.3.3.

3.4 Results and discussion

3.4.1 Adsorption models and assumptions made

The cannabinoid adsorption behavior was evaluated by comparing experimental results to three competing models. These initial models, of course, overestimate adsorption capacities but are useful based on differences in theoretical adsorption in comparison with experimental observations. Table 1 lists the different adsorption models and assumptions made.

Table 3.4.1: Theoretical adsorption models and assumptions made within the calculations.

Adsorption Model	Assumption
1	The total BET surface area of the MOF is adsorption accessible to all of cannabinoid SASA, with 100% adsorption efficiency.
2	Cannabinoid adsorption occurs uniformly across a sphere congruent to the average particle diameter, with 100% adsorption efficiency. Only half of cannabinoid SASA used to account for adsorbate orientation.
3	Cannabinoid adsorption occurs non-uniformly across a sphere congruent to the average particle diameter, with 100% adsorption efficiency. Only half of cannabinoid SASA used to account for adsorbate orientation.

3.4.2 Evaluation of Model 1 using BET and FTIR

The BET surface area of the activated MOF was determined to be 948 m^2/g and was used to calculate theoretical adsorption capacity in Model 1, where all of the MOF surface area is adsorption-accessible. The BET procedure was repeated on MOF exposed to cannabinoid solution and a small decrease in BET surface area was observed. The BET surface area of the cannabinoid-adsorbed sample was 865 m^2/g. The high BET surface area of the MOF after exposure to cannabinoids indicates that most of the pores were open to nitrogen adsorption and thus unoccupied. The decrease in surface area could potentially indicate either that cannabinoids occupied some MOF pores, or it may indicate residual solvent was present in the MOF due to degassing at lower temperatures to reduce thermal degradation of cannabinoids prior to analysis.

The finding that most of the MOF pores were unoccupied is inconsistent with adsorption Model 1. A control experiment was performed, where MOF exposed to ACN was analyzed under identical conditions to the cannabinoid-exposed sample. The BET surface area of the ACN-washed sample was determined to be 597 m^2/g – this corresponds to a 37% decrease in BET surface area (Figure A3). Some variation between BET surface area of the solvated MOF is expected, as solvent is likely trapped in the sample in the analysis. This control measurement is consistent with a decreased BET surface area measured in the cannabinoid-exposed sample

and supports the hypothesis that ACN can pass into the particle interior, but the cannabinoids can't. Nitrogen adsorption isotherms for both the MOF and cannabinoid-exposed MOF are presented in Figure 3.4.1.

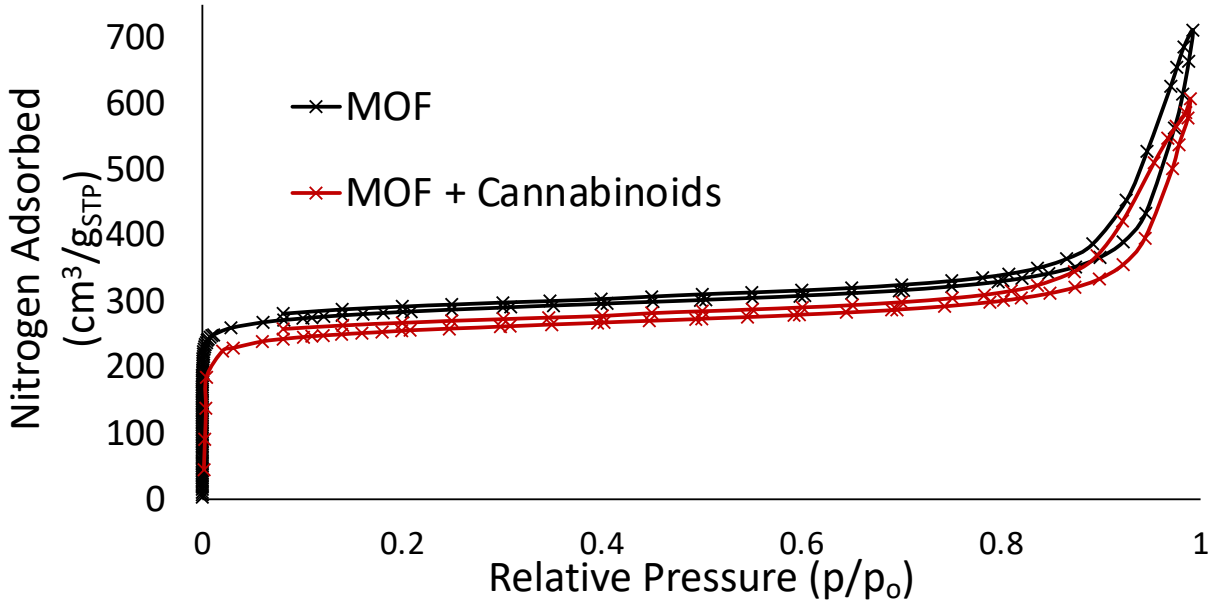

Figure 3.4.1: Overlaid BET nitrogen adsorption isotherms of MIL-53(Al) (black trace) and MIL-53(Al) after exposure to cannabinoid solution (red trace).

FTIR spectra were collected for the activated MOF as well as cannabinoid-exposed MOF. Spectra were evaluated within the characteristic regions of 3085-3060 cm^{-1}, 910-872 cm^{-1}, and 1514-1485 cm^{-1} for CBD, CBN, and THC respectively.[136] Additionally, spectra were inspected for aliphatic C-H adsorption from 3000-2850 cm^{-1}. In all cases, the spectra were indistinguishable between the two samples, indicating that adsorbed cannabinoids were not present in sufficient quantity to be detected by FTIR and thus not present in the bulk of the material. The spectra are shown in Figure 3.4.2. This observation, in combination with the BET analyses, effectively disproves Model 1.

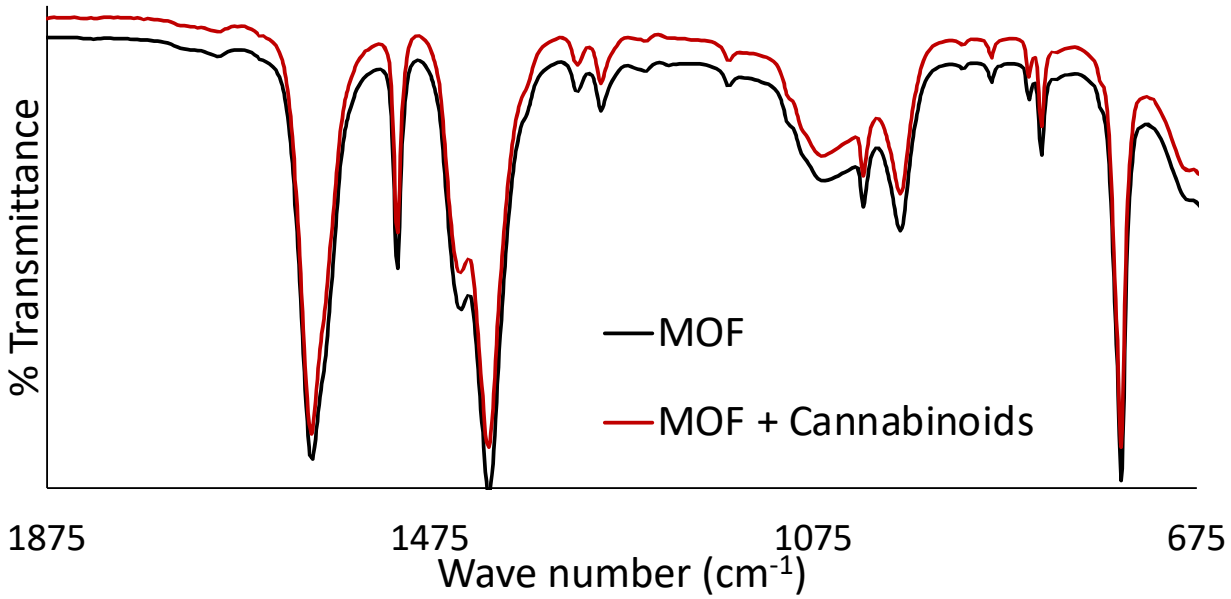

Figure 3.4.2: Overlaid FTIR spectra of MIL-53(Al) (black trace) and cannabinoid-exposed MIL-53(Al) (red trace) in the fingerprint region (675-1875 cm^{-1}). The spectra are indistinguishable, indicating that any adsorbed cannabinoids are present in insufficient quantity to be detected by FTIR, and likely not present within the bulk of the material. The full spectra are presented in Figure B1 in Appendix B.

3.4.3 Particle sizing

DLS was chosen as a preferable particle sizing method over SEM and optical microscopy because the technique allows for measurement in acetonitrile matrix over a much larger sample set. Characteristic SEM images of the activated sample are presented in Figure S2 in the supporting information file. DLS assumes a spherical particle morphology when calculating the hydrodynamic radius. Adsorption calculations for Models 2 and 3 were performed assuming spherical particle morphologies as well for consistency. The DLS Z-avg particle diameter is a reasonable approximation of particle size in the case of the solvated MOF and was used in our calculations of solvent-accessible surface area. The Z-avg was determined to be 322 ± 3 nm (PDI=0.138), and the theoretical external surface area per particle was 0.32 μm^2. The Z-avg was significantly smaller than the sieve diameter used. The reason for the size discrepancy is

hypothesized to be that the bulk MOF material was composed of aggregated, smaller particles. This means we approximated the exterior particle surface area based on measurements in a solvated environment, which better reflects the chemical environment of our system than SEM measurements. Figure 5 shows the DLS particle size intensity graph.

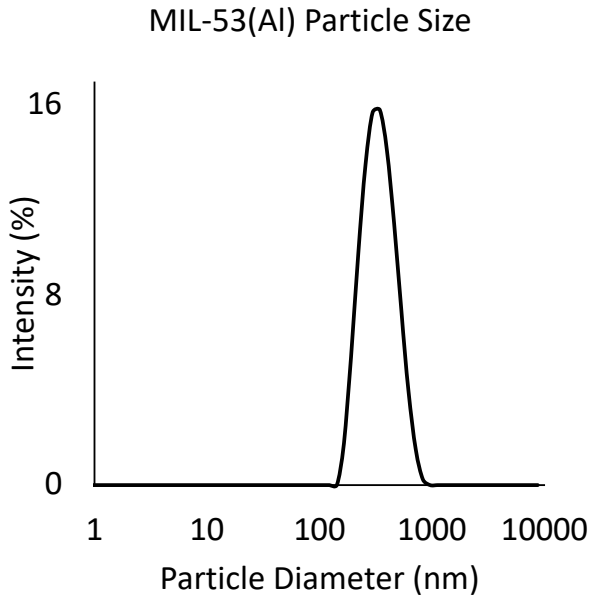

Figure 3.4.3: DLS particle size intensity graph. The Z-average MOF particle size was 322 ± 3 nm (PDI = 0.138).

3.4.4 Computational modeling

Computational modeling was used to estimate adsorptive capacity of cannabinoids by the MOF to evaluate Models 2 and 3 (Table 1). MIL-53(Al) pores are known to constrict when hydrated, but modeling was performed on the open conformation for consistency. The Solvent Accessible Surface Area (SASA) was computed by rolling a sphere of radius 3.26 Å (equal to the radius of ACN) across the surface of the molecule and the accessible area quantified. The surface-limited MOF particles were modeled assuming a spherical particle morphology, uniform framework dimensionality, and that occupied and vacant space are stoichiometrically distributed according to the unit cell composition. The non-uniform adsorption capacity was estimated assuming a stoichiometric relationship between the unit cell SASA and the estimated surface

area of the surface-limited adsorption hypothesis. The effective cannabinoid surface area was calculated as the average cannabinoid SASA. In the surface-limited models, the effective cannabinoid surface area was divided by 2, to account for adsorbate surface area oriented away from the MOF substrate. This means our adsorption models accounted for both the adsorption site and adsorbate orientation.

The MOF pore channel was determined to have an irregular cylindrical shape, with approximate dimensions of $Diameter_1$ = 7.9 Å, $Diameter_2$ = 10.1 Å, and Depth = 6.6 Å. $Diameter_1$ and $Diameter_2$ correspond to radii of 4.0 Å and 5.1 Å, respectively. The radius of gyration for each cannabinoid adsorbate was 4.1 Å and shown in Figure 3.4.4.A. The adsorbate radii of gyration are larger than the minimum pore aperture and implies that the adsorbate diffusion into the pore will be limited, which is reflected in the data for CBD, CBN, THC, and MIL-53(Al). Figures 3.4.4.B and 3.4.4.C show CBD and its radius of gyration superimposed upon the pore aperture and SASA of the MOF, respectively. Figure 6D shows the same view of an ACN solvent molecule for comparison. ACN is not size limited by the pore aperture and can readily diffuse into the MOF bulk (as evidenced by BET results discussed above).

The total SASAs of CBD, CBN, THC, and the $average_{(n=3)}$ which were calculated to be 1020 $Å^2$, 1016 $Å^2$, 1017 $Å^2$, and 1018 ± 2 $Å^2$, respectively (Table 3.4.2). Model 1 assumes that cannabinoids can adsorb to the framework in three dimensions, so the total SASA was used. Models 2 and 3 assume a two-dimensional substrate, where half of the adsorbate is oriented towards the substrate and half oriented away from it. This adsorbate orientation was accounted for by dividing the total cannabinoid SASAs by a factor of two (510 $Å^2$, 508 $Å^2$, 509 $Å^2$, 509 ± 1 $Å^2$, respectively).

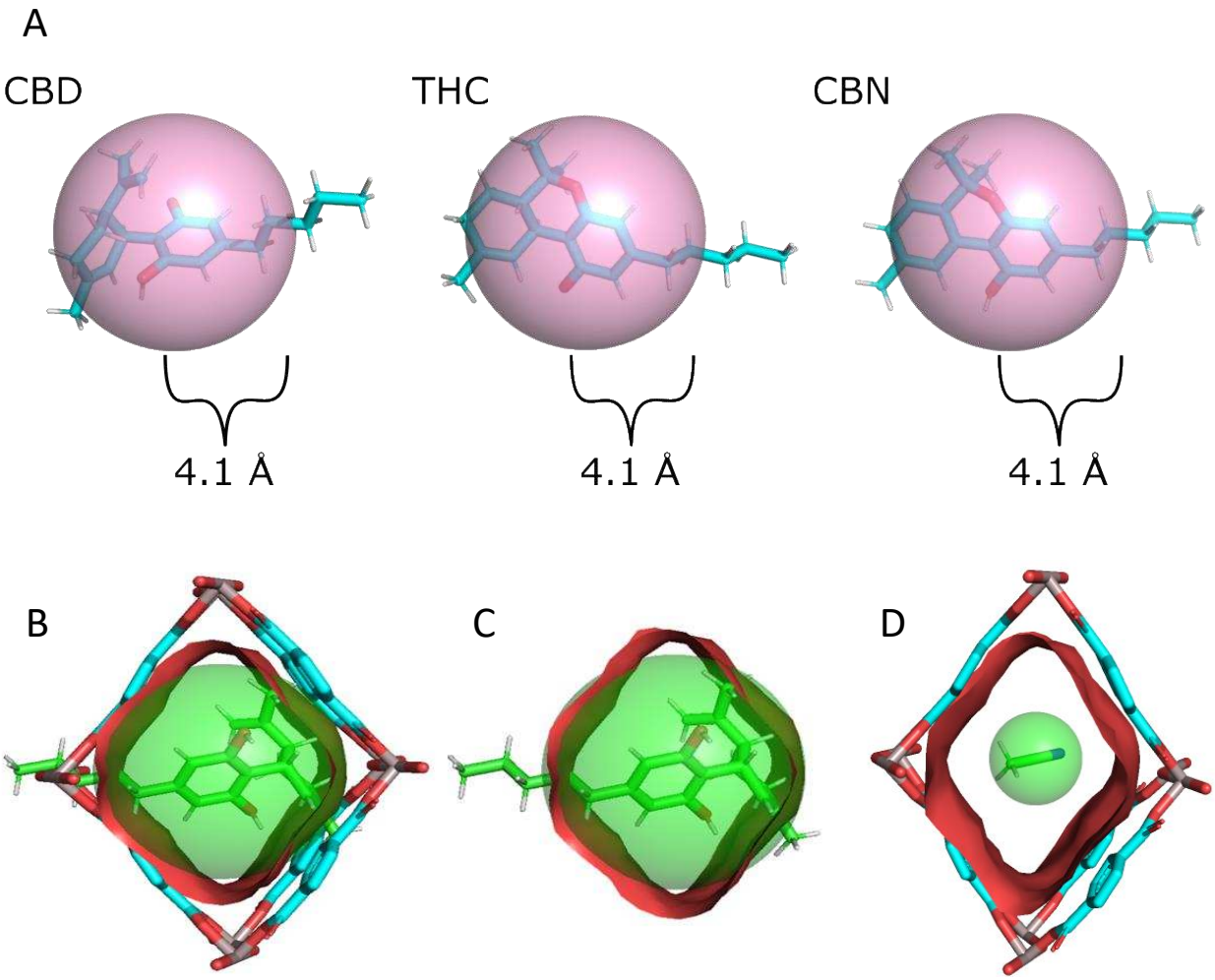

Figure 3.4.4: A) Radii of gyration of CBD, CBN, and THC, respectively. B) CBD and its radius of gyration superimposed upon the pore aperture, C) CBD and its radius of gyration superimposed upon the SASA, and D) ACN and its radius of gyration superimposed upon the pore aperture. Diffusion into the pore by cannabinoids is size limited because the R_g is larger than the pore aperture, whereas ACN readily diffuses into the pore.

Theoretical modeling assumed 100 mg MOF per sample, 3 mL 120 µg/mL total cannabinoids, average cannabinoid SASA, and uniform adsorption across all surfaces. Hence, the values for the Theoretical Adsorption per Cannabinoid in Table 2 are the theoretical upper limit for each model.

Table 3.4.2: Theoretical adsorption models calculated using three modalities for this system.

Adsorption Model	Adsorbate SASA (Å^2)	Theoretical Adsorption-Accessible Surface Area ($\mu m^2/mg_{MOF}$)	Theoretical Adsorption per Cannabinoid ($\mu g_{cannabinoids}/mg_{MOF}$)
1	CBD: 1020 CBN: 1016 THC: 1017 $Avg_{(n=3)}$: 1018 ± 2	9.5×10^{11}	16.2
2	CBD: 510 CBN: 508 THC: 509 $Avg_{(n=3)}$: 509 ± 1	4.7×10^{10}	1.6
3	CBD: 510 CBN: 508 THC: 509 $Avg_{(n=3)}$: 509 ± 1	9.3×10^{9}	0.3

3.4.5 Quantitation of cannabinoids within the MOF soaking solution

HPLC-DAD was used to quantify the cannabinoid concentrations in soaking solution samples. Cannabinoids in the undiluted filtrate were quantified after a separation step and referenced against a control sample of solution unexposed to the MOF. The initial concentrations of cannabinoids were 43.7 ± 0.2 µg CBD/mL, 42.1 ± 0.1 µg CBN/mL, and 42.5 ± 0.3 µg/mL THC. The cannabinoid recoveries in MOF-containing samples were 43.1 ± 0.1 µg CBD/mL, 42.5 ± 0.2 µg CBN/mL, and 42.5 ± 0.5 µg THC/mL. The sample percentage recoveries relative of CBD, CBN, and THC were 98.8 ± 0.1 %, 100.9 ± 0.4 %, and 100.1 ± 1.1 % respectively. Cannabinoid recoveries are shown in Figure 3.4.5. The high recovery rates within the soaking solution indicate very low adsorptive uptake by the MOF and are more favorable for Model 3 than Model 2.

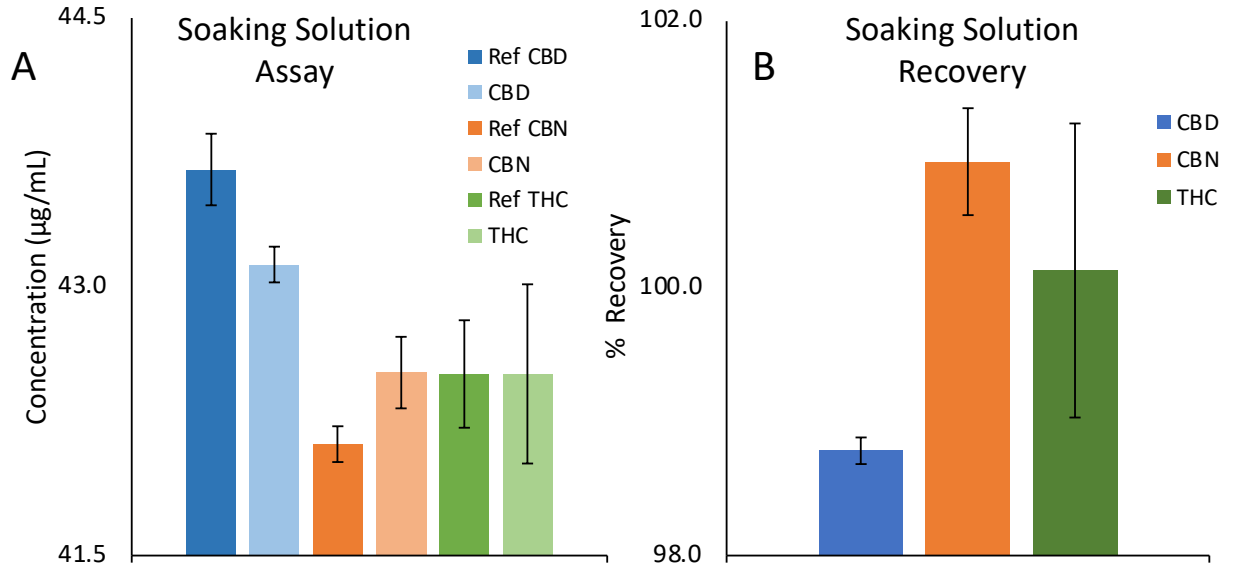

Figure 3.4.5: A) Cannabinoid concentrations of the MOF soaking solution (n=3) compared to reference sample, and B) % recoveries of cannabinoids in samples (n=3) relative to the reference.

A 1.1% decrease in CBD signal corresponds to a 0.013 $\mu g_{cannabinoids}/mg_{MOF}$ decrease in the soaking solution compared to the reference. Given the hypothesis that the predominant physisorption site is the aromatic benzene motif on the terephthalate linker, CBD was expected to have the lowest adsorption affinity because it is the most polar analyte in the system. The percent relative standard deviation of THC corresponds to an uncertainty of 0.012 $\mu g_{cannabinoids}/mg_{MOF}$, and the offset of CBN corresponds to a value of 0.01 $\mu g_{cannabinoids}/mg_{MOF}$. Both THC and CBN are less polar than CBD, respectively, and would be expected to have higher adsorption affinity for the MOF. Measurements of all three cannabinoids fall within AOAC recovery acceptability criteria for 100% assay.[116] We hypothesized that direct measurement of cannabinoids released from the MOF using a more sensitive detection method would enable quantitative evaluation of our system relative to Models 2 and 3. The low adsorptive uptake was therefore evaluated by measurement of the acid soaking solution by the more sensitive HPLC-QQQ.

3.4.6 Quantitation of cannabinoids in acid-digested samples

HPLC-QQQ was used to quantify cannabinoids in the acid-digested MOF samples. Cannabinoid analyte decomposition was observed in the reference during digestion. The decomposition factors in the reference for CBD, THC, and CBN were 87.8%, 87.0 %, and 84.2%, respectively. The level of CBN in the acid degradation samples was below the LOQ and neither CBD nor THC were detected. This uniformly low signal could be a false negative caused by degradation during from the digestion step. Thus, maximum cannabinoid uptake by the MOF was estimated by applying the decomposition factors of the reference to a 100% nominal assay value minus the standard deviation of the reference. Using this method, the maximum cannabinoid uptake was estimated as the Decomposition Corrected RSD as Uptake (DCRU). The DCRU was calculated to be 720 ng/mL, 270 ng/mL, and 980 ng/mL for CBD, CBN, and THC, respectively. The DCRU for all three analytes was less than the LOQ for both CBN and THC, and 0.2 μg/mL greater than the LOQ of CBD, which qualitatively agrees with the HPLC-DAD observations. The greater number of rotatable bonds in CBD could produce greater partial channel accessibility than either THC or CBN due to conformational degrees of freedom. Additional studies are needed to confirm the specific uptake of CBD in this system and elucidate the cause of the apparent greater adsorption than CBN, which was initially hypothesized to have the greatest adsorptive affinity for the MOF. The initial (theoretical) cannabinoid concentration recovered cannabinoid concentrations from the acid digestion reference, and the DCRUs are shown in Figure 3.4.6. The combined low assay results from the HPLC-DAD and HPLC-QQQ methods indicate that Model 2 is less favorable than Model 3, and as will be discussed shortly, suggest that further refinements are necessary to accurately model cannabinoid adsorption by the MOF.

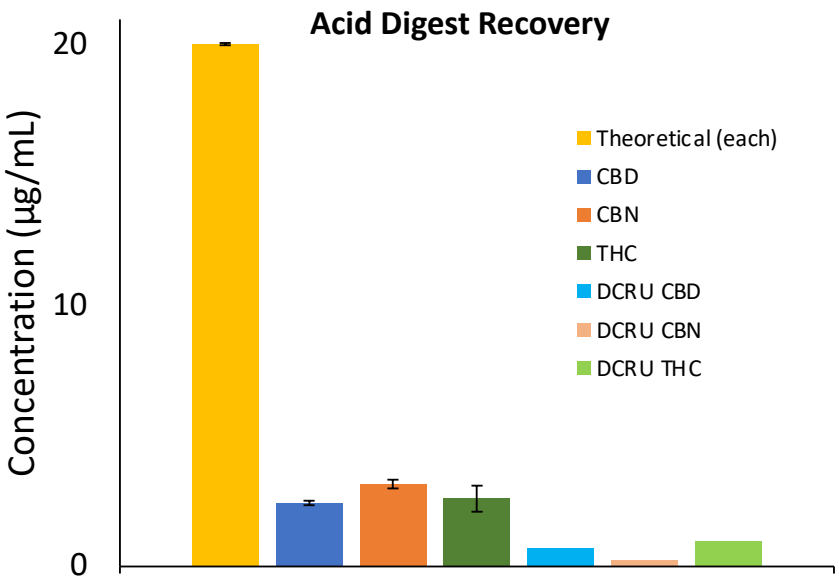

Figure 3.4.6: Cannabinoid recovery of the reference following acid digestion, relative to the theoretical starting concentration (n=3). Also shown, Decomposition-Corrected RSD as Uptake (DCRU) of the HPLC-DAD assay of CBD, CBN, and THC, respectively.

The difference in acid stability can be attributed to structural differences between analytes. Decomposition occurs analogously to polarity of the analyte; CBD (87.8% decomp.) is the most polar of the three, followed by THC (87.0% decomp.), and then CBN (84.2% decomp.). CBN has two benzene moieties whereas THC has only one, although they have the same heteroatom linkers. THC and CBD each have one benzene moiety, but THC is more structurally rigid due to the ether linkage creating three adjacent six-membered rings. The additional aromatic character of CBN provides greater stability in acid when compared to THC. Additional cannabinoid degradation pathways not related to acid digestion are possible, such as thermal degradation while soaking the MOF or drying under N_2 at room temperature were accounted for by use of a reference sample.

3.4.7 Model refinement using DCRU

The observed cannabinoid adsorption was less than estimated by all three models. This observation is expected due to the assumed 100% loading efficiency and exclusion of interferences from solvation shells around the cannabinoids assumed in each model. Model 3 was refined by recalculating the theoretical adsorption of cannabinoids assuming a uniform, monolayer solvation shell, whereby the effective adsorbate diameter was equal to two times the $R_{g(cannabinoids)}$ plus $2R_{g(ACN)}$, maintaining all other assumptions. This refinement is Model 4. The loading percentage of solvated cannabinoids on the MOF, using Model 4, is 3 ± 2%. The theoretical uptake per cannabinoid for each model, and the DCRU of each cannabinoid are shown in Table 3.4.3.

Table 3.4.3: Theoretical uptake per cannabinoid for each model, and the DCRU of each cannabinoid.

Adsorption Model	Theoretical Uptake per Cannabinoid ($\mu g_{cannabinoids}/mg_{MOF}$)
1. Uniform adsorption throughout particle	16.2
2. Uniform Adsorption on Particle Exterior	1.6
3. Adsorption on Particle Exterior Excluding Pore Aperture Area	0.3
4. Adsorption on Particle Exterior Excluding Pore Aperture Area, assuming monolayer solvation shell	0.2
$DCRU_{avg\ (n=3)}$	0.007 ± 0.004

3.5 Conclusions

The observed low uptake of cannabinoids to the MOF is inconsistent with an adsorption model where the full BET surface area is available to the adsorbates, which is most likely due to size-exclusion effects of the adsorbate at the pore aperture. The data are most consistent with a non-uniform, surface-limited adsorption model, where the effective diameter of the adsorbate

accounts for a monolayer solvation shell. The difference between the expected uptake of the non-uniform, surface-limited model and our experimental values necessitates further investigation into the specific adsorption mechanism. However, neither the uptake measured by HPLD-DAD or HPLC-QQQ indicate uniform adsorption throughout the MOF. These results demonstrate that cannabinoid adsorption by the MOF is limited by one or more factors beyond surface area. We hypothesize that adsorption-available surface area is governed primarily by the size of the pore aperture of the MOF relative to the adsorbate. Adsorbates larger than the pore aperture are simply too large to pass into the bulk of the MOF. Adsorption in the liquid phase may be further limited by solvation shells around the adsorbates in the liquid phase. Thus, the suitability of a MOF for adsorptive separations such as liquid chromatography must have an upper size limitation of the analyte. The size exclusion issue may be less prevalent for gas phase adsorptions, where adsorbates are not hindered by the presence of a solvation shell. Future studies may directly evaluate adsorption occurring at the particle exterior by evaluating adsorptive uptake by to MOF relative to varying particle size, where a strong dependence on particle size would be evidence supporting a primarily external adsorption mechanism. Additionally, the proposed adsorbate size limitation can be measured by evaluating the adsorptive uptake of small molecules of incrementally increasing R_g in both the liquid and gas phases.

CHAPTER 4 – DEMONSTRATING A PESTICIDE REMEDIATION STRATEGY FOR PREPARATIVE LIQUID CHROMATOGRAPHY USING HIGH-PERFORMANCE LIQUID CHROMATOGRAPHY[3]

4.1 Summary

Cannabis sativa L. also known as industrial hemp, is primarily cultivated for two major cannabinoids (cannabidiol and Δ9-tetrahydrocannabinol) as a source material for the hemp and marijuana industries. Pesticide contamination during plant growth is a common issue in the cannabis industry which can render plant biomass, extracts, distillates made from contaminated material unusable. Remediation strategies to ensure compliant and safe cannabinoid products are necessary and important to consider for recovering cannabinoids from contaminated materials. The present study evaluated retention times of 11 pesticides relative to 26 cannabinoids plus the cannabinoid precursor molecule olivetol for general suitability of remediation by eluent fractionation. The ten pesticides evaluated for retention times are clothianidin, imidacloprid, piperonyl butoxide, pyrethrins (I/II mixture), diuron, permethrin, boscalid, carbaryl, Spinosad, and myclobutanil. Following these studies, I used three of those pesticides to evaluate spike-recoveries to model extraction efficiency during sample preparation. The sub-study evaluating spike-recovery used carbaryl, Spinosad, and boscalid to model extraction efficiency.

Preparative liquid chromatography (PLC) is an attractive strategy for remediating pesticide contaminants and targeted isolation of phytocannabinoids and would improve on existing liquid-liquid chromatographic methods. To test the feasibility of PLC as a remediation strategy, a

---

[3] The present chapter has been adapted from a manuscript under review in the Springer *Journal of Cannabis Chemistry* with coauthors Dr. James Baumgartner and Dr. Melissa M. Reynolds. Samples were provided by Panacea Life Sciences, Golden, CO.

benchtop-scale high performance liquid chromatographic method was developed as a proof-of-concept for preparative-scale liquid chromatographic separation. Six industrial hemp process matrices were spiked (flower, ethanol crude extract, CO_2 crude extract, distillate, distillation mother liquors, and distillation bottoms) with commonly used pesticides carbaryl, boscalid, and Spinosad. Next, I evaluated differences in spike recovery and pesticide retention in different sample matrices through a 2.7 µm octyldecylsilane column. Pesticides clothianidin, imidacloprid, carbaryl, diuron, Spinosad, and myclobutanil, plus olivetol, eluted in the first 3.6 minutes, and all cannabinoids (except for 7-OH-CBD) eluted in the final 12.6 minutes of the 19-minute gradient for all matrices evaluated. Thus, the present method is suitable for 6/11 pesticides and 25/26 cannabinoids evaluated. 7-OH-CBD (RT: 3.4 min), pyrethrins I and II (RT_A: 6.8 min, RT_B: 10.5 min), permethrin (RT_A: 11.9 min, RT_B: 12.2 min), and piperonyl butoxide (RT_A: 8.3 min, RT_B: 11.7 min), will require additional purification steps than presently reported. Preliminary separations using larger particle-size C18 are ongoing but require further optimization prior to method transfer. The resolution of pesticides from cannabinoids in this method indicates that eluent fractionation is a highly attractive solution for pesticide remediation of contaminated cannabis materials and targeted isolation of cannabinoids.

4.2 Introduction.

The purpose of this study was to develop a benchtop-scale HPLC method for separating 11 pesticides, 26 cannabinoids, the cannabinoid precursor olivetol, and evaluate the theoretical suitability of the method for separating pesticides and cannabinoids from six industrial hemp processing matrices using preparative-scale liquid chromatography (PLC).

Cannabinoids and pesticides have been discussed in depth in previous chapters and will be summarized in brief here. *Cannabis sativa L.* (cannabis) produces a number of physiologically compounds, including phytocannabinoids, terpenoids, flavonoids, and alkaloids.[1] Cannabinoids are a class of molecules that can ligate to endocannabinoid receptors in the body, and phytocannabinoids are a subset of cannabinoids produced by a plant. Phytocannabinoids are triterpenophenolic molecules; perhaps the best known are Δ9-tetrahydrocannabinol (Δ9-THC) and the non-psychoactive cannabidiol (CBD).[90] THC produces the recreational "high" associated with marijuana, and CBD is a non-psychoactive analog that is reported to have antiemetic, anti-seizure, and anti-inflammatory properties.[91] In general, hemp produces CBD in much greater amounts than marijuana, and is thus an important cash crop in the emerging cannabis industry.[23]

Pesticide contamination of cannabis source material is a primary concern in the production of cannabis products, and acceptability criteria for the presence of pesticides are regulated by state agencies.[19] Although direct use of pesticides on hemp products is regulated, occasionally the plants are indirectly exposed to banned pesticides and trace contamination of biomass is an issue when grown next to other crops.[38,95] Hemp grown in proximity to other commodity crops can be contaminated by pesticides from those adjacent fields.[96] This becomes problematic when the pesticides used are banned by commercial cannabis regulations and drift to the hemp crop.

Cannabis products intended for consumption must be tested to ensure compliance with state regulatory agencies; products with pesticide content exceeding acceptability criteria must be remediated prior to sale.[19,20,137] PLC is an attractive remediation strategy that separates sample components using a liquid-solid interface, where solvent composition is modulated as sample moves through a column, and operates on the same principles as analytical High-Performance

Liquid Chromatography (HPLC).[138] Using PLC for pesticide remediation allows for benchtop-scale method development using HPLC, which can then be transferred to the preparative scale.

Liquid chromatography separates analytes by selective partitioning between a solid stationary and liquid mobile phase.[46–49] Components of the Stationary phase is defined as an adsorptive material, such as octyldecylsilane, which is packed into a column. The stationary phase packing and particle size are highly regular throughout the column. A mobile phase is a fluid which carries aliquots of sample through the instrument and drives analytes across the column packed with stationary phase. Mobile and stationary phase compositions are critical parameters in HPLC method development. Stationary phases used in work reported in this chapter were both octyldecylsilane but different particle sizes. The analytical column used in sections 4.4.1- 4.4.4 had a particle size of 2.7 µm. The column used to model analyte retention on the PLC system had a particle size of 10 µm.

Carbaryl, boscalid, Spinosad, imidacloprid, clothianidin, diuron, myclobutanil, piperonyl butoxide, pyrethrins I and II, and permethrin are all pesticides banned from use in cannabis products.[21] Their high chemical and thermal stability make them difficult to remediate from contaminated plant and extract materials, and remediation is further complicated by the complex nature of the cannabis matrix.[139,140] These 11 pesticides are ideal contaminants for demonstrating proof-of-concept of a liquid chromatographic method for remediating pesticides at the benchtop scale, because of their varied chemical composition and unsuitability for cannabis material.[141]

Ideal pesticide remediation methods also maximize cannabinoid recovery in tandem, since cannabinoids are also present in sample matrices.[108] Methods for both cannabinoid and pesticide quantitation have been reported using HPLC, but targeted pesticide separation and assay for scale-up to PLC has not been reported.[16,96,141] Suitability of the present method for each

pesticide was evaluated based on observed retention time. A shorter retention time than that of the cannabinoids in matrix indicates that the method is suitable, whereas pesticides with retention times longer than cannabinoids would require additional separation steps. Pesticides were evaluated as single samples and retention times measured.

The suitability of benchtop-scale method on six processing matrices was evaluated: flower, CO_2 crude extract, ethanol crude extract, distillate, distillation mother liquor, and distillation bottoms. These matrices were selected as representative steps in industrial processing based on recommendation from Panacea Life Sciences. Flower, crude extracts, and distillates having the most direct path to commercial sale, and the distillation mother liquor and bottoms are processing side-products with potentially commercializable components but require additional processing to recover.[7,112,142] Additional spike/recovery analyses were performed using carbaryl, boscalid, and Spinosad to model the extraction efficiency of the method used during sample preparation, and to compare recoveries between sample matrices. The structures of carbaryl, boscalid, and Spinosad A are shown in Figure 4.1.1.[143–145]

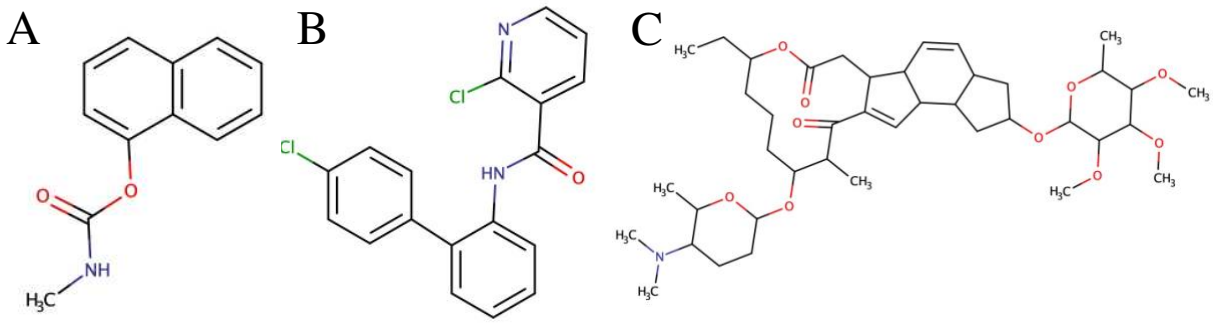

Figure 4.1.1: Molecular structures of three common pesticides regulated by the state of Colorado in cannabis products: A) carbaryl, B) boscalid, and C) Spinosad A.

A limitation of the results reported in section 4.4.3 is that analytes were separated on a column with Agilent Poroshell 120 2.7 µm C18 media.[60] Column dimensions and packing density are expected to be different between benchtop and preparative scale columns, but particle

size is a key consideration in stationary phase selection.[33,146] Currently, 2.7 µm Poroshell stationary phase is not available for bulk purchase and cannot be used for PLC scale up. The stationary phase for preparative-scale separations indicated by this study will be Phenomenex Luna 10 µm C18 PREP media. Preliminary experiments have been performed on a 150 x 4.6 mm Phenomenex Luna 10 µm C18 PREP column to better evaluate suitability of the method. The larger particle size is expected to decrease operating pressure but also decrease method resolution.[47,50,147] Lower resolution is not a critical concern for the proposed preparative method, as long as relative retention times between pesticides and cannabinoids are sufficiently different. Preliminary results collected on the 150 x 4.6 mm 10 µm Luna column are reported however these trials are ongoing.

4.3 Materials and methods

4.3.1 Materials

HPLC-grade acetonitrile (PN A998-4) was purchased from Fisher Scientific. Carbaryl (PN 24139), boscalid (PN 24135), Spinosad A (PN 25649), diuron (PN 24040), myclobutanil (PN 24100), clothianidin (PN 29605), pyrethrins I/II (PN 25814), piperonyl butoxide (PN 25820), imidacloprid (PN 24130), and permethrin (PN 23821) were purchased from Cayman Chemical. EN Method 15662 (QuECHERS) salts were purchased from Agilent (PN 5982-5650). A Sigma Millipore Direct-Q 5 water filtration system was used to deliver 18.0 mΩ•cm water. Cannabis matrix samples were donated by Panacea Life Sciences.

Reference materials of Δ8-tetrahydrocannabinol (Δ8-THC; PN: ISO60158), Δ9-tetrahydrocannabinol (Δ9-THC, PN: ISO60157), Δ9-Tetrahydrocannabinolic acid (Δ9-THCA; PN: 33448), Δ9-tetrahydrocannabutol (Δ9-THCB; PN: 33078), Δ9-tetrahydrocannabihexol (Δ9-

THCH; PN: 33352), Δ9-tetrahydrocannabiphorol (Δ9-THCP; PN: 30171), Δ9-tetrahydrocannabivarin (Δ9-THCV; PN: 18091), Δ9-tetrahydrocannabivarinic acid (Δ9-THCVA; PN: 21259), 7-OH-cannabidiol (7-OH-CBD; PN: 36517), cannabichromene (CBC; PN: 26252), cannabichromeorcin (CBCO; PN: 21742), cannabichromevarin (CBCV; PN: 21974), cannabichromevarinic acid (CBCVA; PN: 32718), cannabidiol (CBD; PN: 21259), cannabidiolic acid (CBDA; PN: 18090), cannabidiolic acid methyl ester (CBDA-ME; PN: 28347), cannabidiphorol (CBDP; PN: 30169), cannabidivarin (CBDV; PN: 20165), cannabielsoin (CBE; PN: 21092), cannabigerol (CBG, PN: 20164), cannabigerolic acid (CBGA PN: 20019), cannabigerol quinone acid (CBGAQ, PN: 31772), cannabigerovarin (CBGV PN: 29117), cannabigerovarinic acid (CBGVA; PN: 25469), cannabicyclol (CBL; PN: 22036), cannabinol (CBN; PN: 25495), cannabicitran (CBT; PN: 21295), and olivetol (PN: 35202) were purchased from Cayman Chemical.

4.3.2 Standard preparation

All standards were prepared at ambient temperatures and stored at -20 °C. Stock standard of 250 µg/mL per pesticide was prepared in acetonitrile. The working standard was prepared by diluting the stock 1:3 in acetonitrile. Calibration standards were prepared by dilution of the working standard and contained 25% matrix blank. Retention time check standards were prepared by dilution of CRMs in 10.0 mL class A volumetric flasks to nominal concentrations of 100 ug/mL.

4.3.3 Sample preparation

Matrix blank: A mass of 100 ± 10 mg sample were massed into 50 mL falcon tubes, soaked in 10 mL water, and vortexed. Then, 10 mL acetonitrile, 4 g $MgSO_4$, 1 g NaCl, 0.5 g disodium citrate sesquihydrate, 1 g sodium citrate, and ceramic agitator were added to the samples. Samples were then rigorously vortexed for 1 minute, centrifuged, and the acetonitrile (top) layer was decanted and transferred into 1.5 mL HPLC vials.

Matrix spikes: A mass of 100 ± 10 mg sample were massed into 50 mL falcon tubes, soaked in 10 mL water, and vortexed. 9.25 mL acetonitrile, 750 µL stock standard solution, 4 g $MgSO_4$, 1 g NaCl, 0.5 g disodium citrate sesquihydrate, 1 g sodium citrate, and ceramic agitator were added to the samples. Samples were then rigorously vortexed for 1 minute, centrifuged, and the acetonitrile (top) layer was decanted and transferred into 1.5 mL HPLC vials. Samples were prepared in triplicate.

4.3.4 Instrument Method

Analytes were separated prior to quantification on an Agilent Infinity II 1260 high performance liquid chromatography with diode array detection (HPLC-DAD). The detection wavelengths used were 208, 220, 230, and 240 nm. Primary studies were performed using an Agilent InfinityLab Poroshell 120 EC-C18 3.0 x 50 mm column with 2.7 µm particle diameter (PN: 699975-302), using a binary gradient. Preliminary studies on Phenomenex Luna 10 µm C18 PREP stationary phase were performed using a 150 x 4.6 mm column (PN: 00G-4616-E0) Mobile phase A was 0.1% (v/v) phosphoric in water. Mobile phase B was 0.1% (v/v) phosphoric acid in acetonitrile. The injection volume was 1 µL. The method gradient was 60% B, 0 min; 60% B, 1 min; 80% B, 8 min; 100% B, 10 min; 100%, 14.5 min; 60 % B, 15 min; 19

min runtime. The method was calibrated using the calibration standard solutions ($R^2 > 0.999$, all cases).

Measurements were quantitated using an external standard calibration. The instrument signal used was defined as the integrated peak area in the DAD chromatogram with units of absorbance over time (mAU*s).

4.3.5 Experimental systems

The work reported in this chapter includes two systems. The first system is comprised of six cannabis processing matrices extracted in ACN, which were spiked with boscalid, carbaryl, and Spinosad A standards in ACN. Sample and standard preparation is reported in sections 4.3.2-4.3.3. Cannabis processing matrices used were raw flower, CO_2 and EtOH crude extract, distillate, distillation mother liquor, and distillation bottoms. A second system comprised of analytical standards containing both pesticides and cannabinoids dissolved in acetonitrile, which were then separated on C18 silica with two different particle sizes: 2.7 and 10 µm. In this case, the stationary phase used is considered part of the system because particle size is an independent variable used to evaluate analyte retention times.

4.4 Results and discussion

4.4.1 Sample cleanup and pesticide recovery (all samples)

Sample cleanup was necessary for each matrix prior to analysis to limit chromatographic interference. Benchtop-scale liquid-liquid extraction between acetonitrile and salt-saturated water provided suitable resolution for this work. Each of the six matrices were spiked with 11.3 µg carbaryl, 18.8 µg boscalid, and 18.8 µg Spinosad. Recovery was calculated based on

standard addition calibration. Initially, pesticide recovery was calculated across all samples (n=18) because the objective of the study was to demonstrate suitability across multiple matrices. Using this approach, the relative standard deviations (RSDs) were greater than 5% for both carbaryl and boscalid. The average recoveries of carbaryl, boscalid, and Spinosad were 63.7 ± 7.8 %, 71.5 ± 19.5 %, and 64.4 ± 4.7 % respectively. To our knowledge, this is the first report of extraction efficiency using this approach. The recoveries are shown in Figure 4.4.1.

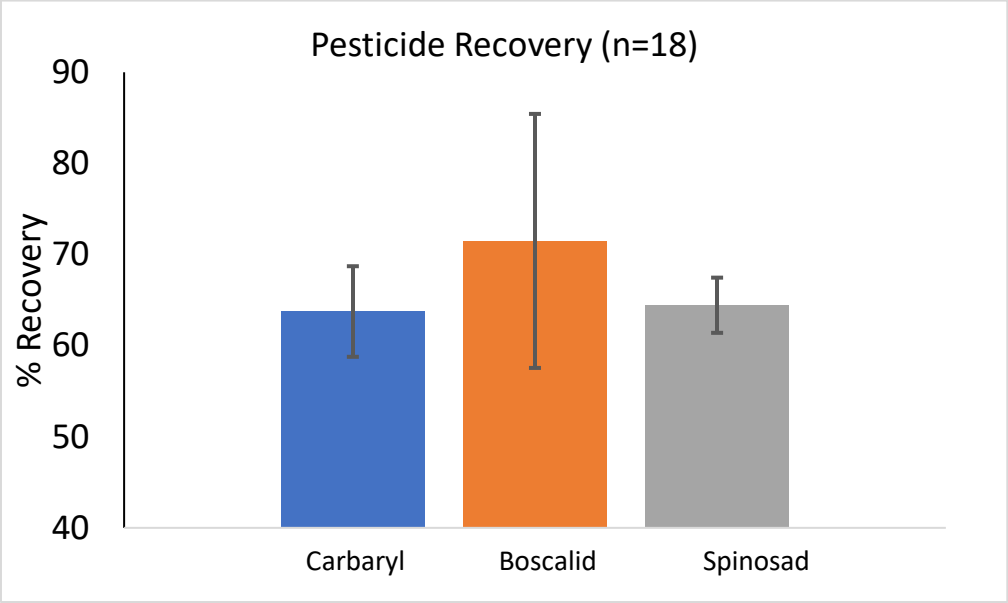

Figure 4.4.1: Percent recovery of carbaryl, boscalid, and Spinosad across all matrices and replicates (n=18, data is shown as the average ± relative standard deviation).

4.4.2 Pesticide spike recovery (matrix specific)

The overall (n=18) pesticide recovery had higher variability than matrices considered individually (n=3). This indicates that the matrix composition – for example, residual EtOH in the EtOH crude extract compared to unprocessed flower – influences pesticide recovery and thus availability for remediation. This is likely the result of greater solubility of pesticides in ethanol than acetonitrile, whereby residual ethanol in the samples increases the carrying capacity of pesticides in the solvent. The highest RSD for individual matrices per pesticide were 1.3%

(distillate), 4.1% (distillate), and 1.2% (flower, CO_2 crude, and bottoms) for carbaryl, boscalid, and Spinosad, respectively. The largest matrix-specific RSDs represented a 6.5%, 15.4%, and 3.5% improvement for carbaryl, boscalid, and Spinosad, respectively. Therefore, when preparing samples for LC separation, pesticide remediation must be considered on a matrix-specific basis, rather than a longitudinal one. The matrix-specific pesticide recoveries are shown in table 4.4.1.

Table 4.4.1: Average percent recovery and relative standard deviation of carbaryl, boscalid, and Spinosad for each of the six analytical matrices.

Sample (n=3)	Carbaryl	Boscalid	Spinosad
Flower	61.3 ± 0.4	60.2 ± 1.3	62.2 ± 1.2
Distillate	64.0 ±1.3	62.6 ± 4.1	66.3 ±0.2
Mother Liquor	62.8 ± 0.6	68.6 ± 0.5	65.5 ± 0.9
EtOH Crude	73.8 ± 1.1	96.9 ± 0.9	68.8 ± 1.1
CO_2 Crude	62.3 ± 0.4	59.7 ± 1.3	63.7 ±1.2
Bottoms	58.3 ±0.4	80.9 ± 1.3	60.0 ± 1.2

Greater pesticide recovery in the context of this work facilitates more efficient remediation by minimizing the number of PLC replicates per sample. The ethanolic crude extract had the greatest spike recovery for all three pesticides. In an industrial context, it may therefore be advantageous to target specific process matrices for pesticide remediation. A similar matrix-specific approach to cannabinoid purification is possible, although cannabinoid isolation is outside the scope of this work. Besides the uniformly high recovery in the ethanolic crude extract, it was observed that the distillation bottoms had a notably larger boscalid recovery (80.9%) compared to carbaryl and Spinosad (58.3% and 60.0%, respectively) within the same matrix. The matrix-specific pesticide recovery is shown in Figure 4.4.2.

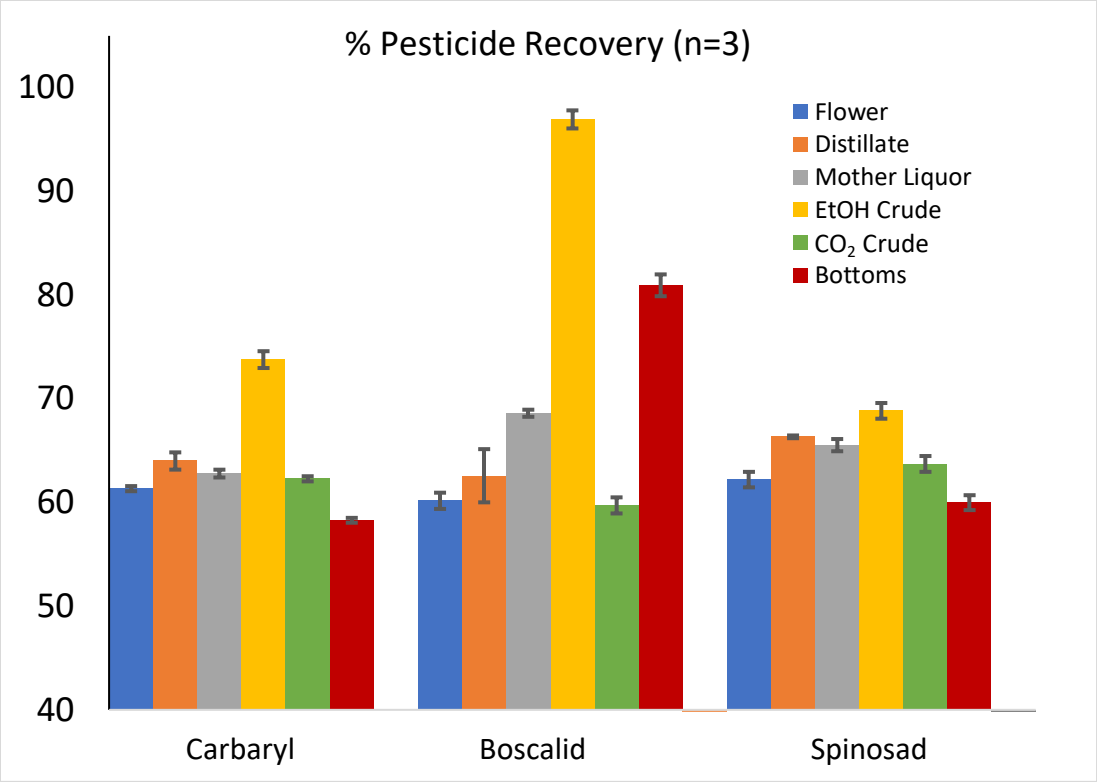

Figure 4.4.2: Matrix-specific recoveries of carbaryl, boscalid, and Spinosad (n=3 each. Data is shown as the average ± relative standard deviation).

4.4.3 Matrix cannabinoid profiles

Additionally, cannabinoids were qualitatively identified in each of the spiked hemp matrices. It was expected that the ratio of acid-form to decarboxylated cannabinoids will be observed in greatest proportion in the raw flower sample, because the biomass is heated prior to crude extraction. CBD/CBDA was observed in greatest relative abundance for each of the matrices except the distillation bottoms, where CBG occurs in greatest abundance. Representative chromatograms for each matrix are shown in Figure 4.4.3.

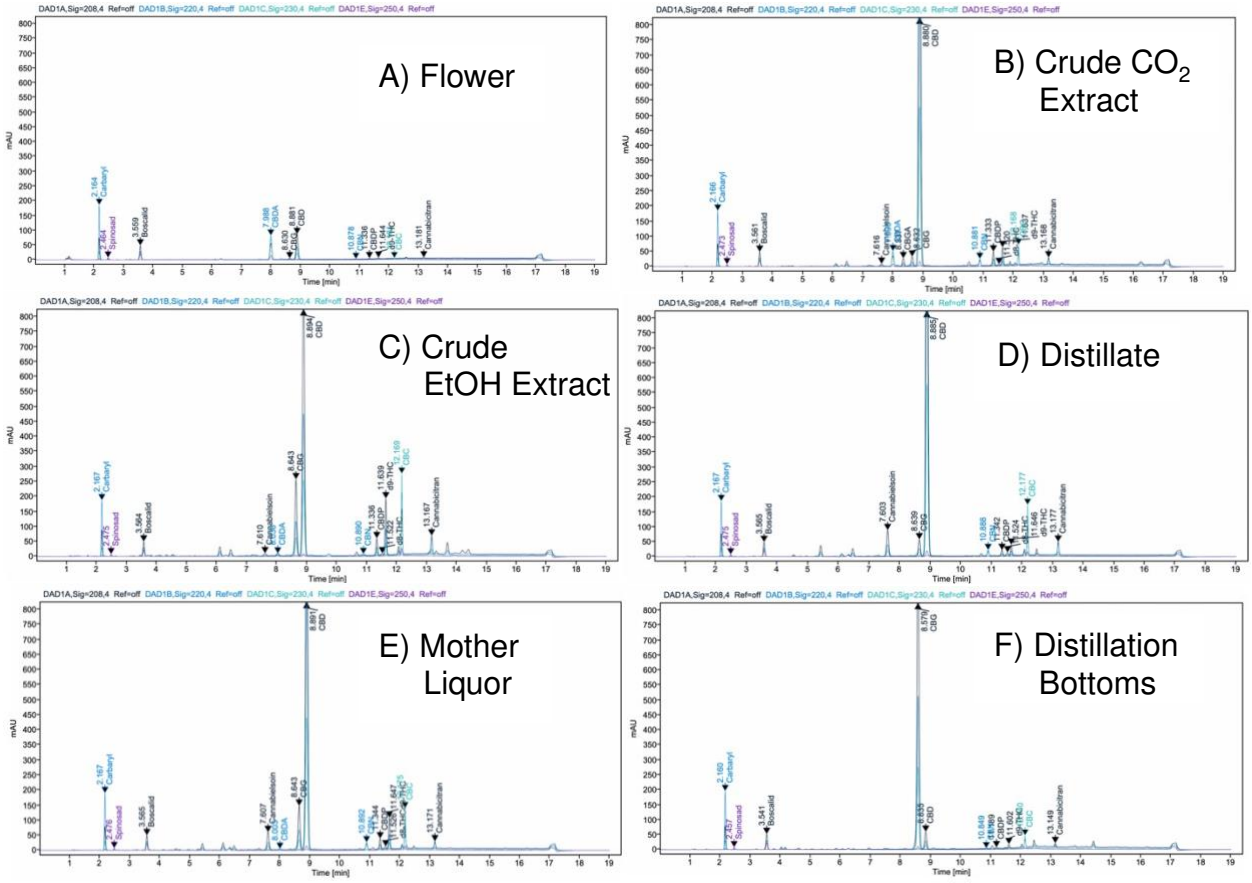

Figure 4.4.3: Representative chromatograms of A) raw flower, B) crude CO_2 extract, C) crude ethanol extract, D) CBD distillate, E) mother liquor, and F) distillation bottoms. The ratio of CBDA to CBD occurs in greatest proportion in the raw flower sample, because the biomass is decarboxylated with heat prior to crude extraction. CBD/CBDA was observed in greatest relative abundance for each of the matrices except the distillation bottoms, where CBG occurs in greatest abundance.

4.4.4 Analyte retention on 2.7 µm Poroshell C18

As expected, carbaryl, boscalid, and Spinosad eluted before the more hydrophobic cannabinoids during spike/recovery trials. Clothianidin, imidacloprid, carbaryl, olivetol, diuron, Spinosad, and myclobutanil eluted in the first 3.6 minutes, and all cannabinoids (except for 7-OH-CBD) eluted in the final 12.6 minutes of the 19-minute gradient for all matrices evaluated. Thus, the present method is suitable for 6/11 pesticides and 25/26 cannabinoids evaluated, by fractionating the first 19% of eluent to waste. Cannabinoid 7-OH-CBD, and pesticides

pyrethrins I and II, permethrin, and piperonyl butoxide will require additional purification steps following the present gradient. Retention times for all analytes are shown in table 4.4.2 and organized both alphabetically and by elution time.

Multiple peaks were observed in Pyrethrins, piperonyl butoxide, and permethrin standards. Structures of piperonyl butoxide, permethrin, and pyrethrins, are shown in Figure 4.4.3. Piperonyl butoxide is sold as a ≥ 95% liquid preparation and it is expected that additional peak is a formulation impurity. Permethrin is sold as a ≥ 95% mixture of isomers, and it's expected that the two observed peaks correspond to cis/trans isomers of the terminal allylic dichlorine motif. Pyrethrin is sold as a mixture of pyrethrins I and II. For cases where multiple peaks were observed, peaks were identified as A and B because their identities could not be deduced from the DAD data. I hypothesize that pyrethrin and piperonyl butoxide peak identities may be elucidated using the LC-QQQ method reported in Chapter 2. Permethrin cis/trans isomers may be elucidated using polarimetry detection.

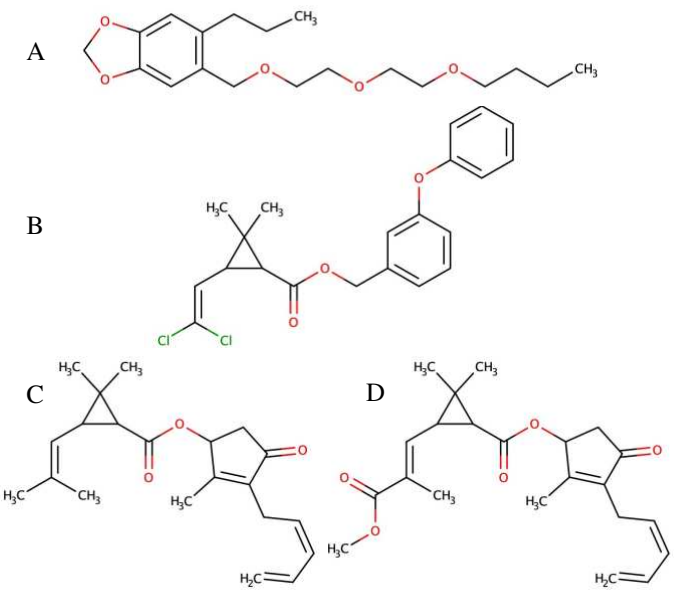

Figure 4.4.3: Molecular structures of standards with more than one eluting peak. A) piperonyl butoxide; secondary peak is likely formulation impurity. B) permethrin; secondary peaks are likely cis/trans isomers of the terminal allylic dichlorine motif. C) pyrethrin I and D) pyrethrin II are both present in the source material.

Table 4.4.2: Elution times for all analytes, organized alphabetically and by elution time. Clothianidin, imidacloprid, carbaryl, diuron, Spinosad, and myclobutanil elute before all cannabinoids and the present method is suitable for remediating them by fractionating the first 19% of eluent to waste.

	Analyte (Alphabetically)	*Retention Time (min)*	*Analyte (Elution order)*	*Retention Time (min)*
1	Δ8-THC	11.510	Clothianidin	1.451
2	Δ9-THC	11.610	Imidacloprid	1.492
3	Δ9-THCA	12.320	Carbaryl	2.160
4	Δ9-THCB	10.678	Olivetol	2.263
5	Δ9-THCH	12.331	Diuron	2.314
6	Δ9-THCP	12.915	Spinosad	2.480
7	Δ9-THCV	9.160	Myclobutanil	3.258
8	Δ9-THCVA	10.646	7-OH-CBD	3.441
9	7-OH-CBD	3.441	Boscalid	3.550
10	Boscalid	3.550	CBGV	6.440
11	Carbaryl	2.160	CBDV	6.490
12	CBC	12.180	CBGVA	6.500
13	CBCO	7.866	Pyrethrin Peak A	6.829
14	CBCVA	11.224	CBGQA	7.136
15	CBD	8.900	CBE	7.636
16	CBDA	8.000	CBCO	7.866
17	CBDA-ME	12.314	CBDA	8.000
18	CBDP	11.269	Pip. But. Peak A	8.327
19	CBDV	6.490	CBGA	8.340
20	CBE	7.636	CBG	8.704
21	CBG	8.704	CBD	8.900
22	CBGA	8.340	THCV	9.160
23	CBGQA	7.136	Pyrethrin Peak B	10.480
24	CBGV	6.440	THCVA	10.646
25	CBGVA	6.500	Δ9-THCB	10.678
26	CBL	12.098	CBN	10.900
27	CBN	10.900	CBCVA	11.224
28	CBTC	13.178	CBDP	11.269
29	Clothianidin	1.451	Δ8-THC	11.510
30	Diuron	2.314	Δ9-THC	11.610
31	Imidacloprid	1.492	Pip. But. Peak B	11.748
32	Myclobutanil	3.258	Permethrin Peak A	11.880
33	Olivetol	2.263	CBL	12.098
34	Permethrin Peak A	11.880	Permethrin Peak B	12.175
35	Permethrin Peak B	12.175	CBC	12.180
36	Pip. But. Peak A	8.327	CBDA-ME	12.314
37	Pip. But. Peak B	11.748	Δ9-THCA	12.320
38	Pyrethrin Peak A	6.829	Δ9-THCH	12.331
39	Pyrethrin Peak B	10.480	Δ9-THCP	12.915
40	Spinosad	2.480	CBTC	13.178

4.4.5 Preliminary tests on 10 µm Luna C18

Preliminary injections using larger particle size were done using 11-component pesticide, olivetol, and 26-component cannabinoid test samples. I evaluated all components, including those deemed unsuitable on the 2.7 µm column, for direct comparison between the two stationary phases. As of September 2022, development is ongoing. Analyte concentrations and scale were not normalized which causes the difference in peak size. Pesticide and cannabinoid elution profiles are similar to those in section 4.4.4, in that cannabinoids elute late in the gradient, and some pesticide peaks overlap with cannabinoids. Representative chromatograms are shown in Figure 4.4.4. Chromatograms A and B used the instrument method reported in section 4.4.4. The solvent front and first eluting species are shifted right in the chromatogram, caused by the 5 cm longer pathlength through the column. The large peak occurring at 11.1 min is likely unresolved late-eluting species such as CBTC and permethrin. Chromatograms C and D used a flow rate of 1.0 mL/min, causing peaks to elute earlier.

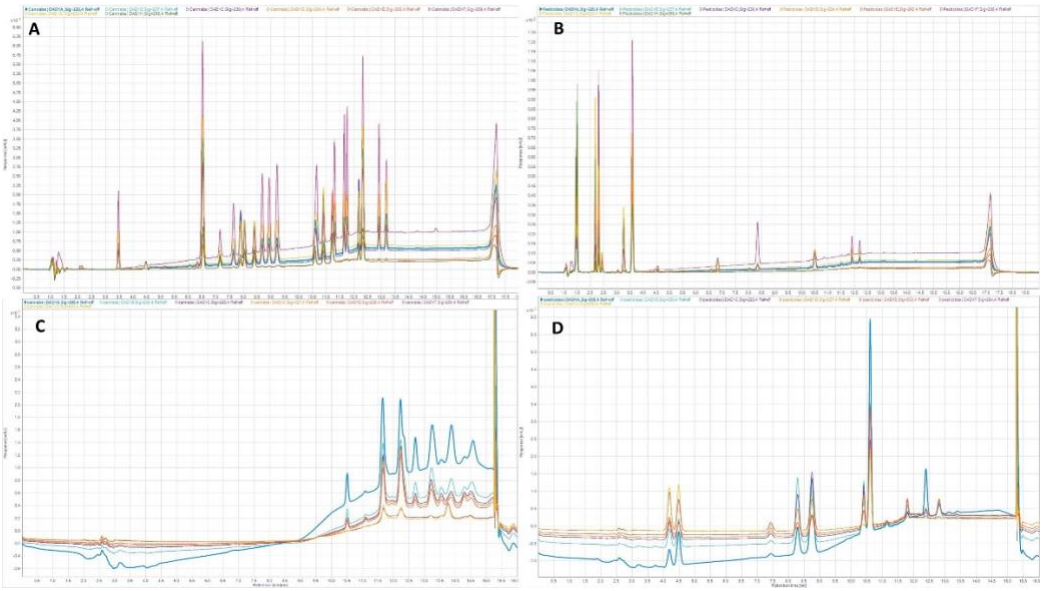

Figure 4.4.4: Representative chromatograms of cannabinoid (A and C) and pesticide (B and D) test samples. Chromatograms A and B used the instrument method reported in section 4.4.4. The large peak occurring at 11.1 min is likely unresolved late-eluting species such as CBTC and permethrin. Chromatograms C and D used a flow rate of 1.0 mL/min, causing peaks to elute earlier.

4.5 Conclusions

The present study evaluated retention times of 11 pesticides relative to 26 cannabinoids, plus the cannabinoid precursor molecule olivetol, for general suitability of remediation by eluent fractionation with PLC. Clothianidin, imidacloprid, carbaryl, olivetol, diuron, Spinosad, and myclobutanil eluted in the first 3.6 minutes, and all cannabinoids (except for 7-OH-CBD) eluted in the final 12.6 minutes of the 19-minute gradient for all matrices evaluated. Thus, the present method is suitable for simple fractionation of 6/11 pesticides and 25/26 cannabinoids evaluated on 2.7 µm C18 Poroshell media. 7-OH-CBD, pyrethrins I and II, permethrin, and piperonyl butoxide will require additional purification steps beyond the present gradient. Preliminary benchtop separations using 10 µm C18 stationary phase are ongoing but require further optimization prior to method transfer.

Carbaryl, boscalid, and Spinosad were spiked into six industrial cannabis processing matrices: flower, ethanol crude extract, CO_2 crude extract, distillate, distillation mother liquor, and distillation bottoms. Percent spike recoveries were calculated for all three pesticides, and it was observed that ethanolic crude extract had the largest recovery for all three pesticides, and the RSDs of spike recoveries of the individual matrices were significantly smaller compared to all samples. A key finding is that matrix composition must be considered when extracting samples for pesticide remediation. The possibility of completely removing pesticides while retaining cannabinoids and other high-value matrix components for further processing makes PLC a highly attractive strategy for separating cannabinoids in large volume and industrial manufacturing of cannabis products.

CHAPTER 5 – CONCLUDING REMARKS AND FUTURE DIRECTIONS

This dissertation reports on investigations into separations of cannabinoids and pesticides in the liquid phase. In Chapter 2, I developed an HPLC-QQQ method to simultaneously measure 25 cannabinoids and 9 pesticides using high-performance liquid chromatography coupled with tandem mass spectrometry. Two key outcomes of Chapter 2 are the capability of resolving Δ8- and Δ9-THC and increasing the number of cannabinoids and pesticides detected in a single HPLC-QQQ method. In Chapter 3, I report the first investigation on the use of a metal-organic framework, MIL-53(Al) for adsorptive separation of Δ9-THC, CBD, and CBN from an ideal system. The key outcome of Chapter 3 was that the MOF was not suitable because cannabinoids were size excluded from the internal surfaces and thus could not adsorb to much of the MOF surface area. In Chapter 4, I present benchtop-scale high performance liquid chromatographic (HPLC) separation of 26 cannabinoids and 11 pesticides, and evaluate spike extraction efficiency of pesticides boscalid, Spinosad, and carbaryl. It was observed during this work are the observation that ethanolic crude extract had the largest recovery for all three pesticides, the RSDs of spike recoveries of the individual matrices were significantly smaller compared to all samples – indicating matrix composition must be considered when extracting samples for pesticide remediation. The benchtop method is suitable for simple fractionation of 6/11 pesticides and 25/26 cannabinoids evaluated. 7-OH-CBD (RT: 3.4 min), pyrethrins I and II (RT_A: 6.8 min, RT_B: 10.5 min), permethrin (RT_A: 11.9 min, RT_B: 12.2 min), and piperonyl butoxide (RT_A: 8.3 min, RT_B: 11.7 min), will require additional purification steps beyond the present gradient.

In future work, the HPLC-QQQ method reported in Chapter 2 is validated in neat solvent, but additional sample clean up and development of a suitable calibration matrix are necessary prior to accurate quantitation and method validation for cannabis samples. Advancing adsorptive separation studies of cannabinoids or pesticides using MOFs reported in Chapter 3 will require a different MOF with larger pore aperture than MIL-53(Al). Ideally, a MOF with the same solvothermal stability as MIL-53(Al), which may require development of new synthetic methods in our research group. Preliminary experiments for benchtop-scale separations reported in Chapter 4 using 10 µm C18 stationary phase are ongoing but require further optimization prior to method transfer to preparative-scale.

A critique of the work reported in this dissertation is that additional time spent during experimental design may have readily facilitated deeper insights into the experimental systems. For example, the use of an external calibration in neat solvent may be intuitively eliminated from use because of the known complexity and potential for matrix interference in cannabis samples. Use of standard addition or internal standards may be more suitable than external standard calibration since an ideal matrix blank is not readily available. Development and qualification of an analogous calibration matrix such as hops could produce a transferable calibration to analyze cannabis samples and would represent a direct improvement on reported methods. However, having performed this work and observed difficulties associated with the matrix extraction using QuECHERS extraction followed by filtration through 0.2 µm PTFE, method development may have been streamlined by using standard addition from the outset. Standard addition alone would not address issues with noise or interference from concomitant species but would more appropriately account for matrix composition in the calibration. Future work using standard

addition calibration would likely greatly improve the reproducibility and transferability of the method.

Experiments for chapter 3 were designed based on prior experience using a metal-organic framework to adsorptively remove uremic toxins - specifically, *p*-cresyl sulfate - from solution with the end goal of using it for dialysis. A critique of the work reported in chapter 3 is that the radii of gyration and pore apertures discussed in section 3.4.4 could have been calculated without benchtop chemistry. The outcomes of experiments reported in chapter 3 clearly support an adsorption model where the internal surface area of the metal-organic frameworks is not accessible to the adsorbate, and the computational data may have been enough to refute adsorption model 1. However, computational data was performed on the back end of this work to evaluate the likelihood of experimental data. There are ample reports in the literature that purport suitability of metal-organic frameworks as adsorptive materials for uremic toxin remediation, which implies a similar suitability may be expected for cannabinoid uptake. The finding that adsorptive uptake by MIL-53(Al) is size-limited contradicts a vast body of work. Thus, experimental trials of the adsorption system were justified at the project outset. Moving forward in future work, the size-limited adsorption findings should be considered at the project outset.

The work reported in chapter 4 may be similarly critiqued as chapter 2, whereby the retention times of pesticides may be rationally predicted without experimentation. Molecular polarity is a parameter that can be computed beforehand, and the relative polarities of cannabinoids and pesticides could be used to estimate relative elution order of analytes prior to experiment. The 11 pesticides evaluated in chapter 4 were selected because of their varying structures and functionalization, but experimental determination of exact retention times may not

be critical to understanding the relative suitability of the method for remediating pesticides from cannabis samples. This is a valid critique and future studies should include a computation of analyte polarity prior to analysis.

A second critique of work reported in chapter 4 is that relative retention times are expected to be congruent for a given set of analytes with the same stationary and mobile phase compositions. A 7.3 µm particle size difference of an octyldecylsilane stationary phase will likely have different resolving power and different retention times due to differences in stationary phase surface area, but the separation is driven by the same relative intermolecular forces in either column. In response to this second critique of chapter 4, an alternative experimental design where the composition of stationary phase is varied with a constant particle size. Analyte separation is driven by partitioning between the stationary and mobile phase, so differences in the stationary phase would be expected to change the elution behavior of analytes on the column. Again, the polarity of analytes could be used to estimate the relative retention of analytes on the column, but experimental observation may be more justified than for the system reported in chapter 4.

The methods described in this dissertation have been developed with the objective of direct transferability to industry laboratories. The majority detection method in an industrial setting is diode-array detection because of the low relative abundances of most cannabinoids relative to Δ9-THC(A) and CBD(A). DAD has a lower operational cost compared to tandem mass spectrometry, so cost may be a gendarme to transferring QQQ methods from chapters 2 and 3 to industry, compared to the benchtop DAD method in chapters 3 and 4. Additional sample preparation steps will be necessary – as discussed previously in chapter 5 – as well as method validation prior to method transfer to outside labs. One approach could be to use a single

laboratory validation protocol in-house, verified on a secondary system on CSU's campus, then verified on an off-site system by different researchers in order to demonstrate the robustness of the method.[63] Once the calibration and robustness are verified, the method can be fortified via the implementation of QC check and limit of quantitation standards into the standard protocol. Completion of these validation protocols and method checks will greatly enhance the generalizability and transferability of the methods described in this dissertation.

The industrial value of this work lies both in the analytical improvements previously discussed but also in the commercial outcomes. Our collaborators at Panacea Life Sciences quoted the current price of crude hemp extract at $5,000/kg, CBD isolate at $10,000/kg, and Δ9-THCV isolate at $40,000/kg. Cannabis extracts contaminated with pesticides represent a serious financial burden to manufacturers, and a robust pesticide remediation method such as that modeled in chapter 4 of this dissertation would allow companies to recover capital that would otherwise lost. The ability to target minor cannabinoids in cannabis matrices and quantify their abundance makes production forecasting easier and potentially reduces overage costs. The ability to then isolate those minor cannabinoids for sale or research purposes is a powerful tool for driving profits and enables new frontiers in cannabinoid research by supplying raw materials for clinical trials. Sample preparation methods described in chapters 2 and 4 use 20 mL of solvent and milligrams of sample – the associated costs and quantities used are dwarfed in comparison to the production scale, and the commercial value of the final products.

Briefly summarized, future iterations and expansion of this work will benefit from a focus on optimized sample preparation, understanding that a benchtop-to-preparative scale drives the commercializability of this work. The finding in Chapter 2 that sample composition influences the pesticide extraction efficiency can likely be extended to cannabinoids as well.

Cannabinoids have a greater solubility in ethanol compared to acetonitrile, so a liquid-liquid sample extraction using ethanol may improve recoveries. I tried this during method development with the QuECHERS materials I've reported and found that the solubility of ethanol in salt-saturated water was such that a biphasic extraction was not observed. There may be other solvent combinations or clarifying methods possible that I did not try. Solvent removal following preparative extraction should also be considered. Using ethanol instead of ACN may reduce post-separation hazards due to the relative toxicity of the two solvents. Recovered fractions of sample plus acidified acetonitrile/water may pose difficulties for solvent removal. The researcher should also consider the toxicity of the acid used if the isolated product is to then be sold for consumption. Food-grade phosphoric acid is used in Coca-Cola, but may be less desirable in a cannabis context. A potential alternative would be acetic acid but issues with odor/taste may be a factor. These are long-term applications beyond the fundamental scope of a dissertation but are relevant to the industrial significance of such research.

One interesting direction for the HPLC methods described in this work would be to track cannabinoid content through the course of processing. Each step, from decarboxylation to extraction to distillation to isolation, will inherently involve some loss. What is the loss associated with each step? Cannabinoids vaporize at different temperatures, so does decarboxylation pre-crude extraction cause some high-value cannabinoids to be lost? Does decarboxylation or distillation in the presence of oxygen increase Δ9-THC oxidation to CBN? If samples are homogenized with heat in a sonicator prior to HPLC analysis, does that cause measurement bias resulting from heat-driven analyte decomposition? Can CBGV, CBDV, CBGA, and CBDA be more easily resolved and isolated using a different stationary phase?

The size-limitation of MOF-mediated adsorption may be inappropriate for cannabinoids, but not necessarily for smaller concomitants in the cannabis matrix. Volatile isoprene and monoterpenes are smaller than the triterpenophilic cannabinoids and may be adsorbed in the gas phase, and research into storage or isolation of these smaller compounds may still be possible. Studies, including those reported by our group, have shown that MOFs can remove heavy metals from solution. MOF-mediated heavy-metal capture in cannabis is a potentially advantageous approach, given that cannabinoid molecules are unlikely to diffuse into the framework, thus remediating heavy metals while preserving the cannabinoid content of the source material. Obviously, the pore dimensions and MOF properties would be a crucial component in this study, and concomitant molecules in the sample may interfere with uptake by clogging the MOF pores. However, if this approach were to work, it would be similarly valuable to the cannabis industry to have a remediation method for metal ions that cannot be remediated using PLC.

BIBLIOGRAPHY

(1) Brenneisen, R. Chemistry and Analysis of Phytocannabinoids and Other Cannabis Constituents. In *Marijuana and the Cannabinoids*; El Sohly, M. A., Ed.; Forensic Science And Medicine; Humana Press: Totowa, NJ, 2007; pp 17–49. https://doi.org/10.1007/978-1-59259-947-9_2.

(2) *Cannabis and Culture*; Rubin, V. D., Ed.; World anthropology; Mouton [u.a.]: The Hague, 1975.

(3) Long, T.; Wagner, M.; Demske, D.; Leipe, C.; Tarasov, P. E. Cannabis in Eurasia: Origin of Human Use and Bronze Age Trans-Continental Connections. *Veg. Hist. Archaeobotany* **2017**, *26* (2), 245–258. https://doi.org/10.1007/s00334-016-0579-6.

(4) Li, H.-L. An Archaeological and Historical Account of Cannabis in China. *Econ. Bot.* **1974**, *28* (4), 437–448.

(5) Shiner, M. Drug Policy Reform and the Reclassification of Cannabis in England and Wales: A Cautionary Tale. *Int. J. Drug Policy* **2015**, *26* (7), 696–704. https://doi.org/10.1016/j.drugpo.2015.03.009.

(6) Decorte, T.; Potter, G. R. The Globalization of Cannabis Cultivation: A Growing Challenge. *Int. J. Drug Policy* **2015**, *26* (3), 221–225. https://doi.org/10.1016/j.drugpo.2014.12.011.

(7) Gould, J. The Cannabis Crop. *Nature* **2015**, *525* (7570), S2–S3. https://doi.org/10.1038/525S2a.

(8) *Marijuana Sales Reports | Department of Revenue*. https://cdor.colorado.gov/data-and-reports/marijuana-data/marijuana-sales-reports (accessed 2022-09-04).

(9) *Phytocannabinoids: Unraveling the Complex Chemistry and Pharmacology of Cannabis Sativa*; Kinghorn, A. D., Falk, H., Gibbons, S., Kobayashi, J., Eds.; Progress in the Chemistry of Organic Natural Products; Springer International Publishing: Cham, 2017; Vol. 103. https://doi.org/10.1007/978-3-319-45541-9.

(10) Cascio, M. G.; Pertwee, R. G.; Marini, P. The Pharmacology and Therapeutic Potential of Plant Cannabinoids. In *Cannabis sativa L. - Botany and Biotechnology*; Chandra, S., Lata, H., El Sohly, M. A., Eds.; Springer International Publishing: Cham, 2017; pp 207–225. https://doi.org/10.1007/978-3-319-54564-6_9.

(11) Breijyeh, Z.; Jubeh, B.; Bufo, S. A.; Karaman, R.; Scrano, L. Cannabis: A Toxin-Producing Plant with Potential Therapeutic Uses. *Toxins* **2021**, *13* (2), 117. https://doi.org/10.3390/toxins13020117.

(12) Grotenhermen, F.; Russo, E. *Cannabis and Cannabinoids: Pharmacology, Toxicology, and Therapeutic Potential*; Psychology Press, 2002.

(13) Borowska, M.; Czarnywojtek, A.; Sawicka-Gutaj, N.; Woliński, K.; Płazińska, M. T.; Mikołajczak, P.; Ruchała, M. The Effects of Cannabinoids on the Endocrine System. *Endokrynol. Pol.* **2018**, *69* (6), 705–719. https://doi.org/10.5603/EP.a2018.0072.

(14) Howlett, A. C. Pharmacology of Cannabinoid Receptors. *Annu. Rev. Pharmacol. Toxicol.* **1995**, *35*, 607-34.

(15) McRae, G.; Melanson, J. E. Quantitative Determination and Validation of 17 Cannabinoids in Cannabis and Hemp Using Liquid Chromatography-Tandem Mass Spectrometry. *Anal. Bioanal. Chem.* **2020**, *412* (27), 7381–7393. https://doi.org/10.1007/s00216-020-02862-8.

(16) Atapattu, S. N.; Johnson, K. R. D. Pesticide Analysis in Cannabis Products. *J. Chromatogr. A* **2020**, *1612*, 460656. https://doi.org/10.1016/j.chroma.2019.460656.

(17) Pinkhasova, D. V.; Jameson, L. E.; Conrow, K. D.; Simeone, M. P.; Davis, A. P.; Wiegers, T. C.; Mattingly, C. J.; Leung, M. C. K. Regulatory Status of Pesticide Residues in Cannabis: Implications to Medical Use in Neurological Diseases. *Curr. Res. Toxicol.* **2021**, *2*, 140–148. https://doi.org/10.1016/j.crtox.2021.02.007.

(18) Walters, K. M.; Fisher, G. G.; Tenney, L. An Overview of Health and Safety in the Colorado Cannabis Industry. *Am. J. Ind. Med.* **2018**, *61* (6), 451–461. https://doi.org/10.1002/ajim.22834.

(19) Subritzky, T.; Pettigrew, S.; Lenton, S. Into the Void: Regulating Pesticide Use in Colorado's Commercial Cannabis Markets. *Int. J. Drug Policy* **2017**, *42*, 86–96. https://doi.org/10.1016/j.drugpo.2017.01.014.

(20) Geesaman, J. Code of Colorado Regulations. Marijuana Enforcement Division – Medical Marijuana Rules. 1 CCR 212-1. https://www.sos.state.co.us/CCR/GenerateRulePdf.do?ruleVersionId=7094&fileName=1%20CCR%20212-1 accessed 10/31/2022.

(21) *Pesticide Use in Cannabis Production Information: Pesticides Allowed for Use on Cannabis*; Colorado Department of Agriculture, 2022; pp 1–47.

(22) Nahar, L.; Onder, A.; Sarker, S. D. A Review on the Recent Advances in HPLC, UHPLC and UPLC Analyses of Naturally Occurring Cannabinoids (2010–2019). *Phytochem. Anal.* **2020**, *31* (4), 413–457. https://doi.org/10.1002/pca.2906.

(23) Nie, B.; Henion, J.; Ryona, I. The Role of Mass Spectrometry in the Cannabis Industry. *J. Am. Soc. Mass Spectrom.* **2019**, *30* (5), 719–730. https://doi.org/10.1007/s13361-019-02164-z.

(24) Elkins, A. C.; Deseo, M. A.; Rochfort, S.; Ezernieks, V.; Spangenberg, G. Development of a Validated Method for the Qualitative and Quantitative Analysis of Cannabinoids in Plant Biomass and Medicinal Cannabis Resin Extracts Obtained by Super-Critical Fluid Extraction. *J. Chromatogr. B* **2019**, *1109*, 76–83. https://doi.org/10.1016/j.jchromb.2019.01.027.

(25) Zivovinovic, S.; Alder, R.; Allenspach, M. D.; Steuer, C. Determination of Cannabinoids in Cannabis Sativa L. Samples for Recreational, Medical, and Forensic Purposes by Reversed-Phase Liquid Chromatography-Ultraviolet Detection. *J. Anal. Sci. Technol.* **2018**, *9* (1), 27. https://doi.org/10.1186/s40543-018-0159-8.

(26) Mudge, E. M.; Murch, S. J.; Brown, P. N. Leaner and Greener Analysis of Cannabinoids. *Anal. Bioanal. Chem.* **2017**, *409* (12), 3153–3163. https://doi.org/10.1007/s00216-017-0256-3.

(27) Fathordoobady, F.; Singh, A.; Kitts, D. D.; Pratap Singh, A. Hemp (Cannabis Sativa L.) Extract: Anti-Microbial Properties, Methods of Extraction, and Potential Oral Delivery. *Food Rev. Int.* **2019**, *35* (7), 664–684. https://doi.org/10.1080/87559129.2019.1600539.

(28) List, A.; Nazar, B.; Nyquist, S.; Harclerode, J. The Effects of Δ9-Tetrahydrocannabinol and Cannabidiol on the Metabolism of Gonadal Steroids in the Rat. *Ism Dispos.* **1977**, *5* (3), 268–272.

(29) Harclerode, J.; Nyquist, S. E.; Nazar, B.; Lowe, D. EFFECTS OF CANNABIS ON SEX HORMONES AND TESTICULAR ENZYMES OF THE RODENT. In *Marihuana Biological Effects*; Elsevier, 1979; pp 395–405. https://doi.org/10.1016/B978-0-08-023759-6.50035-4.

(30) Marchioni, C.; de Souza, I. D.; Acquaro, V. R.; de Souza Crippa, J. A.; Tumas, V.; Queiroz, M. E. C. Recent Advances in LC-MS/MS Methods to Determine Endocannabinoids in Biological Samples: Application in Neurodegenerative Diseases. *Anal. Chim. Acta* **2018**, *1044*, 12–28. https://doi.org/10.1016/j.aca.2018.06.016.

(31) Rustichelli, C.; Ferioli, V.; Baraldi, M.; Zanoli, P.; Gamberini, G. Analysis of Cannabinoids in Fiber Hemp Plant Varieties (Cannabis Sativa L.) by High-Performance Liquid Chromatography. *Chromatographia* **1998**, *48* (3–4), 215–222. https://doi.org/10.1007/BF02467674.

(32) Lee, J. H.; Min, A. Y.; Han, J. H.; Yang, Y. J.; Kim, H.; Shin, D. Development and Validation of LC-MS/MS Method with QuEChERS Clean-up for Detecting Cannabinoids in Foods and Dietary Supplements. *Food Addit. Contam. Part Chem. Anal. Control Expo. Risk Assess.* **2020**, *37* (9), 1413–1424. https://doi.org/10.1080/19440049.2020.1769200.

(33) Bączek, T.; Kaliszan, R.; Novotná, K.; Jandera, P. Comparative Characteristics of HPLC Columns Based on Quantitative Structure–Retention Relationships (QSRR) and

Hydrophobic-Subtraction Model. *J. Chromatogr. A* **2005**, *1075* (1–2), 109–115. https://doi.org/10.1016/j.chroma.2005.03.117.

(34) Pourseyed Lazarjani, M.; Torres, S.; Hooker, T.; Fowlie, C.; Young, O.; Seyfoddin, A. Methods for Quantification of Cannabinoids: A Narrative Review. *J. Cannabis Res.* **2020**, *2* (1), 35. https://doi.org/10.1186/s42238-020-00040-2.

(35) Luca, S. V.; Braumann, L.; Gerigk, M.; Frank, O.; Minceva, M. Separation of Minor Cannabinoids from Hemp Extract with Trapping Multiple Dual Mode Liquid-Liquid Chromatography. *J. Chromatogr. A* **2021**, *1658*, 462608. https://doi.org/10.1016/j.chroma.2021.462608.

(36) Felletti, S.; De Luca, C.; Buratti, A.; Bozza, D.; Cerrato, A.; Capriotti, A. L.; Laganà, A.; Cavazzini, A.; Catani, M. Potency Testing of Cannabinoids by Liquid and Supercritical Fluid Chromatography: Where We Are, What We Need. *J. Chromatogr. A* **2021**, *1651*, 462304. https://doi.org/10.1016/j.chroma.2021.462304.

(37) Wittayanan, W.; Chaimongkol, T. Determination of Pesticides Residue in Cannabis, Cannabis Extract and Cannabis Oil by Gas Chromatography Tandem Mass Spectrometry Technique. *Pharm. Sci. Asia* **2021**, *48* (4), 354–366. https://doi.org/10.29090/psa.2021.04.20.107.

(38) McPartland, J. M.; McKernan, K. J. Contaminants of Concern in Cannabis: Microbes, Heavy Metals and Pesticides. In *Cannabis sativa L. - Botany and Biotechnology*; Chandra, S., Lata, H., El Sohly, M. A., Eds.; Springer International Publishing: Cham, 2017; pp 457–474. https://doi.org/10.1007/978-3-319-54564-6_22.

(39) *Endocannabinoids*; Pertwee, R. G., Ed.; Handbook of Experimental Pharmacology; Springer International Publishing: Cham, 2015; Vol. 231. https://doi.org/10.1007/978-3-319-20825-1.

(40) *Marijuana and the Cannabinoids*; El Sohly, M. A., Ed.; Forensic science and medicine; Humana Press: Totowa, N.J, 2007.

(41) Meah, F.; Lundholm, M.; Emanuele, N.; Amjed, H.; Poku, C.; Agrawal, L.; Emanuele, M. A. The Effects of Cannabis and Cannabinoids on the Endocrine System. *Rev. Endocr. Metab. Disord.* **2022**, *23* (3), 401–420. https://doi.org/10.1007/s11154-021-09682-w.

(42) Calò, L.; Anzillotti, L.; Maccari, C.; Cecchi, R.; Andreoli, R. Validation of a Bioanalytical Method for the Determination of Synthetic and Natural Cannabinoids (New Psychoactive Substances) in Oral Fluid Samples by Means of HPLC-MS/MS. *Front. Chem.* **2020**, *8*.

(43) *phyto- | Meaning of prefix phyto- by etymonline*. https://www.etymonline.com/word/phyto- (accessed 2022-09-04).

(44) *endo- | Meaning of prefix endo- by etymonline*. https://www.etymonline.com/word/endo- (accessed 2022-09-04).

(45) Raber, J. C.; Elzinga, S.; Kaplan, C. Understanding Dabs: Contamination Concerns of Cannabis Concentrates and Cannabinoid Transfer during the Act of Dabbing. *J. Toxicol. Sci.* **2015**, *40* (6), 797–803. https://doi.org/10.2131/jts.40.797.

(46) Kazakevich, Y. V. Department of Chemistry and Biochemistry, Seton Hall University, South Orange, NJ 07079, USA. 32.

(47) Molnár, I. Searching for Robust HPLC Methods – Csaba Horváth and the Solvophobic Theory. *Chromatographia* **2005**, *62* (S13), s7–s17. https://doi.org/10.1365/s10337-005-0645-1.

(48) Fekete, S.; Sadat-Noorbakhsh, V.; Schelling, C.; Molnár, I.; Guillarme, D.; Rudaz, S.; Veuthey, J.-L. Implementation of a Generic Liquid Chromatographic Method Development Workflow: Application to the Analysis of Phytocannabinoids and Cannabis Sativa Extracts. *J. Pharm. Biomed. Anal.* **2018**, *155*, 116–124. https://doi.org/10.1016/j.jpba.2018.03.059.

(49) Zotou, A. An Overview of Recent Advances in HPLC Instrumentation. *Open Chem.* **2012**, *10* (3), 554–569. https://doi.org/10.2478/s11532-011-0161-0.

(50) Neue, U. D.; Kele, M. Performance of Idealized Column Structures under High Pressure. *J. Chromatogr. A* **2007**, *1149* (2), 236–244. https://doi.org/10.1016/j.chroma.2007.03.042.

(51) Papadoyannis, IoannisN.; Samanidou, VictoriaF. Validation of HPLC Instrumentation#. *J. Liq. Chromatogr. Relat. Technol.* **2004**, *27* (5), 753–783. https://doi.org/10.1081/JLC-120029697.

(52) Dong, M. W. *HPLC and UHPLC for Practicing Scientists*; John Wiley & Sons, Incorporated: Newark, UNITED STATES, 2019.

(53) Kazakevich, Y. V. High-Performance Liquid Chromatography Retention Mechanisms and Their Mathematical Descriptions. *J. Chromatogr. A* **2006**, *1126* (1–2), 232–243. https://doi.org/10.1016/j.chroma.2006.05.022.

(54) Unger, K. K.; Liapis, A. I. Adsorbents and Columns in Analytical High-Performance Liquid Chromatography: A Perspective with Regard to Development and Understanding. *J. Sep. Sci.* **2012**, *35* (10–11), 1201–1212. https://doi.org/10.1002/jssc.201200042.

(55) Moldoveanu, S. C.; Caiali, E.; David, V. Results from Solvophobic Theory Applied to Methylene Selectivity in Reversed-Phase HPLC. *J. Liq. Chromatogr. Relat. Technol.* **2018**, *41* (1), 24–32. https://doi.org/10.1080/10826076.2017.1410708.

(56) Snyder, L. R.; Kirkland, J. J.; Dolan, J. W. Appendix I: Properties of HPLC Solvents. In *Introduction to Modern Liquid Chromatography*; John Wiley & Sons, Ltd, 2010; pp 879–886. https://doi.org/10.1002/9780470508183.app1.

(57) Sun, L.; Jin, H.; Tian, R.; Wang, M.; Liu, L.; Ye, L.; Zuo, T.; Ma, S. A Simple Method for HPLC Retention Time Prediction: Linear Calibration Using Two Reference Substances. *Chin. Med.* **2017**, *12* (1), 16. https://doi.org/10.1186/s13020-017-0137-x.

(58) Kaliszan, R.; Wiczling, P.; Markuszewski, M. J. PH Gradient Reversed-Phase HPLC. *Anal. Chem.* **2004**, *76* (3), 749–760. https://doi.org/10.1021/ac034999v.

(59) Hazekamp, A.; Peltenburg, A.; Verpoorte, R.; Giroud, C. Chromatographic and Spectroscopic Data of Cannabinoids from Cannabis Sativa L. *J. Liq. Chromatogr. Relat. Technol.* **2005**, *28* (15), 2361–2382. https://doi.org/10.1080/10826070500187558.

(60) Neue, U. D. *HPLC Columns: Theory, Technology, and Practice*, 1st ed.; Wiley-VCH, Inc., 1997.

(61) Skoog, D.; Holler, F.; Crouch, S. *Principles of Instrumental Analysis, 6th Edition*; 2014.

(62) Parriott, D. *A Practical Guide to HPLC Detection*, 1st ed.; Academic Press, Inc., 1993.

(63) Horwitz, W. AOAC Guidelines for Single Laboratory Validation of Chemical Methods for Dietary Supplements and Botanicals. 2002-12-19. https://s27415.pcdn.co/wp-content/uploads/2020/01/64ER20-7/Validation_Methods/d-AOAC_Guidelines_For_Single_Laboratory_Validation_Dietary_Supplements_and_Botanicals.pdf accessed 10/31/2022.

(64) Dolan, J. W. How Does It Work? Part IV: Ultraviolet Detectors. *LCGC N. Am.* **2016**, *34* (8), 534–539.

(65) Silberberg, M. *Principles of General Chemistry*, 1st ed.; 2007.

(66) Agilent Technologies. Agilent InfinityLab LC Series 1260 Infinity II Quaternary System Manual and Quick Guide, 2016.

(67) Agilent Technologies. Agilent 6460 Triple Quad Mass Spectrometer (6460) System Concepts Guide; The Big Picture, 2016.

(68) Cuchiaro, H.; Thai, J.; Schaffner, N.; Tuttle, R. R.; Reynolds, M. Exploring the Parameter Space of *p* -Cresyl Sulfate Adsorption in Metal–Organic Frameworks. *ACS Appl. Mater. Interfaces* **2020**, *12* (20), 22572–22580. https://doi.org/10.1021/acsami.0c04203.

(69) Furukawa, H.; Cordova, K. E.; O'Keeffe, M.; Yaghi, O. M. The Chemistry and Applications of Metal-Organic Frameworks. *Science* **2013**, *341* (6149), 1230444–1230444. https://doi.org/10.1126/science.1230444.

(70) How Many MOFs Are There in the CSD? https://s27415.pcdn.co/wp-content/uploads/2020/01/64ER20-7/Validation_Methods/d-AOAC_Guidelines_For_Single_Laboratory_Validation_Dietary_Supplements_and_Botanicals.pdf Accessed 10/31/2022.

(71) Millward, A. R.; Yaghi, O. M. Metal−Organic Frameworks with Exceptionally High Capacity for Storage of Carbon Dioxide at Room Temperature. *J. Am. Chem. Soc.* **2005**, *127* (51), 17998–17999. https://doi.org/10.1021/ja0570032.

(72) Farha, O. K.; Eryazici, I.; Jeong, N. C.; Hauser, B. G.; Wilmer, C. E.; Sarjeant, A. A.; Snurr, R. Q.; Nguyen, S. T.; Yazaydın, A. Ö.; Hupp, J. T. Metal–Organic Framework Materials with Ultrahigh Surface Areas: Is the Sky the Limit? *J. Am. Chem. Soc.* **2012**, *134* (36), 15016–15021. https://doi.org/10.1021/ja3055639.

(73) Loiseau, T.; Serre, C.; Huguenard, C.; Fink, G.; Taulelle, F.; Henry, M.; Bataille, T.; Férey, G. A Rationale for the Large Breathing of the Porous Aluminum Terephthalate (MIL-53) Upon Hydration. *Chem. – Eur. J.* **2004**, *10* (6), 1373–1382. https://doi.org/10.1002/chem.200305413.

(74) Li, J.-R.; Sculley, J.; Zhou, H.-C. Metal–Organic Frameworks for Separations. *Chem. Rev.* **2012**, *112* (2), 869–932. https://doi.org/10.1021/cr200190s.

(75) Tuttle, R. R.; Rubin, H. N.; Rithner, C. D.; Finke, R. G.; Reynolds, M. M. Copper Ion vs Copper Metal–Organic Framework Catalyzed NO Release from Bioavailable S-Nitrosoglutathione En Route to Biomedical Applications: Direct 1H NMR Monitoring in Water Allowing Identification of the Distinct, True Reaction Stoichiometries and Thiol Dependencies. *J. Inorg. Biochem.* **2019**, *199*, 110760. https://doi.org/10.1016/j.jinorgbio.2019.110760.

(76) Liu, S.-S.; Yang, C.-X.; Wang, S.-W.; Yan, X.-P. Metal–Organic Frameworks for Reverse-Phase High-Performance Liquid Chromatography. *The Analyst* **2012**, *137* (4), 816–818. https://doi.org/10.1039/C2AN15925B.

(77) Agrawal, M.; Bhattacharyya, S.; Huang, Y.; Jayachandrababu, K. C.; Murdock, C. R.; Bentley, J. A.; Rivas-Cardona, A.; Mertens, M. M.; Walton, K. S.; Sholl, D. S.; Nair, S. Liquid-Phase Multicomponent Adsorption and Separation of Xylene Mixtures by Flexible MIL-53 Adsorbents. *J. Phys. Chem. C* **2018**, *122* (1), 386–397. https://doi.org/10.1021/acs.jpcc.7b09105.

(78) Yang, C.-X.; Liu, S.-S.; Wang, H.-F.; Wang, S.-W.; Yan, X.-P. High-Performance Liquid Chromatographic Separation of Position Isomers Using Metal–Organic Framework MIL-

53(Al) as the Stationary Phase. *The Analyst* **2012**, *137* (1), 133–139. https://doi.org/10.1039/C1AN15600D.

(79) Rallapalli, P.; Patil, D.; Prasanth, K. P.; Somani, R. S.; Jasra, R. V.; Bajaj, H. C. An Alternative Activation Method for the Enhancement of Methane Storage Capacity of Nanoporous Aluminium Terephthalate, MIL-53(Al). *J. Porous Mater.* **2010**, *17* (5), 523–528. https://doi.org/10.1007/s10934-009-9320-5.

(80) Patil, D. V.; Rallapalli, P. B. S.; Dangi, G. P.; Tayade, R. J.; Somani, R. S.; Bajaj, H. C. MIL-53(Al): An Efficient Adsorbent for the Removal of Nitrobenzene from Aqueous Solutions. *Ind. Eng. Chem. Res.* **2011**, *50* (18), 10516–10524. https://doi.org/10.1021/ie200429f.

(81) Saifutdinov, B. R.; Isaeva, V. I.; Alexandrov, E. V.; Kustov, L. M. Study of Selective Adsorption of Aromatic Compounds from Solutions by the Flexible MIL-53(Al) Metal-Organic Framework. *Russ. Chem. Bull.* **2015**, *64* (5), 1039–1048. https://doi.org/10.1007/s11172-015-0973-8.

(82) Kim, J. Y.; Zhang, L.; Balderas-Xicohténcatl, R.; Park, J.; Hirscher, M.; Moon, H. R.; Oh, H. Selective Hydrogen Isotope Separation via Breathing Transition in MIL-53(Al). *J. Am. Chem. Soc.* **2017**, *139* (49), 17743–17746. https://doi.org/10.1021/jacs.7b10323.

(83) Zi, G.; Yan, Z.; Wang, Y.; Chen, Y.; Guo, Y.; Yuan, F.; Gao, W.; Wang, Y.; Wang, J. Catalytic Hydrothermal Conversion of Carboxymethyl Cellulose to Value-Added Chemicals over Metal–Organic Framework MIL-53(Al). *Carbohydr. Polym.* **2015**, *115*, 146–151. https://doi.org/10.1016/j.carbpol.2014.08.065.

(84) Shu, L.; Chen, S.; Zhao, W.-W.; Bai, Y.; Ma, X.-C.; Li, X.-X.; Li, J.-R.; Somsundaran, P. High-Performance Liquid Chromatography Separation of Phthalate Acid Esters with a MIL-53(Al)-Packed Column. *J. Sep. Sci.* **2016**, *39* (16), 3163–3170. https://doi.org/10.1002/jssc.201600364.

(85) Ambroz, F.; Macdonald, T. J.; Martis, V.; Parkin, I. P. Evaluation of the BET Theory for the Characterization of Meso and Microporous MOFs. *Small Methods* **2018**, *2* (11), 1800173. https://doi.org/10.1002/smtd.201800173.

(86) Brunauer, S.; Deming, L. S.; Deming, W. E.; Teller, E. On a Theory of the van Der Waals Adsorption of Gases. *J. Am. Chem. Soc.* **1940**, *62* (7), 1723–1732. https://doi.org/10.1021/ja01864a025.

(87) Cuchiaro, J.; DeRoo, J.; Thai, J.; Reynolds, M. M. Evaluation of the Adsorption-Accessible Surface Area of MIL-53(Al) Using Cannabinoids in a Closed System. *ACS Appl. Mater. Interfaces* **2022**, *14* (10), 12836–12844. https://doi.org/10.1021/acsami.1c24391.

(88) Bonini, S. A.; Premoli, M.; Tambaro, S.; Kumar, A.; Maccarinelli, G.; Memo, M.; Mastinu, A. Cannabis Sativa: A Comprehensive Ethnopharmacological Review of a Medicinal Plant with a Long History. *J. Ethnopharmacol.* **2018**, *227*, 300–315. https://doi.org/10.1016/j.jep.2018.09.004.

(89) Luca, S. V.; Roehrer, S.; Kleigrewe, K.; Minceva, M. Approach for Simultaneous Cannabidiol Isolation and Pesticide Removal from Hemp Extracts with Liquid-Liquid Chromatography. *Ind. Crops Prod.* **2020**, *155*, 112726. https://doi.org/10.1016/j.indcrop.2020.112726.

(90) Citti, C.; Ciccarella, G.; Braghiroli, D.; Parenti, C.; Vandelli, M. A.; Cannazza, G. Medicinal Cannabis: Principal Cannabinoids Concentration and Their Stability Evaluated by a High-Performance Liquid Chromatography Coupled to Diode Array and Quadrupole Time of Flight Mass Spectrometry Method. *J. Pharm. Biomed. Anal.* **2016**, *128*, 201–209. https://doi.org/10.1016/j.jpba.2016.05.033.

(91) Sandler, L. N.; Beckerman, J. L.; Whitford, F.; Gibson, K. A. Cannabis as Conundrum. *Crop Prot.* **2019**, *117*, 37–44. https://doi.org/10.1016/j.cropro.2018.11.003.

(92) McPartland, J. M.; Guy, G. W. Models of Cannabis Taxonomy, Cultural Bias, and Conflicts between Scientific and Vernacular Names. *Bot. Rev.* **2017**, *83* (4), 327–381. https://doi.org/10.1007/s12229-017-9187-0.

(93) Small, E.; Beckstead, H. Common Cannabinoid Phenotypes in 350 Stocks of Cannabis. *LLoydia* **1973**, *36* (2), 144–165.

(94) Hazekamp, A.; Fischedick, J. T. Cannabis - from Cultivar to Chemovar. *Drug Test. Anal.* **2012**, *4* (7–8), 660–667. https://doi.org/10.1002/dta.407.

(95) Wu, Y.; Trejo, H. X.; Chen, G.; Li, S. Phytoremediation of Contaminants of Emerging Concern from Soil with Industrial Hemp (Cannabis Sativa L.): A Review. *Environ. Dev. Sustain.* **2021**, *23* (10), 14405–14435. https://doi.org/10.1007/s10668-021-01289-0.

(96) López-Ruiz, R.; Marín-Sáez, J.; Garrido Frenich, A.; Romero-González, R. Recent Applications of Chromatography for Analysis of Contaminants in Cannabis Products: A Review. *Pest Manag. Sci.* **2022**, *78* (1), 19–29. https://doi.org/10.1002/ps.6599.

(97) Ambach, L.; Penitschka, F.; Broillet, A.; König, S.; Weinmann, W.; Bernhard, W. Simultaneous Quantification of Delta-9-THC, THC-Acid A, CBN and CBD in Seized Drugs Using HPLC-DAD. *Forensic Sci. Int.* **2014**, *243*, 107–111. https://doi.org/10.1016/j.forsciint.2014.06.008.

(98) Hädener, M.; König, S.; Weinmann, W. Quantitative Determination of CBD and THC and Their Acid Precursors in Confiscated Cannabis Samples by HPLC-DAD. *Forensic Sci. Int.* **2019**, *299*, 142–150. https://doi.org/10.1016/j.forsciint.2019.03.046.

(99) Burnier, C.; Esseiva, P.; Roussel, C. Quantification of THC in Cannabis Plants by Fast-HPLC-DAD: A Promising Method for Routine Analyses. *Talanta* **2019**, *192*, 135–141. https://doi.org/10.1016/j.talanta.2018.09.012.

(100) Brighenti, V.; Pellati, F.; Steinbach, M.; Maran, D.; Benvenuti, S. Development of a New Extraction Technique and HPLC Method for the Analysis of Non-Psychoactive Cannabinoids in Fibre-Type Cannabis Sativa L. (Hemp). *J. Pharm. Biomed. Anal.* **2017**, *143*, 228–236. https://doi.org/10.1016/j.jpba.2017.05.049.

(101) Ciolino, L. A.; Ranieri, T. L.; Taylor, A. M. Commercial Cannabis Consumer Products Part 2: HPLC-DAD Quantitative Analysis of Cannabis Cannabinoids. *Forensic Sci. Int.* **2018**, *289*, 438–447. https://doi.org/10.1016/j.forsciint.2018.05.033.

(102) Protti, M.; Brighenti, V.; Battaglia, M. R.; Anceschi, L.; Pellati, F.; Mercolini, L. Cannabinoids from *Cannabis Sativa* L.: A New Tool Based on HPLC–DAD–MS/MS for a Rational Use in Medicinal Chemistry. *ACS Med. Chem. Lett.* **2019**, *10* (4), 539–544. https://doi.org/10.1021/acsmedchemlett.8b00571.

(103) Chang, C.-W.; Tung, C.-W.; Tsai, C.-C.; Wu, Y.-T.; Hsu, M.-C. Determination of Cannabinoids in Hemp Nut Products in Taiwan by HPLC-MS/MS Coupled with Chemometric Analysis: Quality Evaluation and a Pilot Human Study. *Drug Test. Anal.* **2017**, *9* (6), 888–897. https://doi.org/10.1002/dta.2062.

(104) Mandrioli, M.; Tura, M.; Scotti, S.; Gallina Toschi, T. Fast Detection of 10 Cannabinoids by RP-HPLC-UV Method in Cannabis Sativa L. *Molecules* **2019**, *24* (11), 2113. https://doi.org/10.3390/molecules24112113.

(105) Micalizzi, G.; Vento, F.; Alibrando, F.; Donnarumma, D.; Dugo, P.; Mondello, L. Cannabis Sativa L.: A Comprehensive Review on the Analytical Methodologies for Cannabinoids and Terpenes Characterization. *J. Chromatogr. A* **2021**, *1637*, 461864. https://doi.org/10.1016/j.chroma.2020.461864.

(106) Leghissa, A.; Hildenbrand, Z. L.; Schug, K. A. A Review of Methods for the Chemical Characterization of Cannabis Natural Products. *J. Sep. Sci.* **2018**, *41* (1), 398–415. https://doi.org/10.1002/jssc.201701003.

(107) Brenneisen, R.; El Sohly, M. A. Chromatographic and Spectroscopic Profiles of *Cannabis* of Different Origins: Part I. *J. Forensic Sci.* **1988**, *33* (6), 12583J. https://doi.org/10.1520/JFS12583J.

(108) Moulins, J. R.; Blais, M.; Montsion, K.; Tully, J.; Mohan, W.; Gagnon, M.; McRitchie, T.; Kwong, K.; Snider, N.; Blais, D. R. Multiresidue Method of Analysis of Pesticides in Medical Cannabis. *J. AOAC Int.* **2018**, *101* (6), 1948–1960. https://doi.org/10.5740/jaoacint.17-0495.

(109) Raharjo, T. J.; Verpoorte, R. Methods for the Analysis of Cannabinoids in Biological Materials: A Review. *Phytochem. Anal.* **2004**, *15* (2), 79–94. https://doi.org/10.1002/pca.753.

(110) Patel, B.; Wene, D.; Fan, Z. (Tina). Qualitative and Quantitative Measurement of Cannabinoids in Cannabis Using Modified HPLC/DAD Method. *J. Pharm. Biomed. Anal.* **2017**, *146*, 15–23. https://doi.org/10.1016/j.jpba.2017.07.021.

(111) McPartland, J. M.; Russo, E. B. Cannabis and Cannabis Extracts: Greater Than the Sum of Their Parts? *J. Cannabis Ther.* **2001**, *1* (3–4), 103–132. https://doi.org/10.1300/J175v01n03_08.

(112) Aizpurua-Olaizola, O.; Soydaner, U.; Öztürk, E.; Schibano, D.; Simsir, Y.; Navarro, P.; Etxebarria, N.; Usobiaga, A. Evolution of the Cannabinoid and Terpene Content during the Growth of Cannabis Sativa Plants from Different Chemotypes. *J. Nat. Prod.* **2016**, *79* (2), 324–331. https://doi.org/10.1021/acs.jnatprod.5b00949.

(113) Abd-Elsalam, W. H. LC–MS/MS Quantitation of Phytocannabinoids and Their Metabolites in Biological Matrices. *Sample Prep.* **2019**, 22.

(114) Bakro, F.; Jedryczka, M.; Wielgusz, K.; Sgorbini, B.; Inchingolo, R.; Cardenia, V. Simultaneous Determination of Terpenes and Cannabidiol in Hemp (Cannabis Sativa L.) by

Fast Gas Chromatography with Flame Ionization Detection. *J. Sep. Sci.* **2020**, *43* (14), 2817–2826. https://doi.org/10.1002/jssc.201900822.

(115) Aizpurua-Olaizola, O.; Omar, J.; Navarro, P.; Olivares, M.; Etxebarria, N.; Usobiaga, A. Identification and Quantification of Cannabinoids in Cannabis Sativa L. Plants by High Performance Liquid Chromatography-Mass Spectrometry. *Anal. Bioanal. Chem.* **2014**, *406* (29), 7549–7560. https://doi.org/10.1007/s00216-014-8177-x.

(116) AOAC International, Gaithersburg, MD, USA. Official Method 2019.003. *Official Methods of Analysis of AOAC International* **2019**, 21st Ed.

(117) Hazekamp, A.; Simons, R.; Peltenburg-Looman, A.; Sengers, M.; van Zweden, R.; Verpoorte, R. Preparative Isolation of Cannabinoids from Cannabis Sativa by Centrifugal Partition Chromatography. *J. Liq. Chromatogr. Relat. Technol.* **2004**, *27* (15), 2421–2439. https://doi.org/10.1081/JLC-200028170.

(118) Küsgens, P.; Rose, M.; Senkovska, I.; Fröde, H.; Henschel, A.; Siegle, S.; Kaskel, S. Characterization of Metal-Organic Frameworks by Water Adsorption. *Microporous Mesoporous Mater.* **2009**, *120* (3), 325–330. https://doi.org/10.1016/j.micromeso.2008.11.020.

(119) Kim, Y.-H.; Kumar, P.; Kwon, E. E.; Kim, K.-H. Metal-Organic Frameworks as Superior Media for Thermal Desorption-Gas Chromatography Application: A Critical Assessment of

MOF-5 for the Quantitation of Airborne Formaldehyde. *Microchem. J.* **2017**, *132*, 219–226. https://doi.org/10.1016/j.microc.2017.01.032.

(120) Corella-Ochoa, M. N.; Tapia, J. B.; Rubin, H. N.; Lillo, V.; González-Cobos, J.; Núñez-Rico, J. L.; Balestra, S. R. G.; Almora-Barrios, N.; Lledós, M.; Güell-Bara, A.; Cabezas-Giménez, J.; Escudero-Adán, E. C.; Vidal-Ferran, A.; Calero, S.; Reynolds, M.; Martí-Gastaldo, C.; Galán-Mascarós, J. R. Homochiral Metal–Organic Frameworks for Enantioselective Separations in Liquid Chromatography. *J. Am. Chem. Soc.* **2019**, *141* (36), 14306–14316. https://doi.org/10.1021/jacs.9b06500.

(121) Chang, N.; Gu, Z.-Y.; Yan, X.-P. Zeolitic Imidazolate Framework-8 Nanocrystal Coated Capillary for Molecular Sieving of Branched Alkanes from Linear Alkanes along with High-Resolution Chromatographic Separation of Linear Alkanes. *J. Am. Chem. Soc.* **2010**, *132* (39), 13645–13647. https://doi.org/10.1021/ja1058229.

(122) Chen, B.; Xiang, S.; Qian, G. Metal−Organic Frameworks with Functional Pores for Recognition of Small Molecules. *Acc. Chem. Res.* **2010**, *43* (8), 1115–1124. https://doi.org/10.1021/ar100023y.

(123) Yusuf, K.; Aqel, A.; Al Othman, Z. Metal-Organic Frameworks in Chromatography. *J. Chromatogr. A* **2014**, *1348*, 1–16. https://doi.org/10.1016/j.chroma.2014.04.095.

(124) Perfecto-Irigaray, M.; Beobide, G.; Castillo, O.; da Silva, I.; García-Lojo, D.; Luque, A.; Mendia, A.; Pérez-Yáñez, S. [$Zr_6O_4(OH)_4$(Benzene-1,4-Dicarboxylato)$_6$]$_n$: A Hexagonal Polymorph of UiO-66. *Chem. Commun.* **2019**, *55* (42), 5954–5957. https://doi.org/10.1039/C9CC00802K.

(125) Baerlocher, C.; McCusker, L. B. Database of Zeolite Structures, 2019.

(126) Millange, F.; Serre, C.; Guillou, N.; Férey, G.; Walton, R. I. Structural Effects of Solvents on the Breathing of Metal–Organic Frameworks: An In Situ Diffraction Study. *Angew. Chem.* **2008**, *120* (22), 4168–4173. https://doi.org/10.1002/ange.200705607.

(127) Serre, C.; Bourrelly, S.; Vimont, A.; Ramsahye, N. A.; Maurin, G.; Llewellyn, P. L.; Daturi, M.; Filinchuk, Y.; Leynaud, O.; Barnes, P.; Férey, G. An Explanation for the Very Large Breathing Effect of a Metal–Organic Framework during CO2 Adsorption. *Adv. Mater.* **2007**, *19* (17), 2246–2251. https://doi.org/10.1002/adma.200602645.

(128) Serre, C.; Millange, F.; Thouvenot, C.; Noguès, M.; Marsolier, G.; Louër, D.; Férey, G. Very Large Breathing Effect in the First Nanoporous Chromium(III)-Based Solids: MIL-53 or $Cr^{III}(OH)\cdot\{O_2C{-}C_6H_4{-}CO_2\}\cdot\{HO_2C{-}C_6H_4{-}CO_2H\}_x\cdot H_2O_y$. *J. Am. Chem. Soc.* **2002**, *124* (45), 13519–13526. https://doi.org/10.1021/ja0276974.

(129) Neimark, A. V.; Coudert, F.-X.; Triguero, C.; Boutin, A.; Fuchs, A. H.; Beurroies, I.; Denoyel, R. Structural Transitions in MIL-53 (Cr): View from Outside and Inside. *Langmuir* **2011**, *27* (8), 4734–4741. https://doi.org/10.1021/la200094x.

(130) Kato, S.; Otake, K.; Chen, H.; Akpinar, I.; Buru, C. T.; Islamoglu, T.; Snurr, R. Q.; Farha, O. K. Zirconium-Based Metal–Organic Frameworks for the Removal of Protein-Bound Uremic Toxin from Human Serum Albumin. *J. Am. Chem. Soc.* **2019**, *141* (6), 2568–2576. https://doi.org/10.1021/jacs.8b12525.

(131) Wang, Y.; Sun, J.; Qiao, J.; Ouyang, J.; Na, N. A "Soft" and "Hard" Ionization Method for Comprehensive Studies of Molecules. *Anal. Chem.* **2018**, *90* (24), 14095–14099. https://doi.org/10.1021/acs.analchem.8b04437.

(132) Sanner, M. F.; Olson, A. J.; Spehner, J. C. Reduced Surface: An Efficient Way to Compute Molecular Surfaces. *Biopolymers.* **1996**. 38 (3), 305-320.

(133) Ho, B. K.; Gruswitz, F. HOLLOW: Generating Accurate Representations of Channel and Interior Surfaces in Molecular Structures. *BMC Struct. Biol.* **2008**, *8* (1), 49. https://doi.org/10.1186/1472-6807-8-49.

(134) The PyMol Molecular Graphics System, Version 2.4, Schrodinger, LLC.

(135) Lee, S. C.; Kim, S. Y.; Lee, W. S.; Jung, S. Y.; Hwang, B. W.; Ragupathy, D.; Lee, D. D.; Lee, S. Y.; Kim, J. C. Effects of Textural Properties on the Response of a SnO2-Based Gas Sensor for the Detection of Chemical Warfare Agents. *Sensors* **2011**, *11* (7), 6893–6904. https://doi.org/10.3390/s110706893.

(136) Cirrincione, M.; Saladini, B.; Brighenti, V.; Salamone, S.; Mandrioli, R.; Pollastro, F.; Pellati, F.; Protti, M.; Mercolini, L. Discriminating Different Cannabis Sativa L. Chemotypes Using Attenuated Total Reflectance - Infrared (ATR-FTIR) Spectroscopy: A Proof of Concept. *J. Pharm. Biomed. Anal.* **2021**, *204*, 114270. https://doi.org/10.1016/j.jpba.2021.114270.

(137) *Marijuana Tax Data*. Colorado Department of Revenue. https://www.colorado.gov/pacific/revenue/colorado-marijuana-tax-data (accessed 2020-07-24).

(138) De Luca, C.; Buratti, A.; Krauke, Y.; Stephan, S.; Monks, K.; Brighenti, V.; Pellati, F.; Cavazzini, A.; Catani, M.; Felletti, S. Investigating the Effect of Polarity of Stationary and Mobile Phases on Retention of Cannabinoids in Normal Phase Liquid Chromatography. *Anal. Bioanal. Chem.* **2022**. https://doi.org/10.1007/s00216-021-03862-y.

(139) Wylie, P. L.; Westland, J.; Wang, M.; Radwan, M. M.; Majumdar, C. G.; El Sohly, M. A. Screening for More than 1,000 Pesticides and Environmental Contaminants in Cannabis by

GC/Q-TOF. *Med. Cannabis Cannabinoids* **2020**, *3* (1), 14–24. https://doi.org/10.1159/000504391.

(140) do Amaral, B.; Peralta-Zamora, P.; Nagata, N. Simultaneous Multi-Residue Pesticide Analysis in Southern Brazilian Soil Based on Chemometric Tools and QuEChERS-LC-DAD/FLD Method. *Environ. Sci. Pollut. Res.* **2022**. https://doi.org/10.1007/s11356-021-18292-7.

(141) Craven, C. B.; Wawryk, N.; Jiang, P.; Liu, Z.; Li, X.-F. Pesticides and Trace Elements in Cannabis: Analytical and Environmental Challenges and Opportunities. *J. Environ. Sci.* **2019**, *85*, 82–93. https://doi.org/10.1016/j.jes.2019.04.028.

(142) King, J. W. The Relationship between Cannabis/Hemp Use in Foods and Processing Methodology. *Curr. Opin. Food Sci.* **2019**, *28*, 32–40. https://doi.org/10.1016/j.cofs.2019.04.007.

(143) National Center for Biotechnology Information. *PubChem Compound Summary for CID 6129, Carbaryl.* Pubchem. https://pubchem.ncbi.nlm.nih.gov/compound/6129 (accessed 2022-05-10).

(144) National Center for Biotechnology Information. *PubChem Compound Summary for CID 213013, Boscalid*. Pubchem. https://pubchem.ncbi.nlm.nih.gov/compound/213013 (accessed 2022-05-10).

(145) National Center for Biotechnology Information. *PubChem Compound Summary for CID 115003, Spinosad A*. Pubchem. https://pubchem.ncbi.nlm.nih.gov/compound/115003 (accessed 2022-05-10).

(146) Altiero, P. An Introduction to Chromatography Equations. *Agil. Train. Webinar* **2018**, 37.

(147) Morley, R.; Minceva, M. Operating Mode and Parameter Selection in Liquid–Liquid Chromatography. *J. Chromatogr. A* **2020**, *1617*, 460479. https://doi.org/10.1016/j.chroma.2019.460479.

APPENDIX A – SUPPORTING INFORMATION FOR CHAPTER 2

Table A.1: Dilution-corrected assay for cannabinoids and pesticides, detected using the present instrument method (n = 3, all samples). The high sample RSD indicates that these results are not suitable and further optimization is necessary for accurate quantification.

Analyte	*Bottoms (ng/mL)*	*Bottoms RSD*	*Distillate (ng/mL)*	*Distillate RSD*
7-OH-CBD [(-)-7-hydroxy CBD]	41	173	2369	121
Boscalid	43	5	44	2
Carbaryl	ND	ND	ND	ND
CBC (Cannabichromene)	7201	140	19001	132
CBCO (Cannabichromeorcin)	ND	ND	179	143
CBCVA (Cannabichromevarinic Acid)	3	173	92	126
CBD (Cannabidiol)	143823	29	8388212	11
CBDA (Cannabidiol Acid)	ND	ND	ND	ND
CBDA-ME (Cannabidiolic Acid Methyl	23	43	97	115
CBDP (Cannabidiphorol)	215	106	443	125
CBDV (Cannabidivarin)	225	140	10508	118
CBE (Cannabielsoin)	2796	141	28133	107
CBG (Cannabigerol)	3468956	15	71641	9
CBGA (Cannabigerolic Acid)	ND	ND	ND	ND
CBGQA (Cannabigerol Quinone Acid)	53	173	26	173
CBGV (Cannabigerovarin)	689	135	49	116
CBGVA (Cannabigerovarinic Acid)	ND	ND	ND	ND
CBN (Cannabinol)	2557	135	13656	126
CBTC (Cannabicitran)	37349	134	68320	101
Clothianidin	ND	ND	ND	ND
Δ8-THC (Δ8-tetrahydrocannabinol)	1276	138	22629	116
Δ9-THC (Δ9-tetrahydrocannabinol)	21496	131	70168	100
Δ9-THCA (Δ9-tetrahydrocannabinolic	531	74	3100	139
Δ9-THCB (Δ9-tetrahydrocannabutol)	94	18	85	18
Δ9-THCH (Δ9-tetrahydrocannabihexol)	6209	116	362	13
Δ9-THCV (Δ9-tetrahydrovannabivarin)	294	145	539	124
Δ9-THCVA (Δ9-	ND	ND	8	173
Diuron	ND	ND	ND	ND
Imidacloprid	ND	ND	ND	ND
Myclobutanil	11	24	11	25
Pyrethrin I	9528	115	6348	98
Pyrethrin II	681	135	179	68
Spinosad	ND	ND	ND	ND

Table A.1 (*cont'd*):

Analyte	*Mother Liquor*	*Mother Liquor*	*EtOH (ng/mL)*	*EtOH RSD*
7-OH-CBD [(-)-7-hydroxy CBD]	9373	108	3274	126
Boscalid	44	6	44	4
Carbaryl	ND	ND	ND	ND
CBC (Cannabichromene)	29479	122	28796	130
CBCO (Cannabichromeorcin)	144	157	478	161
CBCVA (Cannabichromevarinic Acid)	474	154	142	169
CBD (Cannabidiol)	6549283	2	6167320	8
CBDA (Cannabidiol Acid)	ND	ND	404562	17
CBDA-ME (Cannabidiolic Acid Methyl	133	121	58	102
CBDP (Cannabidiphorol)	816	145	799	141
CBDV (Cannabidivarin)	4660	87	13013	129
CBE (Cannabielsoin)	59809	81	6536	137
CBG (Cannabigerol)	352145	4	454129	14
CBGA (Cannabigerolic Acid)	ND	ND	ND/OQ	ND/OQ
CBGQA (Cannabigerol Quinone Acid)	282	173	836	168
CBGV (Cannabigerovarin)	196	113	158	128
CBGVA (Cannabigerovarinic Acid)	ND	ND	ND	ND
CBN (Cannabinol)	23839	118	5987	135
CBTC (Cannabicitran)	73082	100	87526	113
Clothianidin	ND	ND	ND	ND
Δ8-THC (Δ8-tetrahydrocannabinol)	29039	114	21931	124
Δ9-THC (Δ9-tetrahydrocannabinol)	78728	94	62010	111
Δ9-THCA (Δ9-tetrahydrocannabinolic	6152	119	14194	136
Δ9-THCB (Δ9-tetrahydrocannabutol)	185	45	143	68
Δ9-THCH (Δ9-tetrahydrocannabihexol)	487	27	1197	82
Δ9-THCV (Δ9-tetrahydrovannabivarin)	2343	122	583	135
Δ9-THCVA (Δ9-	147	157	39	173
Diuron	ND	ND	ND	ND
Imidacloprid	ND	ND	ND	ND
Myclobutanil	12	28	12	17
Pyrethrin I	2567	93	2660	104
Pyrethrin II	142	84	117	85
Spinosad	ND	ND	ND	ND

Table A.1 (*cont'd*):

Analyte	*Flower (ng/mL)*	*Flower RSD*
7-OH-CBD [(-)-7-hydroxy CBD]	1142	154
Boscalid	44	6
Carbaryl	ND	ND
CBC (Cannabichromene)	13075	135
CBCO (Cannabichromeorcin)	ND	ND
CBCVA (Cannabichromevarinic Acid)	ND	ND
CBD (Cannabidiol)	1389722	15
CBDA (Cannabidiol Acid)	1520578	16
CBDA-ME (Cannabidiolic Acid Methyl	22	25
CBDP (Cannabidiphorol)	92	110
CBDV (Cannabidivarin)	1136	128
CBE (Cannabielsoin)	2355	156
CBG (Cannabigerol)	52102	21
CBGA (Cannabigerolic Acid)	ND	ND
CBGQA (Cannabigerol Quinone Acid)	57	173
CBGV (Cannabigerovarin)	8	132
CBGVA (Cannabigerovarinic Acid)	ND/OQ	ND/OQ
CBN (Cannabinol)	6058	134
CBTC (Cannabicitran)	18574	138
Clothianidin	ND	ND
Δ8-THC (Δ8-tetrahydrocannabinol)	8450	133
Δ9-THC (Δ9-tetrahydrocannabinol)	22391	129
Δ9-THCA (Δ9-tetrahydrocannabinolic	6339	145
Δ9-THCB (Δ9-tetrahydrocannabutol)	72	9
Δ9-THCH (Δ9-tetrahydrocannabihexol)	ND	ND
Δ9-THCV (Δ9-tetrahydrovannabivarin)	31	173
Δ9-THCVA (Δ9-	1	173
Diuron	ND	ND
Imidacloprid	ND	ND
Myclobutanil	11	23
Pyrethrin I	513	145
Pyrethrin II	103	78
Spinosad	ND	ND

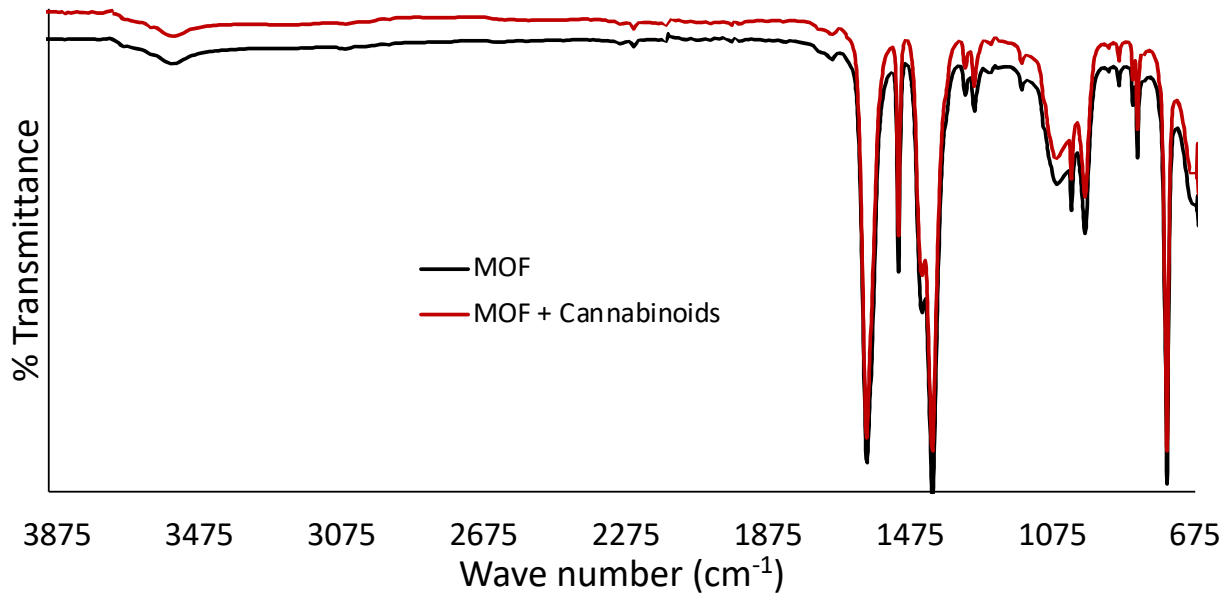

Figure B.1: Overlaid, full FTIR spectra of MIL-53(Al) (black trace) and cannabinoid-exposed MIL-53(Al) (red trace).

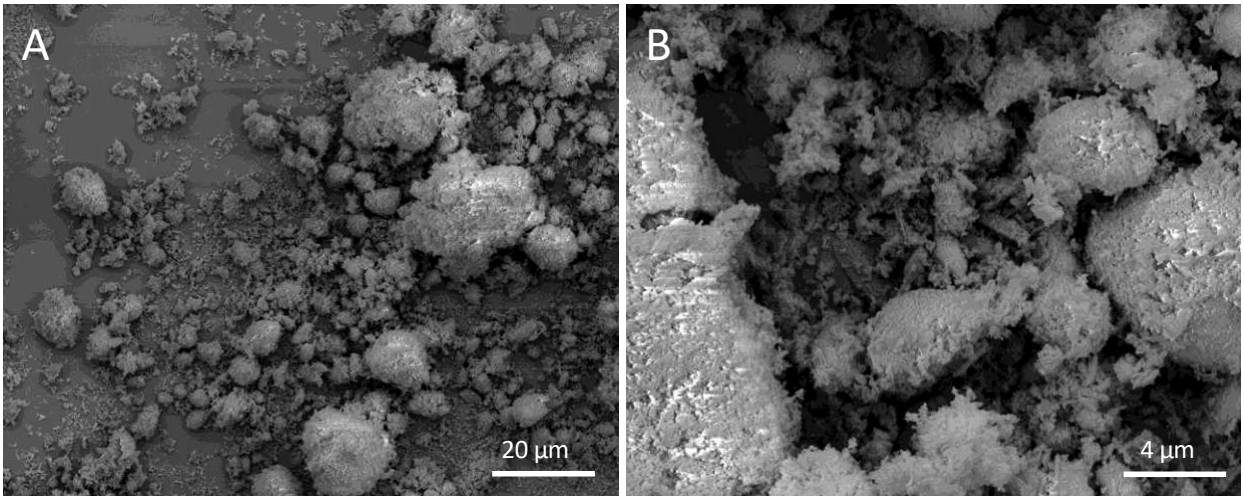

Figure B.2: Characteristic SEM images of the activated MIL-53(Al) sample at A) 1,000x and B) 5,000x magnification.

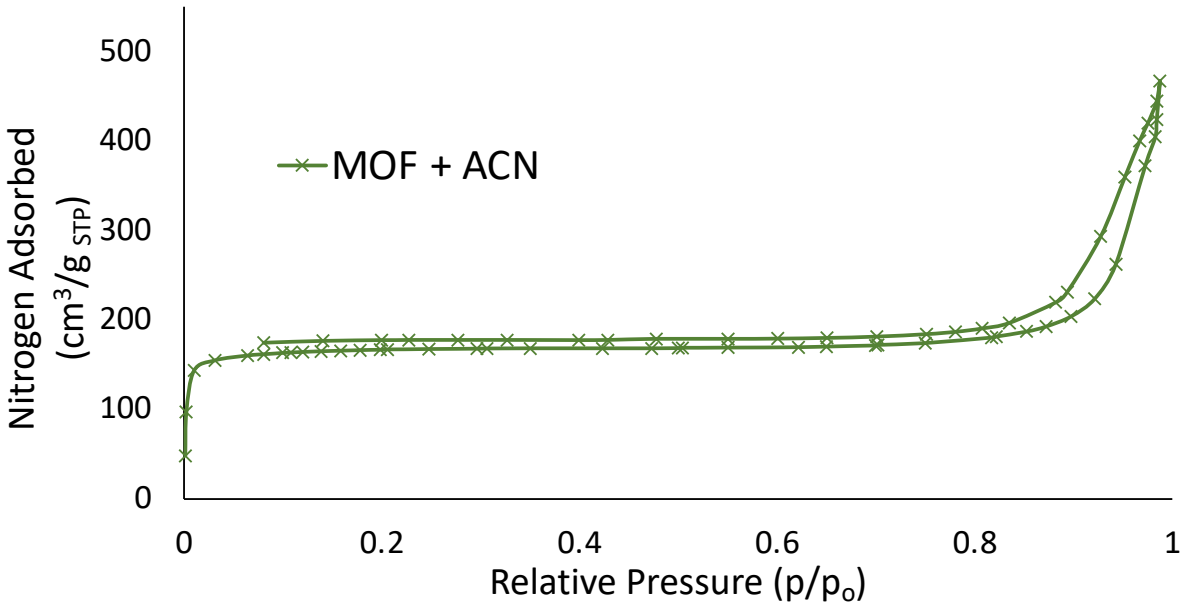

Figure B.3: Nitrogen adsorption isotherm of MIL-53(Al) exposed to ACN and degassed under ambient conditions (control).